Summer 8-9-2017

Analysis of Variable Insensitive Friction Stir Welding Parameters

Robert L. Marrero Jr
University of New Orleans, rlmarrer@Uno.edu

Analysis of Variable Insensitive Friction Stir Welding

A Thesis

Submitted to the Graduate Faculty of the
University of New Orleans
in partial fulfillment of the
requirements for the degree of

Master of Science
in
Engineering
with a concentration in
Mechanical Engineering

by

Robert L. Marrero, Jr.

B.Sc., University of New Orleans, 2012

August, 2017

Dedicated to my late mother who always encouraged me to pursue higher education.

Acknowledgement

I would like to thank Dr. Michael Eller for the guidance and support offered throughout this thesis. I would also like to thank him for bringing the FSW course to UNO, in which without that, this manuscript would not exist.

I would also like to extend my thanks to Dr. Paul Herrington for serving as a committee member for my thesis. His recommendations and support were fundamental to improve the quality of this manuscript.

I would also like to extend my thanks to Dr. Paul Schilling for serving as a committee member for my thesis. His recommendations and support were fundamental to improve the quality of this manuscript.

I would like to express my gratitude to my colleagues Davin Kieff and Shawn Puleo for assisting in the tensile testing. I also extend my thanks to both Anne-Marie and Sarah of Dr. Paul Schilling's material's lab for assisting with the polishing and micro-hardness testing.

Table of Contents

Nomenclature

Δ	Change in Original Value
ε	Strain
σ	Stress
σ_u	Ultimate Tensile Strength
σ_y	Yield Strength
a	Intercept of Regression Line
A	Cross Sectional Area
b_k	Slope of Regression Line
d	Diagonal Length of Hardness Indention
e	Error of Regression Line
E	Modulus of Elasticity
F	Indention Load
HV	Hardness-Vickers
L	Length of Tensile Specimen
P	Applied Load
R^2	Coefficient of Determination
SS_{res}	Sum of Squared Distances Between the Actual and Predicted Values
SS_{tot}	Sum of Squared Distances Between the Actual Values and their Mean
X_k	Independent Variable of Regression Line
Y	Dependent Variable of Regression Line

List of Figures

List of Tables

Abstract

Friction Stir Welding (FSW) was used to perform a Design of Experiment (DOE) to determine the welding parameters effects on yielding consistent mechanical properties across the length of the weld. The travel speed was varied across set forge force and RPM conditions, to find a dataset that will yield consistent mechanical properties independent of the travel speed. Six different welds were completed on two different aluminum panels, the advancing side being Aluminum alloy 2195-T8 at a thickness of .350", with the retreating side being Aluminum alloy 2219-T851 with a gauge thickness of .360". A Left-hand Right-hand self-reacting pin tool was used for each weld. The mechanical properties of interest are the Ultimate Tensile Strength, Yield Strength, Elasticity and Hardness. The strengths were evaluated by tensile testing, with the Elasticity being measure post break. Specimens were then polished where macrograph and micrograph analysis was completed. Micro-hardness testing was then completed on the weld nuggets.

Keywords: Friction Stir Welding; Welding Parameters; Variable Insensitive; Travel Speed; Pin Tool;

Chapter 1: Introduction

Oftentimes, when developing a weld scheme for friction stir welding it is completed on a flat plane in ideal conditions. When transferring the same weld scheme to a production model, the different geometries experienced can have an effect on the overall welding parameters. An example would be a curved surface in which the travel speed will not be constant as it travels up and down at different points along the curvature. This is because not all friction stir welding equipment are able to maintain a constant parameter, or not optimized to maintain a particular parameter, resulting in deviations from the welding input. Insensitivity would be the means to find out which combination of two welding parameters would make the third parameter have no effect on the overall mechanical properties.

Variable insensitivity in Friction Stir Welding was initially presented by Lockheed Martin Corporation. The idea behind the theory is that there exists a set of two welding parameters when used in combination on a weld schedule, the third welding panel will have no effect on the final mechanical properties. This is important as predictability in welding is important for manufacturing tolerances. An example of past research can be seen in the Figure 1.1.

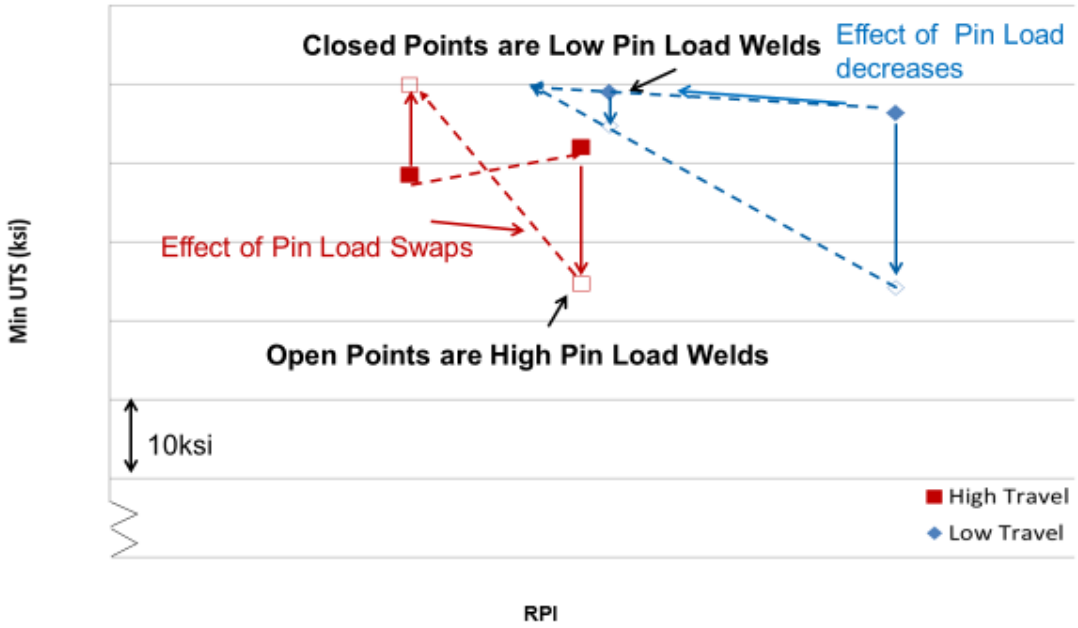

Figure 1.1: Effect of Load Insensitivity on Friction Stir Welds [1]

The above figure shows the results of two different experiments. The one on the left in red shows two different forge forces, a constant high travel speed and varied rotational speeds for the tool. The set on the right in the blue shows similar input variables with the exception being that a low travel speed was used instead of the high travel speed. All welding parameters and final mechanical properties of the original experiment is considered proprietary information and was not publicly released. Only the original idea behind variable insensitivity was presented. When looking at the above red "bowtie", the trend lines cross between them showing a point where one value of UTS is achieved for both values of the forge force.

The aluminum alloys used in this experiment were 2219-T851 (2219 hereafter), and Aluminum 2195-T8 (2195 hereafter) which are typical in aerospace applications. Much of the metal that was used in this experiment was leftovers from the original NASA Ares project that was cancelled. These are unique in that the 2000 series Aluminum is often considered unweldable by common techniques due to increase concentration of Copper causing an increased sensitivity to hot cracking

[2]. The base mechanical properties are tabulated below and these values will be used in the final comparison of the weld integrities.

Table 1.1
Mechanical Properties for Aluminum Alloys

Property	Aluminum 2219-T851 [3]	Aluminum 2195-T8 [5][4]
σ_u	60 ksi	78 ksi
σ_y	42 ksi	73 ksi
E	10.1 msi	11 msi
HV	130	180

This current research will be building upon the original theory and examining the effect of the travel speed on the final mechanical properties and general weld quality. This manuscript will also build upon pull research completed by the Friction Stir Welding course at the University of New Orleans, as their previous data was used to help select the weld parameters which is further explained in Chapter 3.

Knowing the above information, this manuscript will propose to investigate the effects of variable insensitivity in friction stir welding process parameters, specifically focusing on the travel speed.

Chapter 2: Literature Review

2.1 Friction Stir Welding

Friction Stir Welding was created by The Welding Institute in 1991, and later officially patented in 1995 **[6]**. It is a solid-state welding process. A solid-state welding process is defined as the joining of two materials in which the surface Temperature does not reach the melting point **[7]**. A solid-state weld allows for higher quality welds as the lack of material melting has an absence of solidification cracking, porosity, oxidation and other defects commonly occurring in fusion welds **[8]**. The primary method for the material joining is through plastic deformation along the interface of the tool and material.

Friction Stir Welding is completed by having a rotating pin tool penetrate the base material. The pin tool is rotated at a pre-determined RPM and allowed to generate enough heat through the friction between the both the rotating tool and the work piece before traveling. This localization of heat allows the material to undergo plastic deformation. Once enough heat is generated to prevent too cold of a weld, the pin tool then traverses along the weld seam. This will continuously generate frictional heat between the surface contact points, allowing plastic deformation to continue to occur along the weld seam. This can be illustrated in Figure 2.1.1.

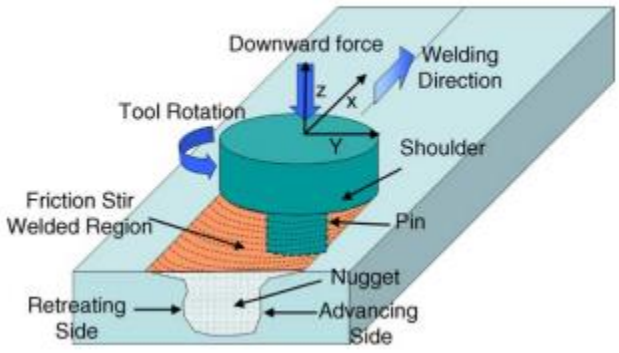

Figure 2.1.1: Schematic of Friction Stir Welding [9]

It can be seen from the above figure that the collection of terms is made with respect to the pin tool. Each panel is divide into either the advancing side or the retreating side. The advancing side is where the tool's tangential velocity is the same as the welding direction. While the retreating side possesses a tangential velocity opposite that of the weld direction. This can be illustrated below in Figure 2.1.2.

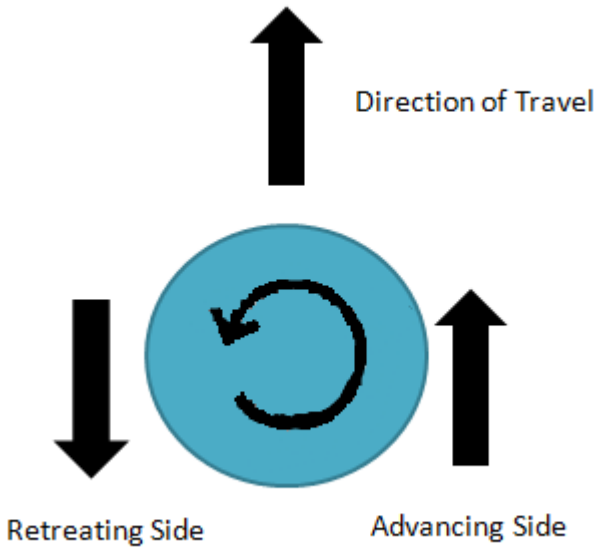

Figure 2.1.2: Velocity Profile of Pin Tool

Friction stir welds are characterized by their welding parameters. The three primary welding parameters are the forge force, pin RPM and pin travel speed.

The forge force pushes down on the work piece and extrudes the material around the pin tool. This allows for material flow to occur. Because of the forge force pressing down upon the work piece, each side must be clamped down to prevent the plate from separating. If this were not the case, the workpiece would not be able to extrude properly and the advancing and retreating side would push away from each other **[7]**.

The second welding parameter is the pin tool RPM. The RPM directly correlates to the amount of heat produced by the pin tool. A low RPM will cause less heat to be generated resulting in more cold work being applied to the work piece. An increase in RPM will yield much more friction heat, but will also have a softer weld. An optimal amount of heat should be applied to use the benefits of both the cold and hot work being applied to the workpiece.

The last welding parameter and the focus of this study is the pin tool travel speed. The travel speed is set at a constant velocity across the seam. The pin tool travel speed also has an effect on the heat output to the work piece. As the pin tool travels at a much slower rate, more frictional heat will be applied to the work piece. This is analogous to that of a heat exchanger.

All three welding parameters can be seen visually in Figure 2.1.3. on the next page. This is shown as a self-reacting pin tool type which will not include an anvil for the panels to rest on. This will in turn make the pin tool pinch together at the set forge force instead of having an anvil with a reaction force.

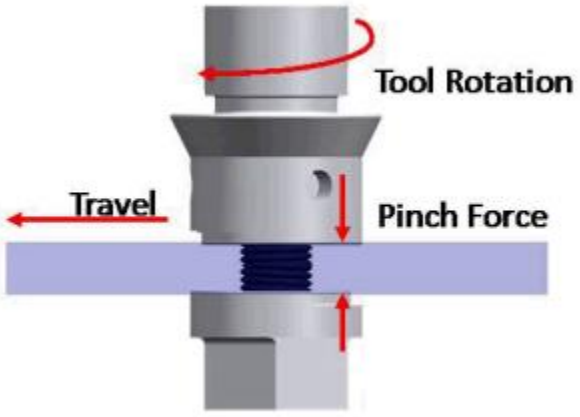

Figure 2.1.3: Three Welding Parameters as seen on a Self-Reacting Pin Tool [10]

2.2 Frictional Heat

One of the more important factors of determining the effectiveness of the weld is to examine the heat input from the pin tool to the work piece. It is estimated for a self-reacting weld, the generated heat can be transferred to the work piece through conduction, lost to the ambient air through convection and radiation, or transferred to the pin tool through conduction **[7]**. It is estimated that at most 95% of the frictional heat can be transferred to the work piece **[11]**. The main methods of varying the input heat is by changes in the weld parameters. The table below shows the relation of the welding parameters with respect to the amount of frictional heat generated.

Table 2.2.1
Frictional Heat vs. Welding Parameter [12]

Welding Parameter	Decrease Parameter	Increase Parameter
Forge Force	Reduce Frictional Heat	Increase Frictional Heat
Tool RPM	Reduce Frictional Heat	Increase Frictional Heat
Travel Speed	Increase Frictional Heat	Reduce Frictional Heat

As the work piece receives less heat the pin tool is then forced to apply more cold work to plasticize the materials. This will allow the strength to increase along with the amount of proportional cold work **[11]**. This is good in theory, but practically it requires much stronger pin tools, as they will also bear stress of this increased cold work, resulting in potential fracturing of the pin tool. The colder the weld will also yield a more brittle final product. The opposite of that in which a surplus of heat is added to the work piece. This will result in a much more ductile weld.

The amount of heat will have an impact on the grain structure of the work piece. An increase in the total heat supplied to the work piece will result in an enlarged grain structure. This is due to the work piece experiencing recrystallization for a much longer period. Recrystallization is

defined as a process in which new strain-free grains are allowed to nucleate and replace previously damaged grains **[13]**.

2.3 Metallurgy

As the pin tool travels across the weld seam, the microstructure is modified. This allows sections of the material to receive different heat treatments. These sections are divided up into the following: Unaffected Material; Heat Affected Zone (HAZ); Thermomechanically affected zoned (TMAZ); and, Weld Nugget **[7]**. Figure 2.3.1 shows a representation of the areas with respective sizes. The amount of heat transferred to the work piece will also affect the total reach of the heat affected zone.

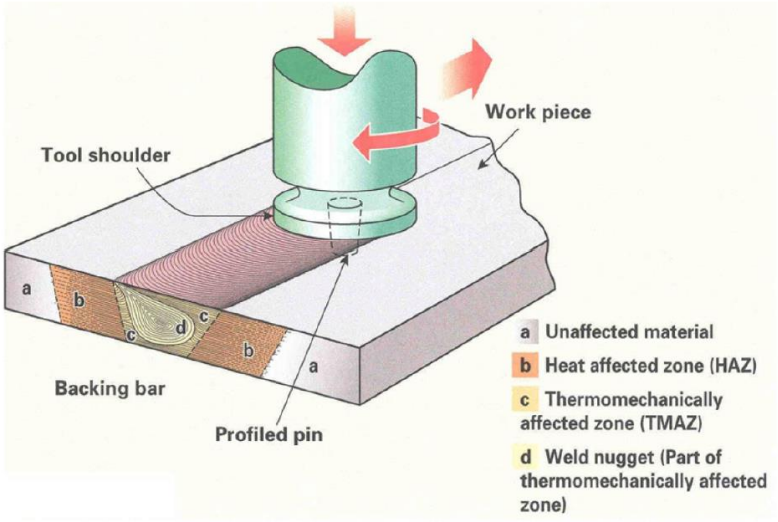

Figure 2.3.1: Microstructure of a Friction Stir Weld [7]

The unaffected material will be the area of the panel that will still retain the original grain size and orientation. The negligible amount of heat received in this area will not result in any microstructure changes. If the panel has any specific grain size or orientation before the welding occurs, then this can be used as a comparison tool for post weld analysis.

The next area of interest is the Heat Affected Zone. The HAZ will have a grain structure that undergoes recrystallization. The orientation of the grains will also remain constant and not change, retaining the original orientation of the parent material. The grain size will also larger than the nugget and TMAZ as it only undergoes static recrystallization and recovery.

The third area, the Thermomechanically Affected Zone, will experience more heat transfer than the previous two zones, which this zone will start showing indications of the material flow. The grain orientation will start following the material flow path instead of retaining the orientation of the base material's orientation. The grains in the TMAZ will experience similar conditions to hot working on metal. As of what happens to the grains themselves, they will experience both dynamic and static recrystallization and growth. This will cause the grain size to become even smaller, but some larger grains can exist.

The last but most important zone is the weld Nugget. The nugget represents a highly turbulent and complex zone with material flow, and varying stresses and different strains acting on the material. The grain structure in this zone experiences full recrystallization which will result in the most refined grain size that have an equiaxed orientation.

These four zones can then be identified on metallurgical macrograph pictures, in which an example can be found in Figure 2.3.2

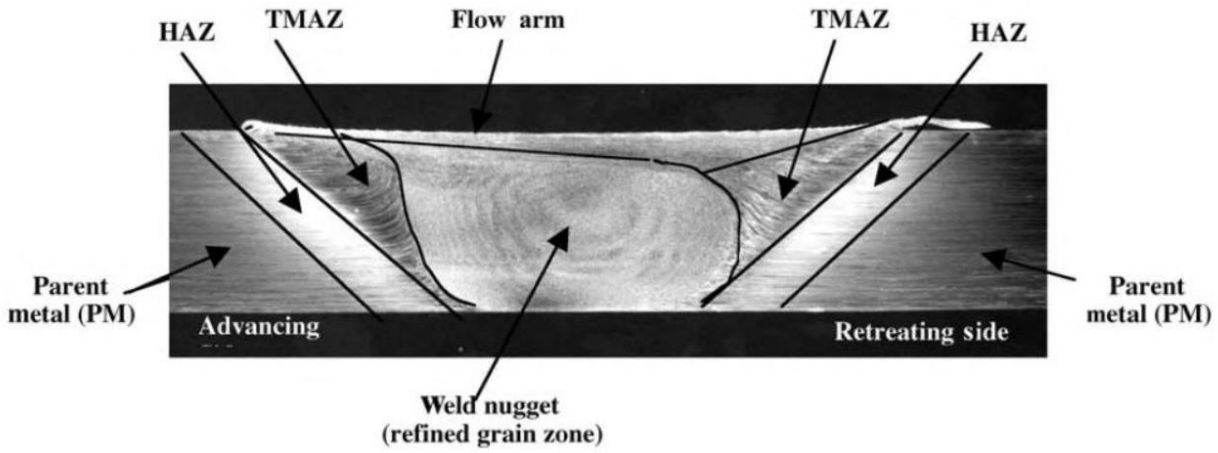

Figure 2.3.2: Zone Classification of a Friction Stir Weld [9]

2.4 Strength of Materials

The strength of the material is defined as the stress required to break the material under question. The stress is the applied load on the subject material normalized by the cross-sectional area. This can be equated below **[14]**:

$$\boldsymbol{\sigma = \frac{P}{A}} \qquad \textbf{Eq. 2.4.1}$$

The strain of the material is not the same as the stress, as it is a mathematically representation of how far the atoms at any point in the solid are being pulled apart. This is normalized by the unit length of the material in question. This can also be express mathematically as seen in Eq 2.4.2. Engineering strains are often very small, and are often expressed in percentages instead of absolute quantities **[14]**.

$$\boldsymbol{\varepsilon = \frac{\Delta L}{L}} \qquad \textbf{Eq. 2.4.2}$$

These two units can be graph together to determine how a material reacted under various loading scenarios. This can also be used as a predictor for future loading scenarios and for this instance,

future welds to be completed under similar conditions. A typical stress-strain curve is depicted in Figure 2.4.1 and shows the various regions of interest.

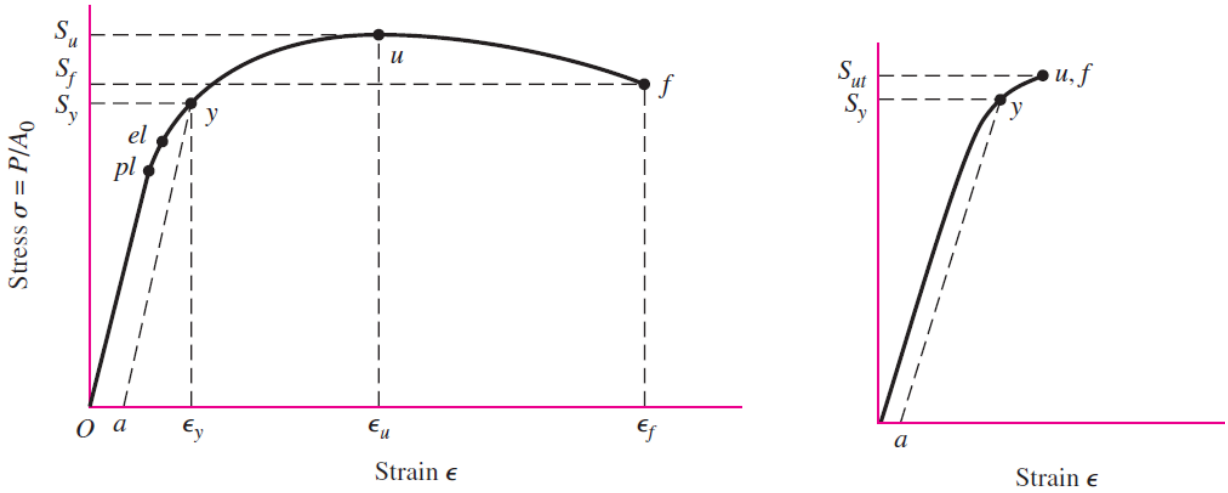

Figure 2.4.1: Typical Stress-Strain Curve [15]

In the figure above, the graph on the left shows a typical stress-strain relation for a ductile material, while the graph on the right side shows a graph for a typical brittle material. There are several points of interest in the above stress-strain curves. The *pl* is the proportional limit which is the maximum stress for which the linear relationship is valid. The *el* is marked as the elastic limit. This is the region in which any applied deformations will yield back to the original condition and not result in any permanent deformations. After the elastic region, any the recovery of the material will be parallel to the straight line of the curve and will result in permanent deformation. This is known as the plastic region. The yield point, *y*, is very close to the elastic point, and is often considered where the plastic region begins. The ultimate strength is marked by *u* and is the maximum stress a material can support without fracture. The last point of interest is the fracture strength, labeled as *f*, in where the material actually fails. For ductile materials, the fracture strength is actually less than the ultimate strength, this is because the material will neck down much more than that of a brittle material that accompanies high plastic strains. As the cross-

sectional area of the material will neck down, less applied load is required to pull the tensile specimen at the designated rate **[16] [17]**.

Engineering stress is one method of analyzing the stress-strain curve and for most purposes, is a good approximation of the true stress. This is completed by calculating the stress per area using the original unloaded tensile dimensions. When a material specimen undergoes loading, the cross-sectional area will reduce under the applied load. The true stress will involve calculating the stress with the continuous reductions in area. This is more instrument intensive as more data will have to be collected. The stress and strain calculated in this report will be the engineering stress/strain.

Materials can be categorized into different groups based on the mechanical property: Ultimate Strength, Yield Strength & Modulus of Elasticity. A *strong* material has a high ultimate strength, whereas a *weak* material will have a low ultimate strength. A *tough* material will yield greatly before fracturing, also known as a ductile material. A brittle material will yield very little before fracture. When examining the Modulus of Elasticity, a *hard* material will have a high Modulus of Elasticity versus a *soft* material, which will have a low modulus of material. All of these groups are not inherently good or bad, but is dependent on the application of the material **[16]**. Combinations of these material types can be represented in Figure 2.5.2 by the below stress-strain curves.

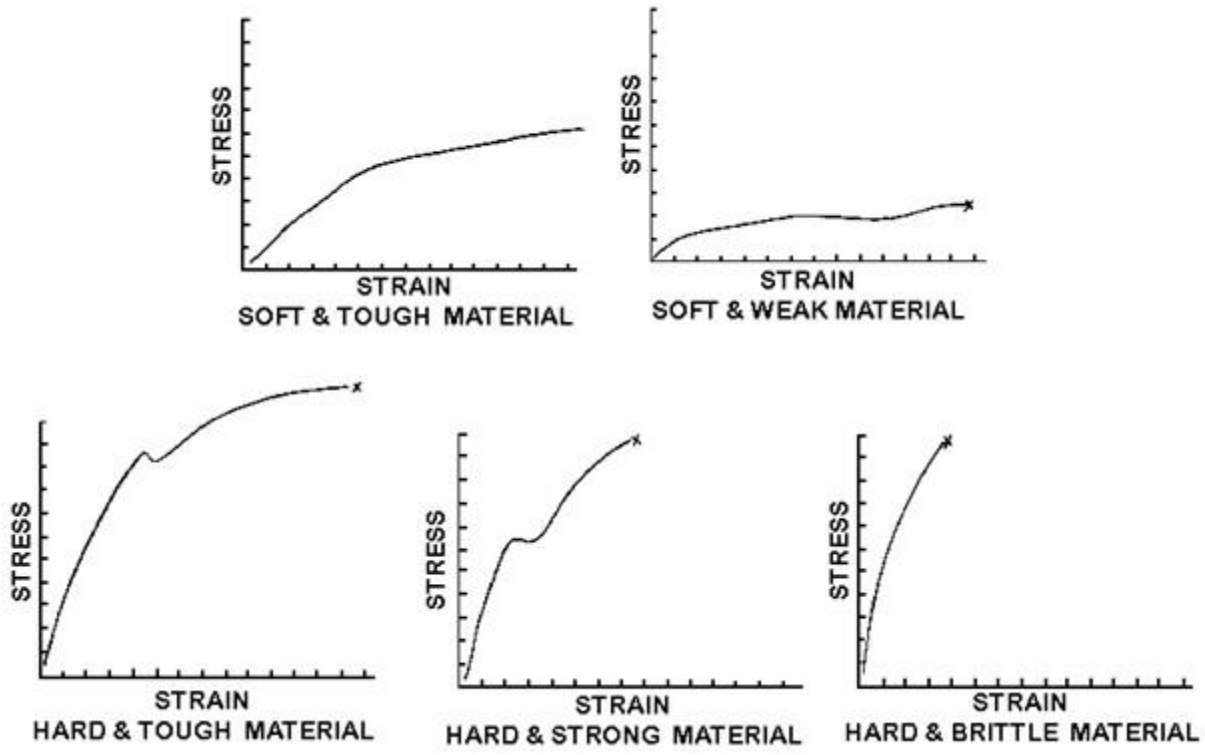

Figure 2.4.2: Stress-Strain Curves for Various Material Types [18]

The categories listed above can be visually seen from the above graphs. More ductile materials are tough as opposed to brittle, while strong materials will have a much higher slope in the elastic region than weak materials, which can as high as 45°.

Another means of determining how brittle versus ductile the material is to examine the fracture type post tensile testing. Figure 2.4.2 shows the possible outcomes of a tensile test for different types of materials.

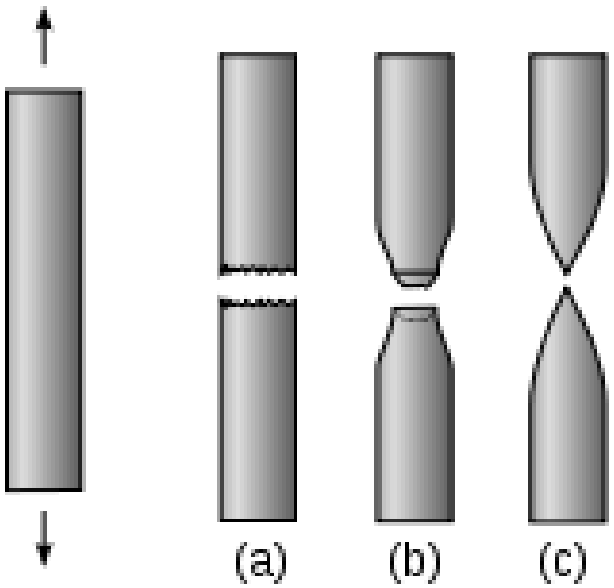

Figure 2.4.2: Fracture Types for Tensile Testing [19]

The materials can then be classified as brittle materials (a), Semi-ductile materials (b), or ductile materials (c). The semi-ductile materials are typical for metals, which is what should be expected for the results of this study.

2.5 Hardness

Hardness is the measure of a material's resistance to deformation by surface indentation or by abrasion **[13]**. Hardness testing is a simple and inexpensive method for determining the mechanical properties of a material. One method of measuring the hardness of the material is through the Vickers Hardness test. This is completed through the means of a diamond shaped tool, that is pressed against the surface of the material, creating an indentation. Hardness testing is completed by having a diamond indented into the specimen. A smooth, firmly supported flat surface is required, in which the load is normally applied for 30 seconds **[20]**. Typical loads for these types of testing can range from 1 and 1000 grams **[13]**. The hardness of the material is then related to the indention load, and the diagonal length of the diamond, which can be seen mathematically in Eq 2.5.1 **[21]**. A correction constant is usually applied after dependent on the

method of hardness testing. To acquire these diagonal lengths, an optical microscopy must be utilized.

$$HV \propto \frac{F}{d^2} \qquad \textbf{Eq. 2.5.1}$$

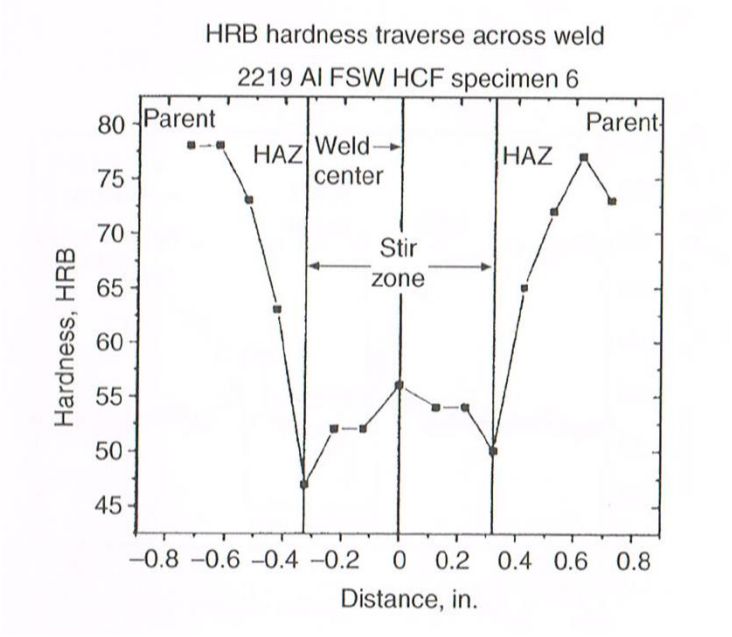

Figure 2.5.1: Typical Hardness Across Friction Stir Weld [7]

When examining typical mechanical properties of 2000 series aluminum alloys post friction stir welding, it can be seen that the hardness per distance from the center follows a "W" pattern. This means that the nugget is not the softest location on a friction stir weld. The TMAZ/HAZ interference will have the lowest hardness, which is seen in the above figure at the sharp downturns from the Parent material through the HAZ. This is due to the dissolution and growth of the precipitates, which will in turn reduce the joint efficiency **[22]**. This is important to know as the material will fail at the weakest point, which is not the nugget itself, in which it will often fail on the side of the weaker material.

2.6 Tool Geometry

There are three different types of pin tool orientations that can be utilized for friction stir welding. There are fixed pin, self-reacting pin, and adjustable pin. The welding done in this experiment utilizes a self-reacting pin tool. A self-reacting pin tool is one in where no anvil is present. This is practical as an anvil is not always available on welding certain structures. A self-reacting pin tool consists of the normal shoulder and pin tool, but in addition to this, a bottom shoulder is attached. The bottom shoulder is placed underneath the work piece in where the anvil would normally be placed. This is completed by having the welding machine pull the bottom shoulder up against the work piece while the top shoulder normally presses down against the work piece. Both shoulders having the same pressing force against the workpiece as to not cause any vertical deformation. This method will result in the total net force on the work piece to be zero **[23]**.

An important aspect of pin tool selection to note would be that of the pin thread orientation. Most standard pin tools have either a left-hand or right-hand thread orientation. These can be seen in the two following figures.

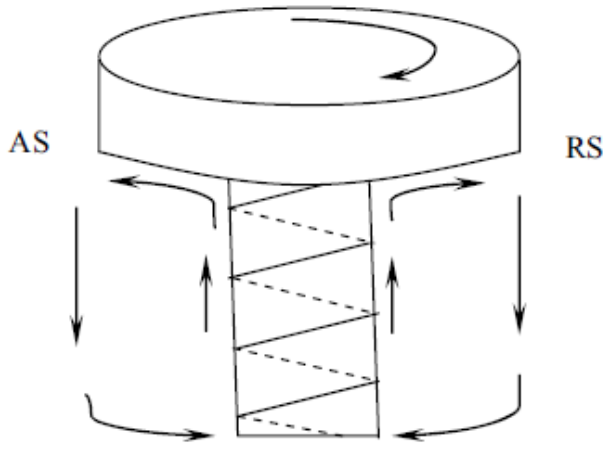

Figure 2.6.1: Material Flow of a Right-Hand Thread Pin Tool [24]

The above figure is a pin tool with a right-hand thread orientation. This is because the threads follow the right-hand grip orientation. It can be seen from the above that a weld that is completed using a right-hand threaded pin tool, in the clockwise direction, the material will flow up towards the top shoulder.

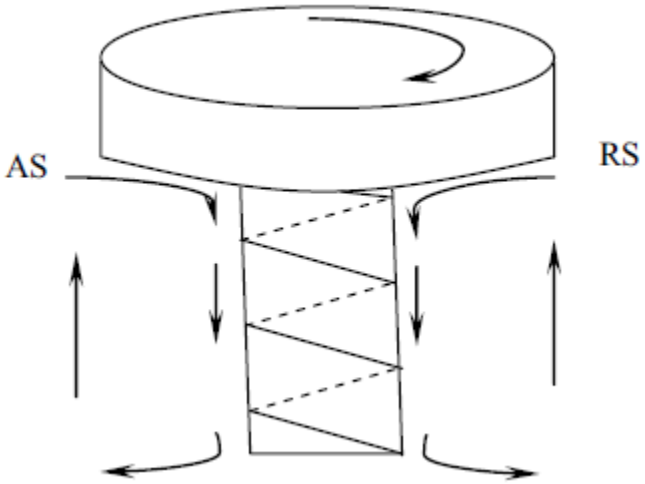

Figure 2.6.2: Material Flow of a Left-Hand Thread Pin Tool [24]

The above figure is a pin tool with a left-hand thread orientation. This is because the threads are opposite to that of the right-hand grip orientation. It can be seen from the above that a weld that is completed using a left-hand threaded pin tool, in the clockwise direction, the material will flow down towards the bottom anvil, and in the case of self-reacting pin tool, the bottom shoulder.

The pin tool that was used for this experiment was a 3/8" pin tool with a Left-Hand Right-Hand thread orientation. The total thread length was 7/16", which provides plenty of clearance for the .36" thickness of the workpiece. The welds were completed in a clockwise manner. This orientation can be expressed visually in the Figure 2.7.3. It is noted that the shoulders are not visually present in the figure for ease of viewing.

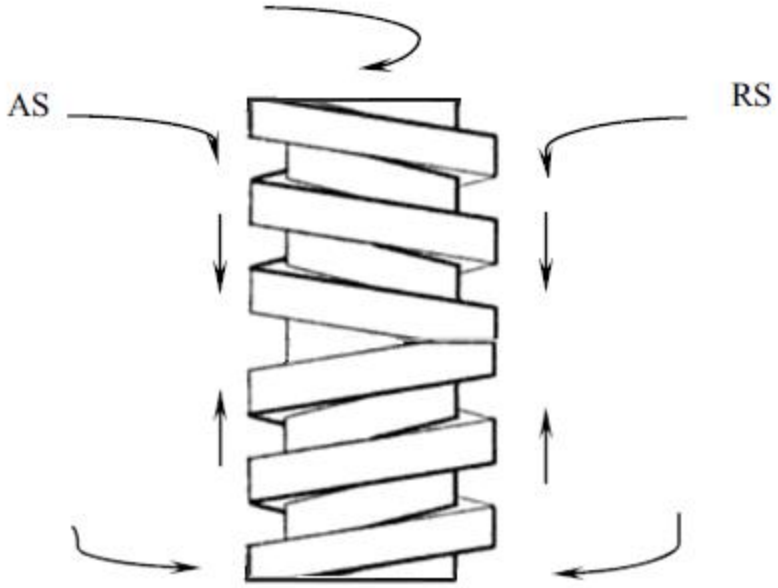

Figure 2.6.3: Left-Hand (Top) Right-Hand (Bottom) Threads Together

Examining the properties of material flow for each of the thread orientations, and then combining them, it can be realized that the material for a Left-hand Right-hand pin tool used in a clockwise manner will force the material to flow towards the center of the work piece.

It is also noted that having a pin tool with either a Left-Hand only thread orientation, or Right-Hand only thread orientation that pushes the material in one direction will cause material to flow towards one of the shoulders. This will cause the material to stick to either the top or bottom shoulder, which will cause a lack of plasticized material for the remaining areas **[25]**. This will cause an increase in the possibility of a weld to form porosity or lack-of bonding defects **[26]**. This is because there will not be enough material for uniform mixing to occur in the weld which will increase the probability of defects to form. In order to counter the material from flowing into one of the shoulders in a self-reacting weld, a left-hand right-hand pin tool should be used in a manner that causes the material to flow towards the center, as opposed to outwards towards both shoulders.

2.7 Design of Experiments

Design of Experiments (DOE) is a statistical approach of experimental design where several variables will need to be altered over the course of the experiment. DOE was originally invented by Ronald Fisher **[27]**. One of the main advantages of using a DOE approach as opposed to a trial-and-error manner is that a range of process variables can be systematically tested in an organized and much more efficient manner.

DOE consists of varying a set number of variables over a range of predetermined values. This allows for the widest range and encompassing approach to an experiment but it can make the experiment a lengthy process depending on the number of variables that are required. Design of Experiments is defined by what is called the factorial. The number of variables and range can be express in the equation below **[28] [29]**.

$$Experiment\ Runs = Level\ per\ Variables^{Number\ of\ Variables} \qquad \textbf{Eq. 2.7.1}$$

Each variable will have different individual values, or levels, that it will be cycled through. This is dependent on the process variables and the range that they will be varied through. Looking at how friction stir welding has three primary process variables, forge force, travel speed and spindle RPM, it can be deduced that a full three factorial DOE should be used for an experiment of this magnitude. An example of a three-factorial approach in where an experiment would have three variables with three different levels per variable is tabulated in Table 2.7.1. This would result in a total of 27 different runs in the experiment.

Table 2.7.1

3^3 Factorial Approach

Trial	Variable A	Variable B	Variable C	Trial	Variable A	Variable B	Variable C
1	-1	-1	-1	15	0	0	1
2	-1	-1	0	16	0	1	-1
3	-1	-1	1	17	0	1	0
4	-1	0	-1	18	0	1	1
5	-1	0	0	19	1	-1	-1
6	-1	0	1	20	1	-1	0
7	-1	1	-1	21	1	-1	1
8	-1	1	0	22	1	0	-1
9	-1	1	1	23	1	0	0
10	0	-1	-1	24	1	0	1
11	0	-1	0	25	1	1	-1
12	0	-1	1	26	1	1	0
13	0	0	-1	27	1	1	1
14	0	0	0				

Due to the lengthy process required by a full three factorial approach and the large number of weldable panels required, a modified three factorial approach was used, in where one variable of the three variables was held constant, the second variable only had two process levels and the third was fully varied through three separate levels. An example of this can be seen below in Table 2.7.2 in where this would be deemed a 1^1 2^1 3^1 Factorial Approach. Using Eq 2.7.1 to multiply the total number would result in a total 6 experimental runs.

Table 2.7.2
$1^1 2^1 3^1$ Factorial Approach

Trial	Variable A	Variable B	Variable C
1	1	-1	-1
2	1	-1	0
3	1	-1	1
4	1	0	-1
5	1	0	0
6	1	0	1

Once the experiments are run, the finished data can be input into a linear regression analysis. A regression analysis is a statistical technique for investigation and modeling the relationship between variables and explain any possible relationships between them **[30]**. The goal of the linear regression model is to determine the relationship between the dependent variables and the independent variables expressed in the Eq 2.7.2

$$Y = a + b_1 X_1 + b_2 X_2 + \ldots + b_k X_k + e \qquad \textbf{Eq. 2.7.2}$$

This equation can be used for several variables, but for this experiment a two-variable case will be utilized. For the two-variable case, in where the travel speed and Force/RPM will be analyzed, the slopes of each dependent variable can be solved for in the below equations:

$$b_1 = \frac{(\sum x_2^2)(\sum x_1 y) - (\sum x_1 x_2)(\sum x_2 y)}{(\sum x_1^2)(\sum x_2^2) - (\sum x_1 x_2)^2}$$

$$b_2 = \frac{(\sum x_1^2)(\sum x_2 y) - (\sum x_1 x_2)(\sum x_1 y)}{(\sum x_1^2)(\sum x_2^2) - (\sum x_1 x_2)^2} \qquad \textbf{Eq. 2.7.3}$$

The above two equations require further manipulation of the data by solving for the product of squares which can be done using the next equations.

$$\sum x_1 y = \sum X_1 Y - \frac{(\sum X_1)(\sum Y)}{N}$$
$$\sum x_2 y = \sum X_2 Y - \frac{(\sum X_2)(\sum Y)}{N} \qquad \textbf{Eq. 2.7.4}$$
$$\sum x_1 x_2 = \sum X_1 X_2 - \frac{(\sum X_1)(\sum X_2)}{N}$$

The only remaining variable which is needed to model the regression line will be the intercept, which can be solved by inputting all known quantities into Eq. 2.7.2 and solving for the last remaining variable **[31]**. From there the values of the actual dependent variables versus the predicted dependent variable can be plotted together to determine the accuracy of the linear regression line. When these values are plotted together, the residual will become apparent. The residual is known as the difference between the predicted value and actual value. Looking at Figure 2.7.1, the actual value would be the black dots and the predicted value is the straight line between them calculated using the regression model. The vertical lines connecting the two objects is the residual amount **[32]**.

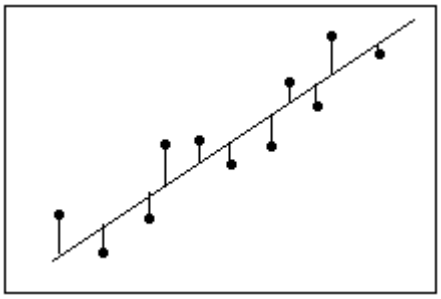

Figure 2.7.1: Graphical Representation of Residual

The accuracy of the regression line can be expressed using the R^2 value of the computed data. The R^2 value is a number that is always ranges from 0 to 1, or 0% to 100%. The R^2 is also a good indicator of the total residual for the linear regression model. The coefficient of determination can

then be calculated based on the following equation or computationally through readily available programs like Microsoft Excel **[33]**.

$$R^2 = 1 - \frac{SS_{res}}{SS_{tot}} \qquad \textbf{Eq. 2.7.5}$$

Once an actual value for R^2 is defined, the fit of the linear regression model can then be determined. A low value indicates that the linear regression model is not a good predictor of the data points, while a number closer to 1 indicates that it will. Figure 2.7.2 below shows a linear regression model for a set of data points with an R^2 value closer to 1. This is because the linear regression model does not miss many of the data points by a significant amount and is a good predictive model for a trend.

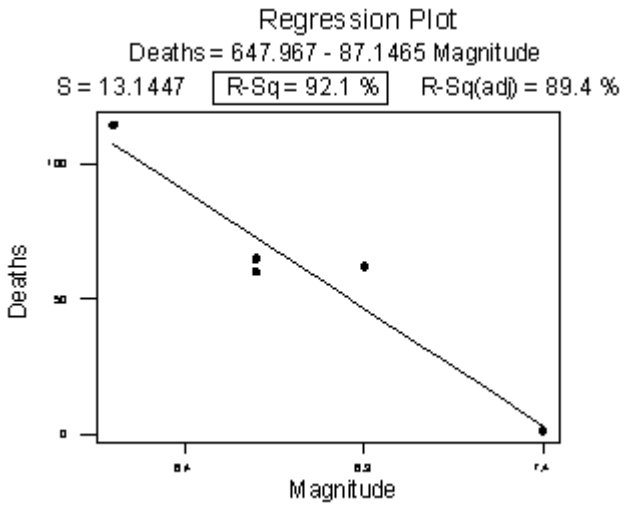

Figure 2.7.2: Example Linear Regression Model with High R^2 Value [34]

Once the final values of the regression model the error can be quantified by the Eq. 2.7.6 labeled below.

$$\textbf{\textit{Error}}\ (\%) = \frac{|\textbf{\textit{Measured Value} - \textbf{\textit{Predicted Value}}|}}{\textbf{\textit{Measured Value}}}\ \boldsymbol{x}\ \mathbf{100} \qquad \textbf{Eq. 2.7.6}$$

Chapter 3: Research Conducted

3.1 Welding & Machining

The researched that was completed consisted of determining of weld parameters, welding the test panels together, tensile testing, macrograph analysis and micro-hardness testing.

The first step in the research was to determine the welding parameters. It was decided to vary the travel speed as a pin tool previously broke when a forge force of 4000 lbf was applied. With respect to the integrity of the equipment, a more conservative weld scheme was selected due to limited supplies. The final weld parameters were chosen based off of the previous research conducted by the undergraduate Friction Stir Welding class final projects. The original scope of their research project did not include variable insensitivity.

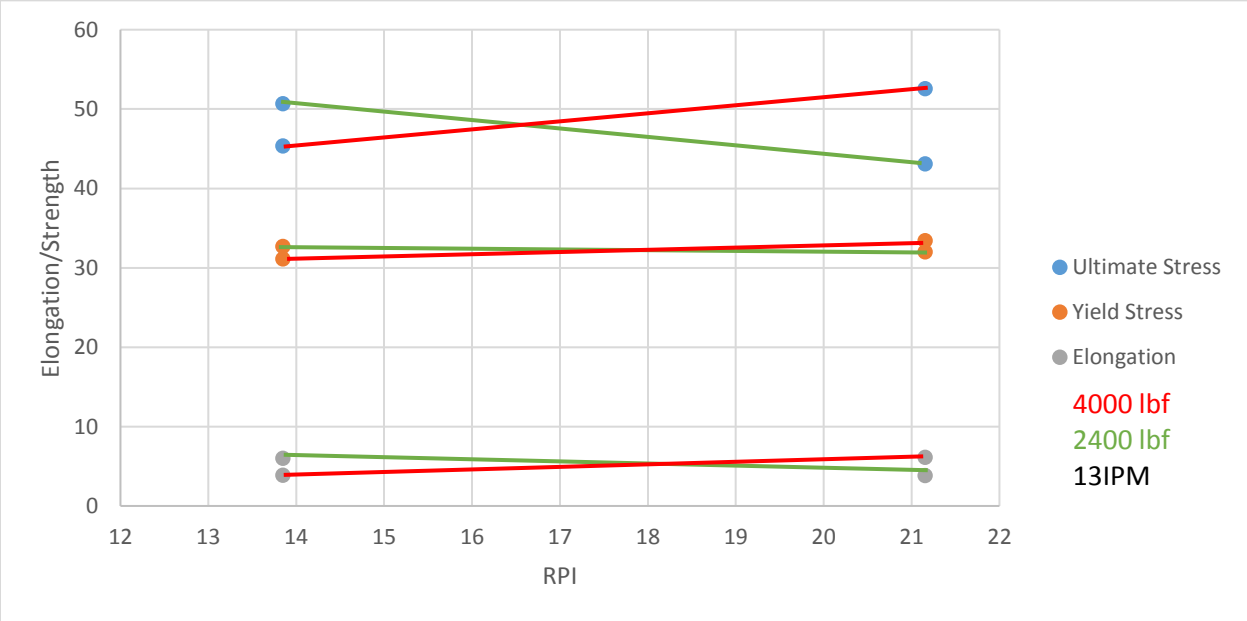

Figure 3.1.1: Previous Nominal Dataset [35]

Figure 3.1.1. above is important as it shows the forge force variable insensitivity of the previous nominal dataset. The importance of this graph shows that a certain combination of welding parameters will have mechanical properties independent of forge force. The bow-tie affect that is

desired is clearly on display and it is one of the goals of this manuscript to recreate this affect by varying different welding parameters. This provided a prediction to create welding parameters that can be seen in Table 3.1.1 that would result in the desired output instead of trial and error. This dataset varies the forge force similar to the original experiment discussed in Chapter 1.

It can be seen that a Rotation per Inch (RPI) range of 14 to 21 can be used to recreate the desired bow-tie effect. With this knowledge in hand, similar process variables were developed based off of this fact. For this experiment, the RPI was chosen to be in the range of 13 to 25 to encompass a larger range as it was noted that the bow-tie effect would diminish under lower travel speeds, but this data was inferred from a smaller data range. A middle point between the two extremes was selected to see if the insensitive point could be recreated. The complete results in this experiment will be displayed with respect to Force/RPM instead of RPM/IPM since the travel speed was varied instead of the forge force.

Table 3.1.1
Welding Parameters Used in the Experiment

Weld	Forge Force	IPM	RPM	Force/RPM
W1	2400	13	180	13.33
W2	2400	13	215	11.16
W3	2400	13	275	8.72
W4	2400	11	180	13.33
W5	2400	11	215	11.16
W6	2400	11	275	8.72

The advancing side was Aluminum 2195 with a gauge thickness of .35”, while the retreating side was Aluminum 2219 with a thickness of .36”. As to why the weld panels did not possess the same thickness, the weld panels were chosen amongst readily available materials. Each weld panel is 24” long, with a width of 4”. There was a total of 12 weld panels used in the course of this experiment, 6 Aluminum 2195 panels and 6 Aluminum 2219 panels.

Each weld was completed at NASA Michoud Assembly Facility using the ISTIR PDS, seen in Figure 3.1.2. This equipment is owned by the National Center of Advanced Manufacturing (NCAM), and is able to be used by college students of state owned Louisiana colleges. This machine possesses customizable tool heads, allowing it to also be the same machine that the specimens were fly cut on.

Figure 3.1.2: ISTIR PDS

Each weld had a start hole drilled to allow for the self-reacting pin tool to be put into place. This means that the pin tool does not plunge into the material like that of a fixed pin or retractable pin. The welds were then clamped down, as shown below, as to prevent any displacement of the plate itself. This was completed using side 8 side clamps, 4 per side, resting along a clamp bars. This is to distribute the clamp force evenly along the length of the weld, and to prevent each side clamp from digging into the weld panels. If the weld panels did not have a distributed clamp force, this

would cause localized bending stresses along the weld panel and this could compromise the integrity of the weld.

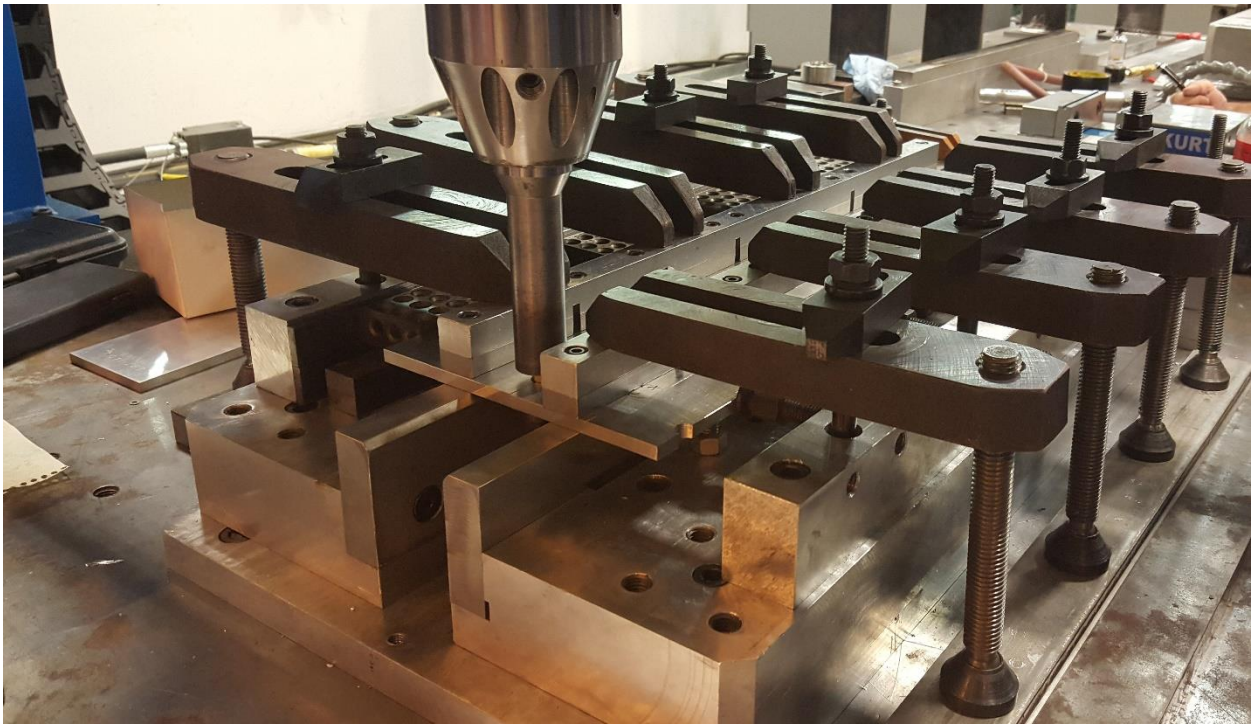

Figure 3.1.3: Typical Set-up for each Weld

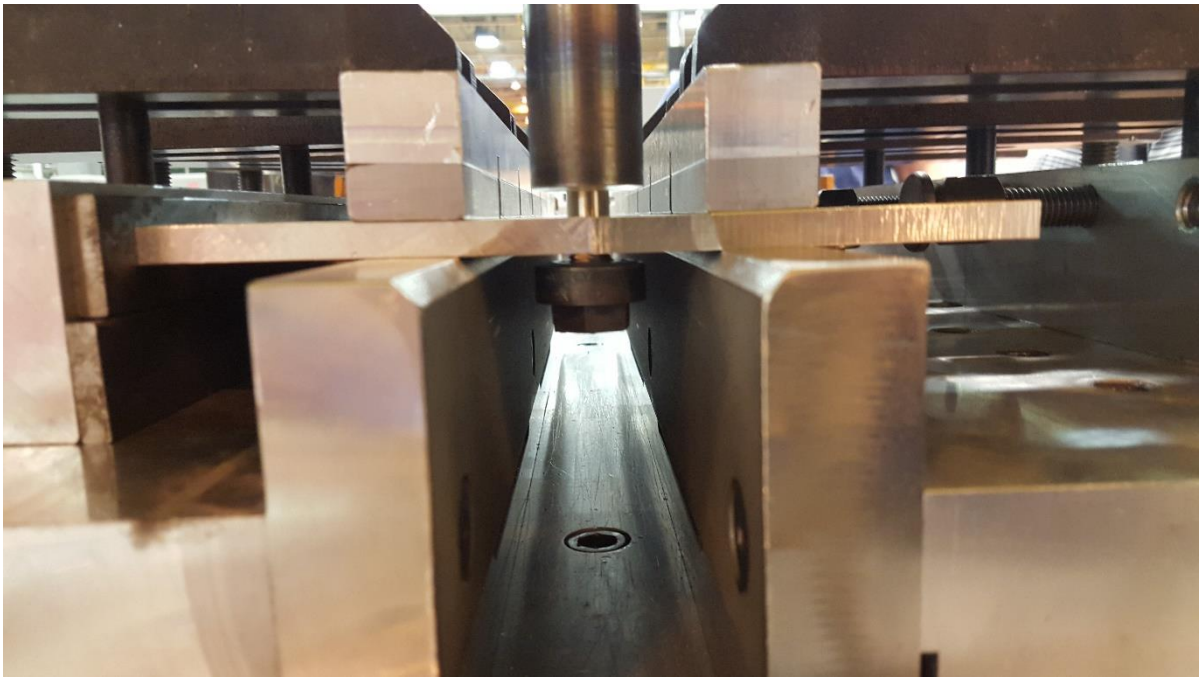

Figure 3.1.4: Typical Set-up for each Weld

The welds are completed by the ISTIR PDS with a preset program. These programs tell the machine where to start and finish the weld, how fast each part spins or moves, and how long of a warm up period is required to create a good weld.

Once the welds are completed using the above methods, they were then removed from the clamping apparatus and then taken to have the scroll lines removed. These scroll lines need to be removed as to prevent stress concentrations during tensile testing. They were removed using a medium grit 3M™ Scotch-Brite™ Roloc™ Surface Conditioning Disc. Both sides of the welded panel had any scroll lines removed down to a smooth surface, but not so much removed as to where the disc would dig into weld causing unwanted low points. The pin tool and shoulder were then subsequently cooled between each weld to prevent residual heat from being transferred to the next weld.

Figure 3.1.5: Completed Weld with Scroll Lines Still Present

After the scroll lines were removed, the welded panel was then separated into nine individual specimens by use of a band saw. Six were to be used as tensile specimens, while the remaining three were to be used for macrographs and hardness testing. The locations of each of the tensiles and macros in this experiment are labelled in Figure 3.1.6. Each cut is 1.2" wide with pre-measured spacing in between each specimen resulting in a total of nine specimens. This was completed for each weld resulting in a total of 36 tensile specimens and 18 macrograph/hardness specimens. Due to the inaccuracy of the band saw and human error present along the seams of the cut, the specimens then had to be further machined down to a uniform width across each specimen.

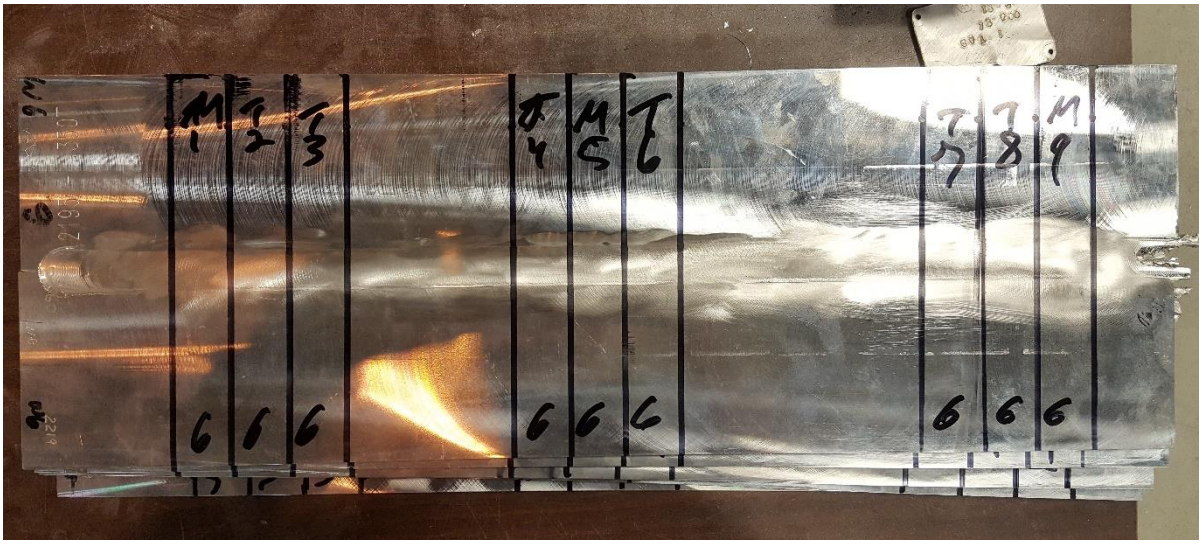

Figure 3.1.6: Tensile and Macrograph Locations

As mentioned before, the ISTIR PDS has interchangeable tools that allowed for the fly cutting to occur. Figure 3.1.7 dictates an image of the process, in where the fly cutter was spun at a preset speed of 1300 RPM, in where the tool was then passed across the specimens removing at a maximum of .020" of the thickness each time. This process was repeated until the side being worked on had a smooth finish. This was then repeated on the other side of the specimens until a smooth side was present. This resulted in the specimens for that particular weld to have a uniform width. The nine specimens for each weld were completed individual to the other welds, this was

to ensure that the tensile specimens for one weld all had the same dimensions. It was noted by clamping the specimens together that any scribe marks that were placed on the sides of a specimen were imprinted on the adjacent specimen. These had to removed post fly-cutting by use of the Scotch Brite pads.

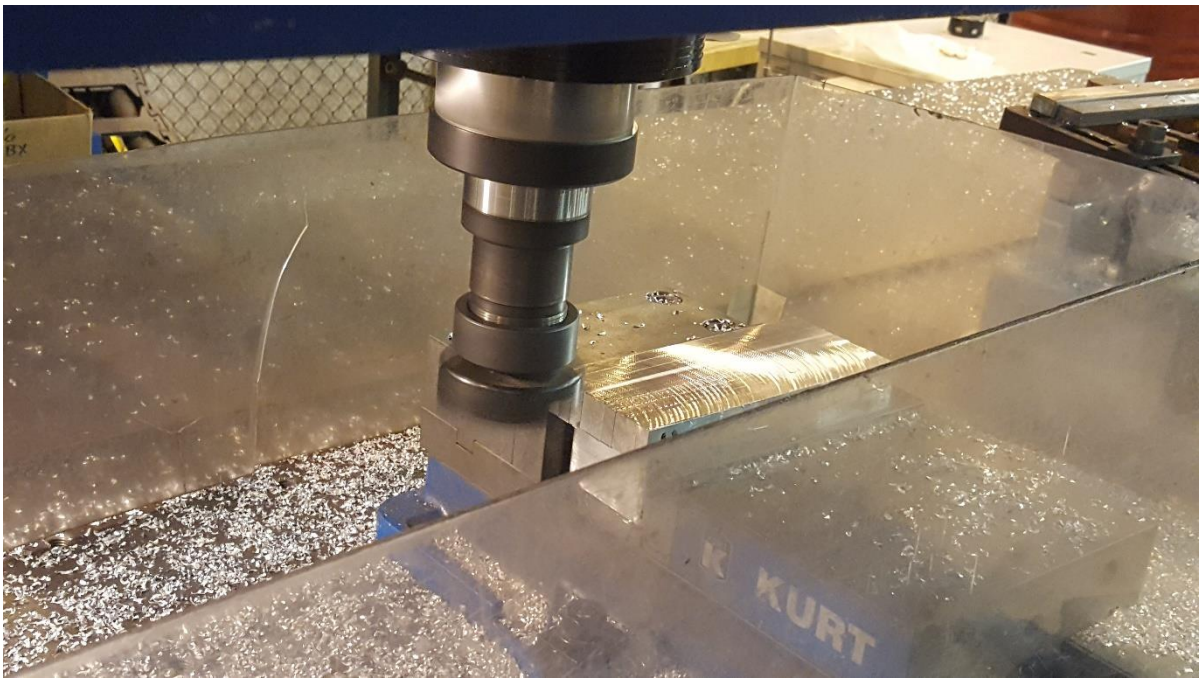

Figure 3.1.7: Machining Tensiles to Uniform Width

3.2 Tensile Testing

Once the tensile specimens were machined down to uniform widths, they then underwent tensile testing. The gauge length of 4" was used for the tensile testing. This was to have a wider area to allow for necking. If a shorter gauge length was used, this would allow the possibility of the specimen necking outside of the predetermined area. The exact measurement that was used for the gauge length was 3.94".

The tensile tests were completed on an MTS 810 material testing machine. This is completed by inputting a feed rate and then the machine will determine and output the force necessary to keep a constant feed rate. As the material begins to neck down, the output force required to keep a

constant feed rate will lower as the cross-sectional area reduces. This will explain why the fracture stress is lower than the ultimate stress for more ductile materials.

Figure 3.2.1 shows a tensile test post fracture. The larger of the two load cells was used (55 kip vs 22 kip). The 55 kip load cell was used because previously the 22 kip load cell was almost at full capacity at breaking .320" thick specimens. The specimens in this experiment were larger, and a more conservative approach was taken with regards to maximum force output.

The MTS 810 outputs all data points recorded during the testing period on an excel spreadsheet. Each tensile has its own unique spreadsheet with the data recorded. The data points collected are the displacement, the force and if an extensometer is utilized, the deformation can also be recorded. The elongation was then calculated by the displacement recorded from determining the spring constant of the machine itself.

Figure 3.2.1: Tensile Testing of Specimens

After each tensile was broken, the specimen was then removed and the final elongation was recorded. This was completed by pressing the specimen back together and recording the distance between the grip marks on the specimen. This number was then used with the original 3.94" gauge length to calculate the final elongation of the specimen.

3.3 Polishing & Macrographs

When examining Figure 3.1.6, the specimens that are labelled M1, M5, and M9 are to be used for polishing and further macrograph analysis. For each weld, three areas were collected and analyzed. This was the beginning of the weld, the center and the end of the weld. These three zones will show the effects the weld has on the microstructure as it progresses through. This resulted in a total of 18 separate macrographs which will then be later hardness tested.

The first part of process was to cut the tensile so that only 1.2" would be present centered through the weld seam so that it may be mounted. This would allow all heat affected zones to be present as a Macrograph and including some parent material for comparison. Once this was done, the samples were then placed in a CitoPress to be mounted.

Figure 3.3.1: CitoPress [37]

This was done by first applying anti-stick cream to the inner area and then placing the specimen inside. 50 mL of MultiFast red was then placed on top to cover the specimen. The sample was then subjected to high temperature and pressure cycle to solidify the resin. Each sample was run at 200 bars for a 2-minute heating period at 180 °C and then cooled for 1.5 minutes.

Once all specimens were fully mounted, they were then placed in a TegraMin to have semi-automated specimen preparation completed, seen in Figure 3.3.2. The grinding and polishing of the specimens to a finished product was completed in a process with a total of eight steps.

Figure 3.3.2: TegraMin [38]

This first step in this process is to rough grind the specimen. This was completed by mounting the specimens on a rotating head that spins at 150 RPM at 25N, with a 220-grit abrasive pad rotating in the opposite direction at 300 RPM. This step was run for a total of 1:10 minutes. In all subsequent steps the specimen holder is run at these conditions, with varying input forces, and the pad is co-rotated.

The second step was to fine grind the specimen using the same setpoints as step 1, but instead use a 500-grit abrasive pad. This step was run for a total of 4 minutes.

The third step utilized a Largo Disc, which is a composite disc for fine grinding, that was rotated at 150 RPM and had a 20 N force applied for a 5-minute duration.

The fourth step utilized a Mol Disc, which is a woven wool disc for fine grinding, that was rotated at 150 RPM and had a 20 N force applied for a 6-minute duration with the specimen rotating at the predetermined setpoints.

The fifth step is the first of the polishing steps and uses a Mol cloth polishing disc and run under the same conditions as Step 4.

The sixth step, fine polishing, has a Dur polishing cloth being used, which has typical uses for fine grinding of metals. The force was lowered to 15 N and the duration was increased to 7 minutes.

The seventh step, extra fine polishing, utilized a Plus polishing cloth disc, where the force was lowered even more to 10 N and the duration was further increased to 10 minutes.

The eighth step utilized a Struers Chem polishing pad with agglomerated alumina lubricant for a twenty-minute duration at 10 Newtons force while the polishing pad was rotated at 80RPM co-directionally with the specimen holder as it rotated 150 RPM. Lastly, oxidative polishing utilized a separate Chem pad and etchant which entailed concentrated hydrogen peroxide to enhance etching properties. The oxidative polishing step lasted a 30:00-minute duration at 10 Newtons force while the chem pad was rotated 70 RPM counter rotationally as the specimen holder, which was also rotated at 150 RPM.[1]

Once completed the polished and mounted specimens had a 9% hydrogen peroxide solution applied via the Chem disc used in step 8 for 20 minutes, and after this final step, macrographs were then taken of each sample.

3.4 Hardness Testing

The specimens that were ground and polished for macrographs then had micro-hardness testing completed. Micro-hardness is completed by indenting a diamond shaped indenter with a constant size and force into the surface of the material. The test was performed using the Vickers pyramidal

[1] The process for grinding and polishing the specimens was developed by the University of New Orleans Metallography Research Laboratory. Micro-hardness testing was subsequently completed by the same group.

indenter at a force of 50 kg. Hardness testing requires bringing the specimen to a mirror-fine polish. The specimen surface must be completely smooth and free of deformities as any deformities would result in inaccurate readings. The hardness tester used for this experiment is the Shimadzu hardness tester.

Figure 3.4.1: Shimadzu Hardness Tester [39]

Chapter 4: Results

The first process in examining the welds will be to look at the physical aspects of the welds themselves post welding, post tensile breaking and macrographs. Figure 4.1 shows the tensile specimens of Weld 1 after they were broken. The advancing side is on the left, while the retreating side is on the right. The tensiles in the figure are laid in an increasing order with Tensile #2 at the top, and Tensile #8 at the bottom. Looking at the cracks, the beginning of the weld was more likely to break on the advancing side, but along the length of the weld, the crack size and location begins to change. The cracks become more jagged and begin to break along the center of the weld nugget instead of the TMAZ. This could mean that a proper material mixing was not achieved along the weld seam over the length of the weld. Examining the fracture break direction, tensiles 7 and 8 are much different than the previous four tensiles. The break type is more in line with a brittle material as opposed to a ductile material due to the rough jagged edges. It can also be seen that on tensile 7, there is a hairline crack normal to the applied force during the testing.

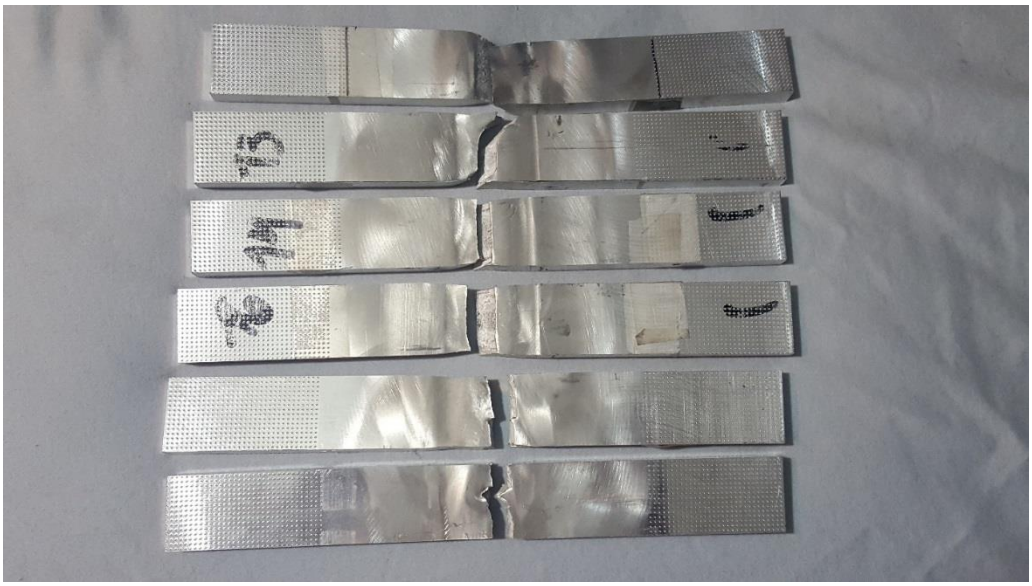

Figure 4.1: Weld #1 Post Tensile Break

Figure 4.2 shows the tensile specimens of Weld 2 after they were broken. The advancing side is on the left, while the retreating side is on the right. The tensiles in the figure are laid in an increasing order with Tensile #2 at the top, and Tensile #8 at the bottom. Weld 2 shows an increase in consistent ductility over Weld 1. This can be seen as fractures are cleaner and slight necking is noticed along the edges. The tensiles are not jagged which is normally seen on brittle material fractures. The tensiles also consistently broke near the retreating side of the TMAZ. The fracture type throughout the six tensiles was largely consistent with very little variance in fracture angle and type. Each tensile broke at a roughly 45° angle and did not show any signs of rough jagged edges.

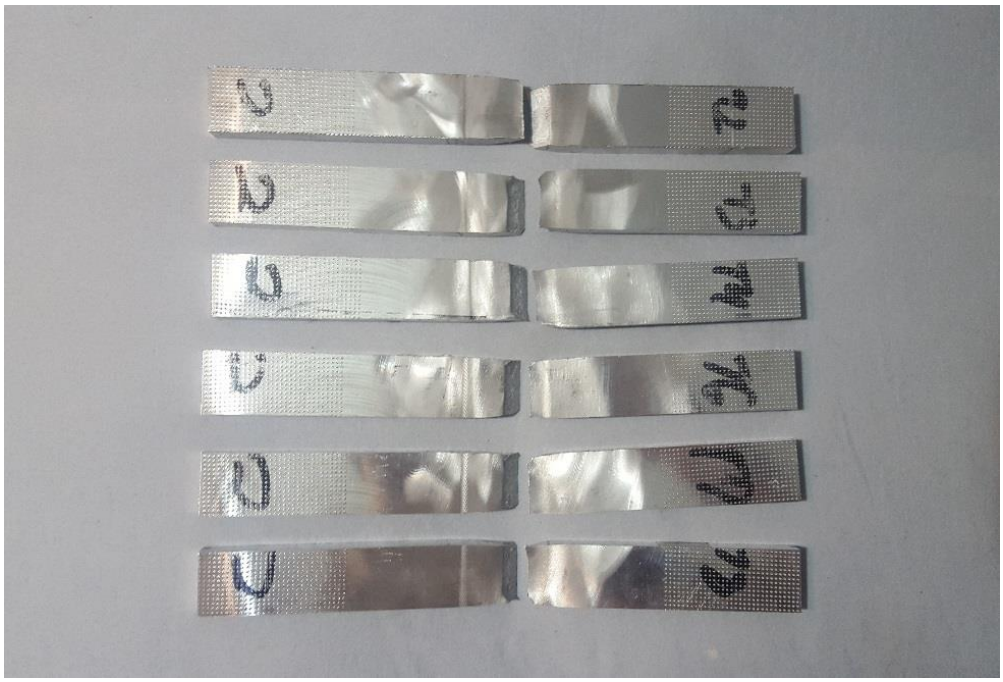

Figure 4.2: Weld #2 Post Tensile Break

Figure 4.3 shows the tensile specimens of Weld 3 after they were broken. The advancing side is on the left, while the retreating side is on the right. The tensiles in the figure are laid in an increasing order with Tensile #2 at the top, and Tensile #8 at the bottom. The welds are displaying

a decrease in ductility from weld 2 as the breaks are no longer a ta 45° plane. The fracture was found to be close to the TMAZ on the advancing side of the weld which is counterintuitive as the metal on the advancing side has higher mechanical properties, making it the stronger side.

Figure 4.3: Weld #3 Post Tensile Break

Figure 4.4 shows the tensile specimens of Weld 4 after they were broken. The advancing side is on the left, while the retreating side is on the right. The tensiles in the figure are laid in an increasing order with Tensile #2 at the top, and Tensile #8 at the bottom. Weld 4 had similar input parameters as Weld 1 and when comparing the two, they are similar in terms of how the tensiles are experiencing brittle fractures. The last tensile does experience a slight change in the fracture type as it becomes more brittle then the previous 5 tensiles. This indicates, like weld 2, that improper mixing must be occurring at the later stages of the weld causing a drop in ductility. The tensiles also had a tendency to break towards the advancing side along what appears to be the TMAZ.

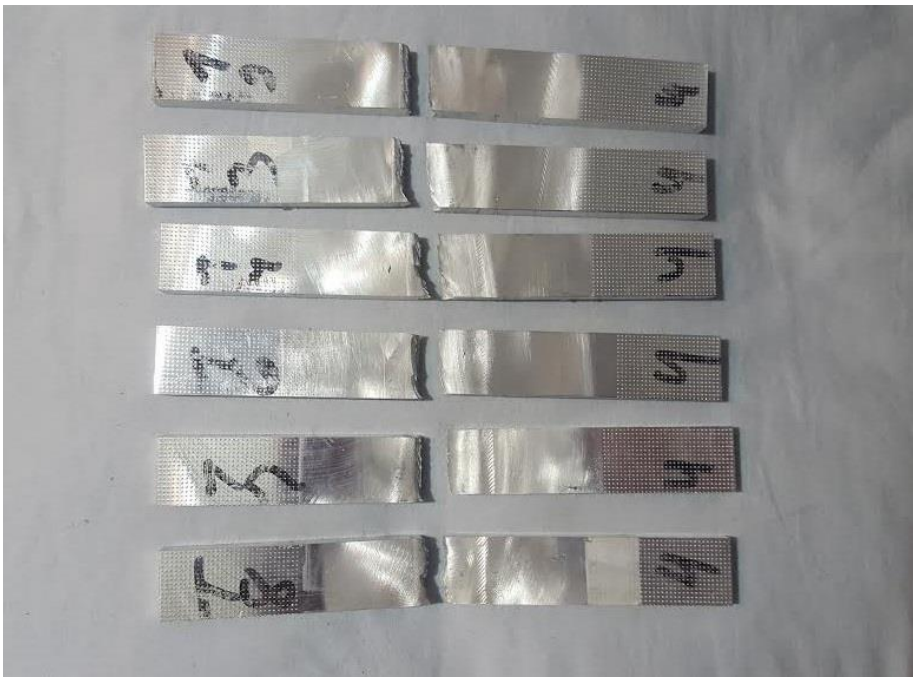

Figure 4.4: Weld #4 Post Tensile Break

Figure 4.5 shows the tensile specimens of Weld 5 after they were broken. The advancing side is on the left, while the retreating side is on the right. The tensiles in the figure are laid in an increasing order with Tensile #2 at the top, and Tensile #8 at the bottom. When comparing to the previous welds, the input parameters are closest to that of weld 2. The fractures do indicate a decrease in ductility as the lack of a noticeable necking region along with the more jagged edges. The fractures were close to the advancing side along the weld nugget which is opposite to that of weld 2, in where the retreating side contained the fracture.

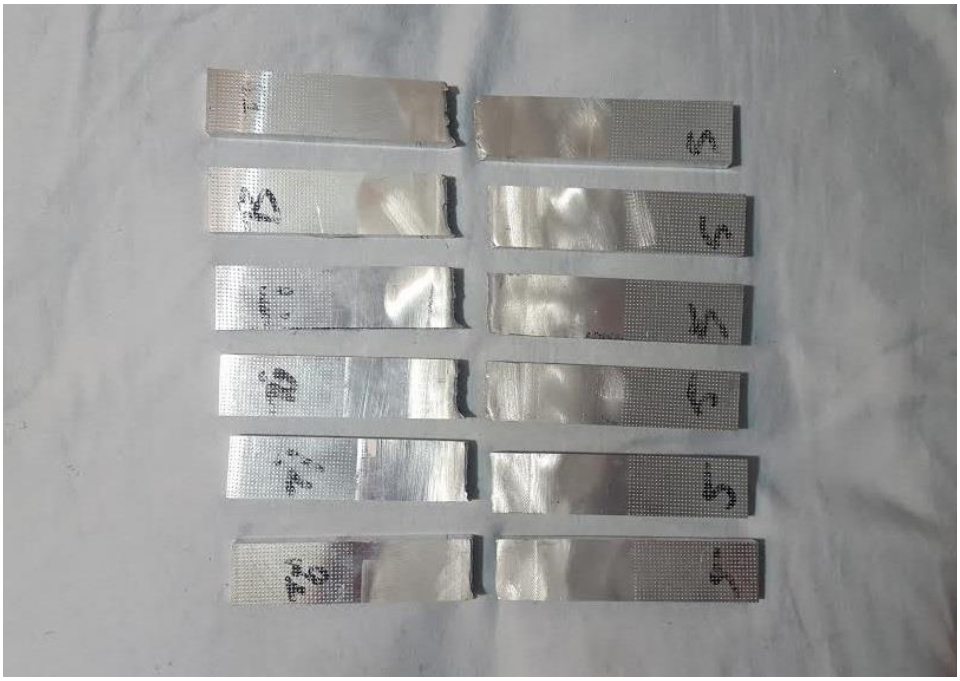

Figure 4.5: Weld #5 Post Tensile Break

Figure 4.6 shows the tensile specimens of Weld 6 after they were broken. The advancing side is on the left, while the retreating side is on the right. The tensiles in the figure are laid in an increasing order with Tensile #2 at the top, and Tensile #8 at the bottom. When comparing these tensiles post break to Weld 3, which had similar welding parameters, a drop-in ductility can be noticed from the crack propagation and lack of necking on the edges. The fractures were also closer to the advancing side of the weld nugget, which is similar to the comparable weld 3.

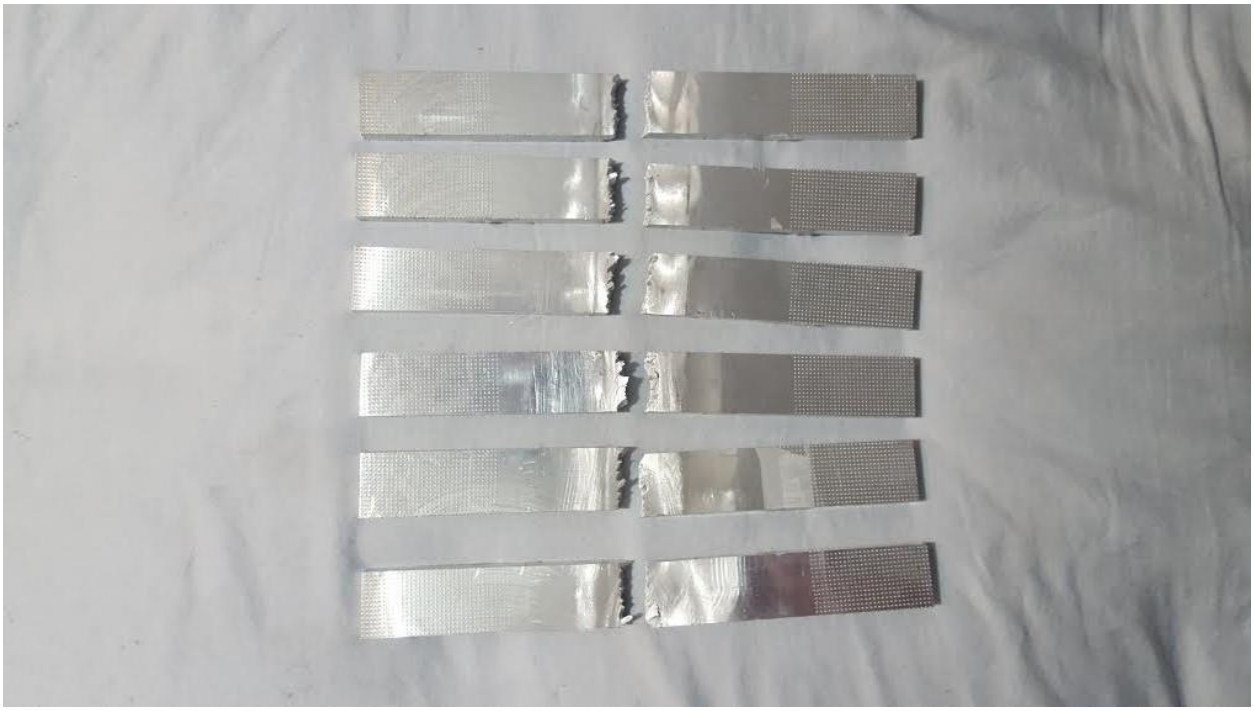

Figure 4.6: Weld #6 Post Tensile Break

It is noted that Weld 3 and 6 both experience a weld defect known as lack of consolidation. This can be seen in the Figure 4.7 below, with a red circle identifying the area of concern. There is a visual indication that the weld was not properly consolidated under these input parameters. The common similarity between Weld 3 and 6 is that both of them are using the highest RPM setting at 275. The welds with lower rotations per inch did not show signs of lack of consolidation from external examination.

Figure 4.7: Lack of Consolidation Welds 3 & 6

The results of all testing are organized by the mechanical properties: elongation, the yield strength and the ultimate strength; the macrograph analysis; and the hardness testing. The results will be compared to the original abstract of this experiment in where it will be determined if certain properties will be insensitive to variations of welding parameters and provide consistent results independent of the travel speed.

Table 4.1
Elongation for Tensiles

Speed = 13 IPM											
Force = 2400 lbf, Rotation = 180 RPM				Force = 2400 lbf, Rotation = 215 RPM				Force = 2400 lbf, Rotation = 275 RPM			
Tensile	Final Length (inches)	ΔL (inches)	Elongation (%)	Tensile	Final Length (inches)	ΔL (inches)	Elongation (%)	Tensile	Final Length (inches)	ΔL (inches)	Elongation (%)
W1T2	4.252	0.312	7.92	W2T2	4.271	0.331	8.40	W3T2	4.188	0.248	6.29
W1T3	4.215	0.275	6.98	W2T3	4.2155	0.2755	6.99	W3T3	4.254	0.314	7.97
W1T4	4.19	0.25	6.35	W2T4	4.2385	0.2985	7.58	W3T4	4.129	0.189	4.80
W1T6	4.271	0.331	8.40	W2T6	4.425	0.485	12.31	W3T6	4.182	0.242	6.14
W1T7	4.159	0.219	5.56	W2T7	4.219	0.279	7.08	W3T7	4.152	0.212	5.38
W1T8	4.192	0.252	6.40	W2T8	4.257	0.317	8.05	W3T8	4.2225	0.2825	7.17
Speed = 11 IPM											
Force = 2400 lbf, Rotation = 180 RPM				Force = 2400 lbf, Rotation = 215 RPM				Force = 2400 lbf, Rotation = 275 RPM			
Tensile	Final Length (inches)	ΔL (inches)	Elongation (%)	Tensile	Final Length (inches)	ΔL (inches)	Elongation (%)	Tensile	Final Length (inches)	ΔL (inches)	Elongation (%)
W4T2	4.1905	0.2505	6.36	W5T2	4.139	0.199	5.05	W6T2	4.1705	0.2305	5.85
W4T3	4.133	0.193	4.90	W5T3	4.1865	0.2465	6.26	W6T3	4.0765	0.1365	3.46
W4T4	4.1895	0.2495	6.33	W5T4	4.2865	0.3465	8.79	W6T4	4.1575	0.2175	5.52
W4T6	4.144	0.204	5.18	W5T6	4.0855	0.1455	3.69	W6T6	4.165	0.225	5.71
W4T7	4.139	0.199	5.05	W5T7	4.19	0.25	6.35	W6T7	4.0755	0.1355	3.44
W4T8	4.1015	0.1615	4.10	W5T8	4.202	0.262	6.65	W6T8	4.217	0.277	7.03

Table 4.2
Yield Stress for Tensiles

Speed = 13 IPM					
Force = 2400 lbf, Rotation = 180 RPM		**Force = 2400 lbf, Rotation = 215 RPM**		**Force = 2400 lbf, Rotation = 275 RPM**	
Tensile	σ_y (ksi)	Tensile	σ_y (ksi)	Tensile	σ_y (ksi)
W1T2	31.88	W2T2	33.25	W3T2	33.383
W1T3	32.09	W2T3	32.58	W3T3	33.22
W1T4	31.9	W2T4	32.45	W3T4	33.38
W1T6	32.34	W2T6	32.42	W3T6	33.58
W1T7	19.93	W2T7	33.43	W3T7	32.67
W1T8	36.29	W2T8	33.67	W3T8	32.64
Speed = 11 IPM					
Force = 2400 lbf, Rotation = 180 RPM		**Force = 2400 lbf, Rotation = 215 RPM**		**Force = 2400 lbf, Rotation = 275 RPM**	
Tensile	σ_y (ksi)	Tensile	σ_y (ksi)	Tensile	σ_y (ksi)
W4T2	31.86	W5T2	31.74	W6T2	29.63
W4T3	31.44	W5T3	31.57	W6T3	28.43
W4T4	31.87	W5T4	31.04	W6T4	28.84
W4T6	31.78	W5T6	32.33	W6T6	30.40
W4T7	32.07	W5T7	31.95	W6T7	29.53
W4T8	32.08	W5T8	31.44	W6T8	29.37

Table 4.3
Ultimate Strength for Tensiles

Speed = 13 IPM											
Force = 2400 lbf, Rotation = 180 RPM				Force = 2400 lbf, Rotation = 215 RPM				Force = 2400 lbf, Rotation = 275 RPM			
Tensile	Maximum Force (lbf)	Area (in2)	σ_u (ksi)	Tensile	Maximum Force (lbf)	Area (in2)	σ_u (ksi)	Tensile	Maximum Force (lbf)	Area (in2)	σ_u (ksi)
W1T2	17,923	0.36	49.79	W2T2	16,540	0.32	50.99	W3T2	17,731	0.36	49.25
W1T3	18,092	0.36	50.26	W2T3	15,998	0.32	49.43	W3T3	18,115	0.36	50.32
W1T4	18,076	0.36	50.21	W2T4	16,156	0.32	49.92	W3T4	16,933	0.36	47.04
W1T6	18,060	0.36	50.17	W2T6	16,072	0.32	49.66	W3T6	17,556	0.36	48.77
W1T7	9,610	0.36	26.69	W2T7	16,042	0.32	50.64	W3T7	17,123	0.36	47.57
W1T8	14,474	0.31	47.01	W2T8	16,102	0.32	50.83	W3T8	16,867	0.36	46.85
Speed = 11 IPM											
Force = 2400 lbf, Rotation = 180 RPM				**Force = 2400 lbf, Rotation = 215 RPM**				**Force = 2400 lbf, Rotation = 275 RPM**			
Tensile	Maximum Force (lbf)	Area (in2)	σ_u (ksi)	Tensile	Maximum Force (lbf)	Area (in2)	σ_u (ksi)	Tensile	Maximum Force (lbf)	Area (in2)	σ_u (ksi)
W4T2	13,746	0.36	38.18	W5T2	14,064	0.36	38.87	W6T2	10,992	0.34	32.14
W4T3	14,338	0.36	39.83	W5T3	13,260	0.37	35.94	W6T3	10,960	0.34	32.05
W4T4	14,483	0.36	40.64	W5T4	14,523	0.38	38.42	W6T4	11,116	0.34	32.50
W4T6	13,719	0.36	38.11	W5T6	13,524	0.35	38.53	W6T6	11,543	0.34	34.11
W4T7	14,342	0.36	40.24	W5T7	12,836	0.35	36.57	W6T7	11,187	0.34	32.71
W4T8	13,134	0.36	36.85	W5T8	11,783	0.35	33.57	W6T8	11,224	0.34	33.26

All macrographs can be found in Chapter 7. Upon examining the macrographs, it is noted that the shape of the weld 2195 portion of the weld nugget is changed as the RPM increases. The lower RPM welds have the nugget looking more like a flame as it is not as compact and waviness is found throughout. As the RPM increases, the welds begin to consolidate more in the middle and have a thinner overall layer of material across the latitudinal centerline.

Looking at the shape of the macros it can be deemed that the welding parameters have an effect on the overall shape of the weld nugget. The higher RPM welds have less waviness overall and a more concise 2195 material profile. This is because the spindle is able to mix the material more and cause a more concise weld. When comparing the same RPM values the travel speed also has an effect on this, as the slower travel speed has less waviness. This is because the spindle is allowed more contact with a particular location on the weld itself. The voids tend to be more apparent on the lower RPM welds, also because the spindle is not able to uniformly mix the material together and instead is leaving voids as it is passing through the area.

Looking at the size of the 2195 material length, or nose, in the weld nugget, the center of the welds, or M5, possesses the larger weld nuggets when compared to the M1 & M9, the beginning and end of the weld respectively. This was consistent across all welds, as the beginning of the weld and end of the weld were normally thinner. Normally in friction stir welding the start point and end point are completed on raised lips and these cut off post machining to avoid this type of irregularities in the microstructure.

The nose length for most of the welds had a trend where it increased over the length of the weld, where the alternative would be the center of the weld had a decrease in nose length, and the outer edges had a much longer nose. The lower RPM welds tended to have shorter nose lengths, on

average. This could be due to the fact that the higher RPM would produce more heat, allowing the material to be extruded and flow much more easily.

The length of the nose has an effect on the material properties, with W5M9 being a great example as it has a very long nose, and the properties are trending downward as they approach this sample location. When comparing the required forces to break each tensile, as the material had a longer nose on that particular point of the weld, a lower force was required to break the tensile specimen. It is expected that this nose length would also be determined by the forge force as a higher forge force will allow the material to extrude further, but cannot not be confirmed in this study, as all welds were completed at the same forge force value.

Voids were present in the weld and it can be seen in the macrographs. They appear as white spots as the silicon used in the grinding/polishing process was lodged into them and filled the void. The silicon was unable to be removed, but it did make finding the voids much easier. The voids are present more in the higher travel speed welds when compared to the lower travel speed welds. Figure 4.9 shows the locations of these voids on a particular weld. The voids are prevalent on both sides from the TMAZ to centerline of the weld nugget with no dominance in a particular zone.

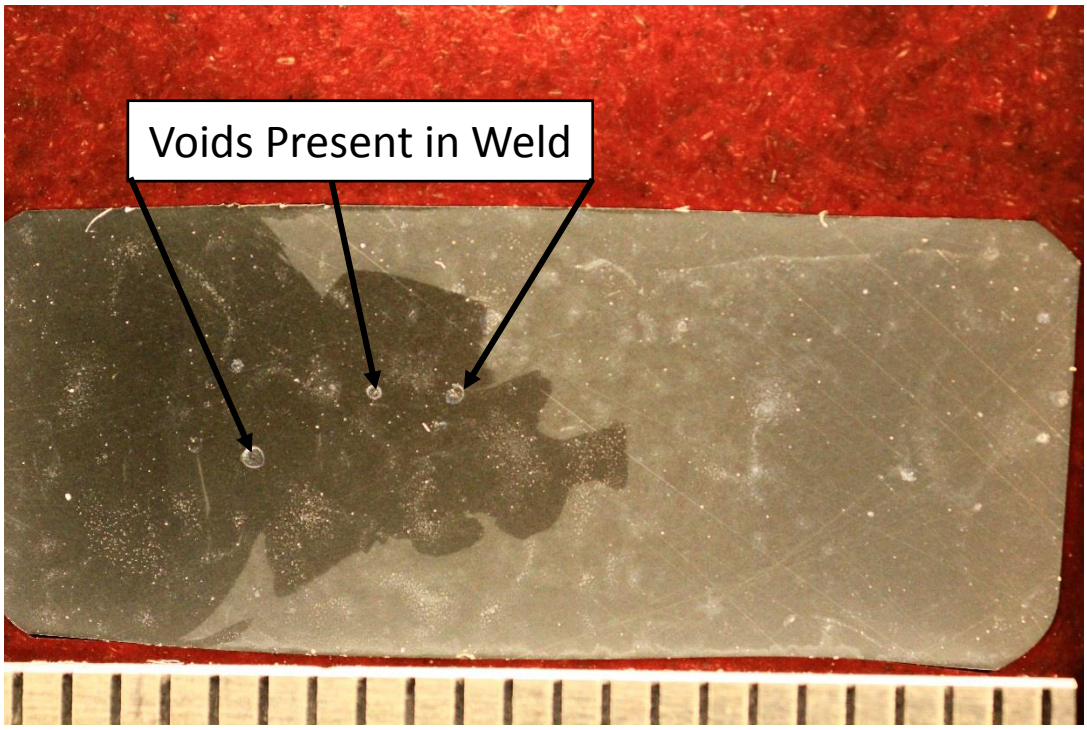

Figure 4.8: Voids in Weld

As noted early in this paper, a lack of consolidation defect was noted on the surface of welds 3 & 6. It appears that this defect is closer to the advancing side. This can be also seen in the macrographs, displayed in Figure 4.10. On the advancing side, it is seen where the discoloration is noted as lack of consolidation. This shows that those areas are not a coherent bond.

Figure 4.9: Lack of Consolidation

The hardness testing results can be seen tabulated below in Table 4.5 which shows the total range of the hardness values on each side of the weld, while the remaining hardness data plots can be found in Chapter 7. These values are taken from the HAZ to the point of the 2195/2219 material interface. This is not always in the center of the weld as the interface between the two metals was

not always in a consistent spot. So, reading the below table for W1M1 the 2195 side of the nugget would be 124.8 HV and the next data point would be on the 2219 material at 101.9 HV.

Table 4.4
Range of Hardness Data

Weld	2195 HAZ & Nugget	2219 HAZ & Nugget	Weld	2195 HAZ & Nugget	2219 HAZ & Nugget
W1M1	107.6 – 124.8	77.4 – 101.9	W4M1	97.1 – 114.3	78.5 –94.5
W1M5	109.4 – 125.4	77.1 – 116.3	W4M5	101.5 – 115.2	73.4 – 94.4
W1M9	105.4 – 120.2	76.9 – 114.8	W4M9	89.1 – 113.8	75.5 – 108.5
W2M1	111.8 – 128.9	81.4 – 110.4	W5M1	90.8 – 115.2	78.8 – 102.2
W2M5	106.7 – 123.7	80.3 – 93.3	W5M5	88.4 – 115.7	80.8 – 86.1
W2M9	102.4 – 115	81.4 – 96	W5M9	104.9 – 122.6	N/A
W3M1	100.3 – 120.4	78.8 – 92.6	W6M1	109.9 – 124.3	81.4 – 115
W3M5	98.3 – 107.6	90.8 – 94.8	W6M5	93.3 – 117.8	78.8 – 91.5
W3M9	103.2 – 130.7	83.9 – 99.5	W6M9	95.6 – 120.4	85.5 – 96.7

This is compared to the parent material hardness of each alloy. Aluminum 2219-T851 has a typical hardness of 130 HV, while Aluminum 2195-T8 has a typical of value of 180 HV. Typically, the hardness data for the welds in this experiment experience a drop-in hardness from the parent material to weld nugget of about 50 HV, while typical drops in friction stir welds of aluminum alloys have drops of approximately 30HV from the parent material to the weld nugget **[36]**. This larger than normal drop in hardness data is expected to stem from the inward mixing material. This is because the material is being forced into each other causing it to be worked more.

It is noted that due to the shape of the weld nugget, sample W5M9 had all data points collected on 2195 portion of the weld nugget. This is why the hardness range is not available for the 2219 section. These shapes effect the total hardness distribution along the face of the macro, as the length of the nose of 2195 dictates when the drop-in hardness will be. This is because the material is not fully mixing and having a 50/50 distribution along the weld nugget. There is a large drop

from the last data point on the 2195 and the first data point of the 2219, although both being in the weld nugget. For This is unusual as it is expected to have a proper mix of the two material types, but since it is a bi-alloy friction stir weld, the properties of the 2195 are still dominant and present.

Looking at the difference between a Left-Hand Right-Hand threaded pin tool and compare it to a typical Right Hand threaded pin tool, the microstructure of the weld is different. In the next two figures, there are two macrographs of welds with similar conditions. Both welds used self-reacting pin tools. The weld input parameters were also similar as the forge force was 2400 lbf, and the travel speed was also 13 IPM. The only different factors would be that the LHRH weld had 215 RPM, while the RH weld had 200 RPM, and the retreating side material is different aluminum alloys, 2195 vs 2050. This difference is approximately 0.5% more copper in 2050 and another <0.5% of other alloying materials, so there is not a larger difference between the two materials. If anything, the Al 2050 would be less resistant to material flow.

When examining the differences in microstructure between the two welds, it can be clearly seen that the LHRH weld has the material consolidated in the center as opposed to being spread out like the RH. This is an expected result as the LHRH pin tool pushes the material to the center of the weld. It is hypothesized that the larger drop in hardness values than expected is due to the LHRH pin tool, as the material is being worked more as it is compacted into the center.

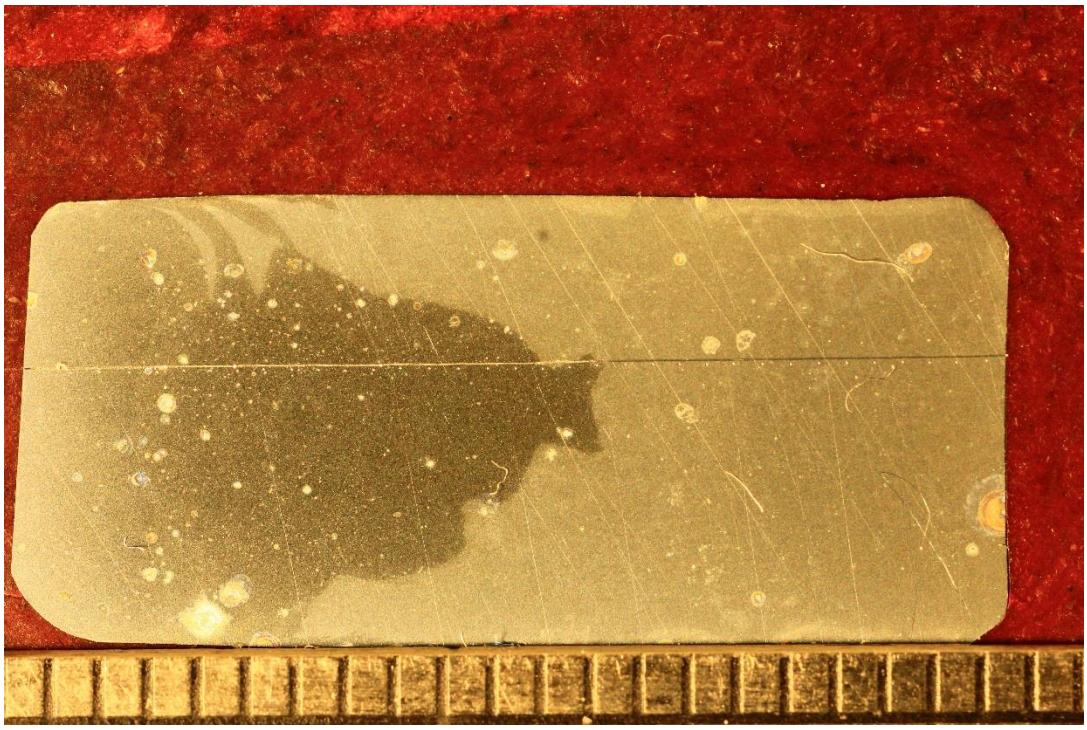

Figure 4.10: Left-Hand Right-Hand Threaded Pin Tool

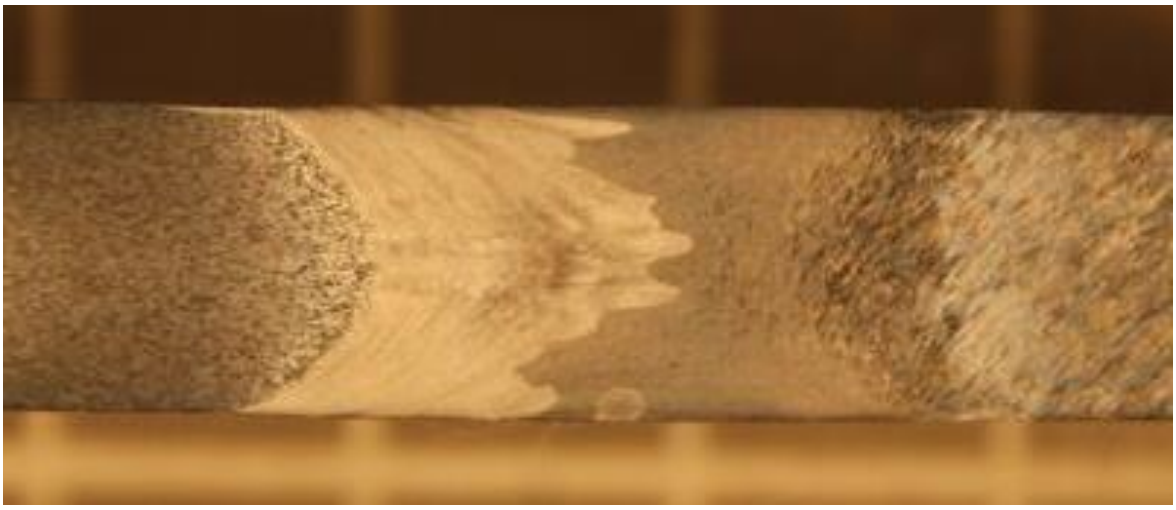

Figure 4.11: Right-Hand Threaded Pin Tool

Once the final results from the experiment were completed and recorded, the data from the tensile testing was input into a linear regression model using the methods described in Chapter 2. The linear regression model was completed for each of the three mechanical properties, the elongation,

the yield strength and the ultimate strength, which resulted in three separate final formulas as dictated below and the following equations were derived from the data collected in this experiment.

$$\frac{\Delta L}{L} = -4.71138 + .834391 * Travel\ Speed + .096901 * Force/RPM \quad \textbf{Eq 4.1}$$

$$\sigma_y = 23.52757 + .658861 * Travel\ Speed + .017165 * Force/RPM \quad \textbf{Eq 4.2}$$

$$\sigma_u = -33.27562 + 5.91297 * Travel\ Speed + .404985 * Force/RPM \quad \textbf{Eq 4.3}$$

These equations were then used to calculated a value (dependent value) that the regression model would output with the input parameters (independent variables) used for each trial run. Looking at the above three equations, it can be seen that the effects of the Travel Speed are much greater than that of the Force/RPM. It was noted that multiplying constant of the Travel Speed is several orders of magnitude higher than the secondary constant for the Force/RPM, meaning that the final mechanical property is much more dependent on the travel speed than the Force/RPM.

Comparing the results of a linear regression to the measured data, it can be seen from the next three figures that a linear regression model fits the dataset of the ultimate tensile strength but not for the yield strength and the elongation based on the R^2 values.

Before looking at the three regression models, it must be noted that each weld on the model is represented by one vertical line. Due to the tensiles all having the same input parameters, the linear regression model will all yield the same predicted value for that particular weld. This causes a flaw in the linear regression model being that each of the six tensiles will have a different actual result per the same predicted value. Any unaccounted variances in the welding process and post machining process will not be expressed in this regression model. This can be further emphasized when examining the large error of the model. The error was calculated for each data point, but can be visually seen by the examining how far each vertical line is stretched. The more error present, the longer the vertical line; with the less error present, the data points will be clumped

around the predicted value, being very precise. When looking at the actual trendline in the next three figures, the closer the slope is to 1, a better predictor the regression model was for that particular dataset.

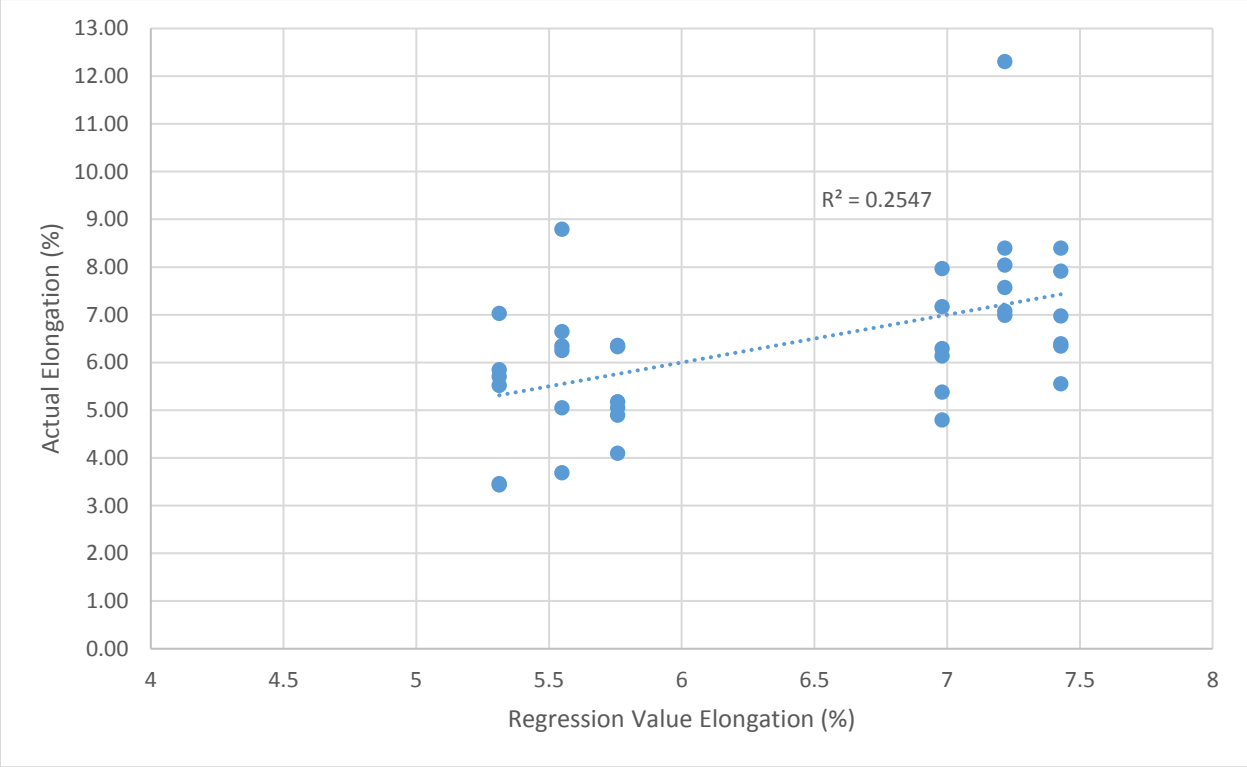

Figure 4.12: Actual Elongation vs. Regression Value Elongation

Overall this regression model for the elongation was not a good model to predict data points. The values are not very precise or accurate, which can be seen in the large experimental error between the actual value vs predicted value. Although looking at the data vs. the trendline, it can be seen that the regression model is good at predicting an average value. So if a weld scheme was characterized by its average value, then the regression model could be more useful.

Table 4.5
Linear Regression Model Elongation

Elongation ΔL/L							
Weld	Actual	Regression Value	Percent Difference	Weld	Actual	Regression Value	Percent Difference
W1T2	7.92	7.43	6.20%	W4T2	6.36	5.76	9.42%
W1T3	6.98		6.42%	W4T3	4.90		17.57%
W1T4	6.35		17.06%	W4T4	6.33		9.06%
W1T6	8.40		11.59%	W4T6	5.18		11.23%
W1T7	5.56		33.63%	W4T7	5.05		14.02%
W1T8	6.40		16.13%	W4T8	4.10		40.50%
W2T2	8.40	7.22	14.09%	W5T2	5.05	5.55	9.86%
W2T3	6.99		3.22%	W5T3	6.26		11.31%
W2T4	7.58		4.74%	W5T4	8.79		36.91%
W2T6	12.31		41.37%	W5T6	3.69		50.25%
W2T7	7.08		1.92%	W5T7	6.35		12.55%
W2T8	8.05		10.29%	W5T8	6.65		16.56%
W3T2	6.29	6.98	10.91%	W6T2	5.85	5.31	9.19%
W3T3	7.97		12.40%	W6T3	3.46		53.35%
W3T4	4.80		45.54%	W6T4	5.52		3.76%
W3T6	6.14		13.66%	W6T6	5.71		6.97%
W3T7	5.38		29.75%	W6T7	3.44		54.48%
W3T8	7.17		2.63%	W6T8	7.03		24.43%

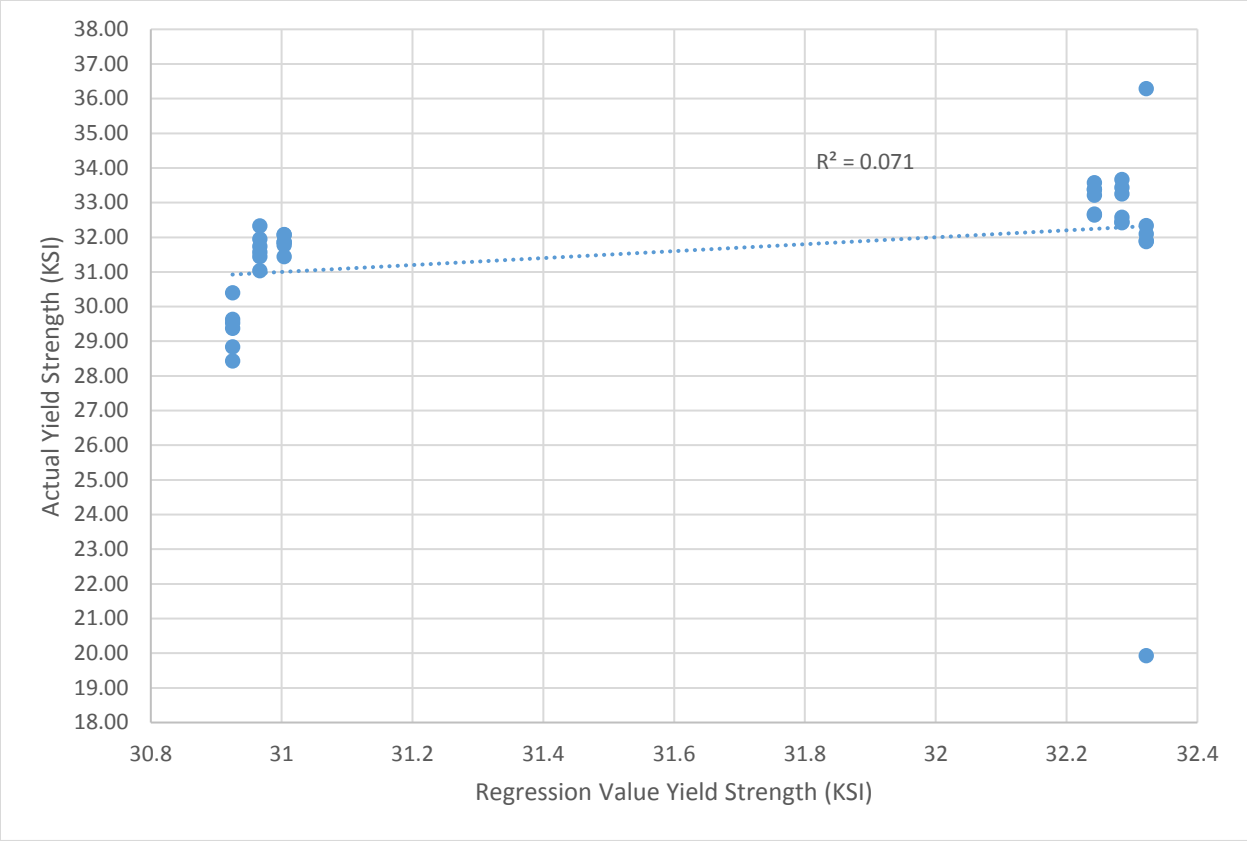

Figure 4.13: Actual Yield Strength vs. Regression Value Yield Strength

Looking at the above linear model in Figure 4.14, it can be seen from how the data points are not tightly bound around a central point that the linear regression model is not a good fit. The values are not very precise or accurate, which can be seen in the large experimental error between the actual value vs predicted value. Although looking at the data vs. the trendline, it can be seen that the regression model is not good at predicting an average value as when looking at the trendline, it is not anywhere near the center of the data points for a particular weld.

Table 4.6
Linear Regression Model Yield Strength

Yield Strength σY							
Weld	Actual	Regression Value	Percent Difference	Weld	Actual	Regression Value	Percent Difference
W1T2	31.88	32.32	1.40%	W4T2	31.86	31.00	2.69%
W1T3	32.09		0.71%	W4T3	31.44		1.39%
W1T4	31.90		1.32%	W4T4	31.87		2.71%
W1T6	32.34		0.05%	W4T6	31.78		2.43%
W1T7	19.93		62.17%	W4T7	32.07		3.33%
W1T8	36.29		10.93%	W4T8	32.08		3.36%
W2T2	33.25	32.28	2.91%	W5T2	31.74	30.97	2.44%
W2T3	32.58		0.91%	W5T3	31.57		1.91%
W2T4	32.45		0.51%	W5T4	31.04		0.24%
W2T6	32.42		0.41%	W5T6	32.33		4.22%
W2T7	33.43		3.43%	W5T7	31.95		3.08%
W2T8	33.67		4.11%	W5T8	31.44		1.51%
W3T2	33.38	32.24	3.42%	W6T2	29.63	30.92	4.37%
W3T3	33.22		2.93%	W6T3	28.43		8.78%
W3T4	33.38		3.40%	W6T4	28.84		7.23%
W3T6	33.58		3.97%	W6T6	30.4		1.73%
W3T7	32.67		1.31%	W6T7	29.53		4.72%
W3T8	32.64		1.21%	W6T8	29.37		5.29%

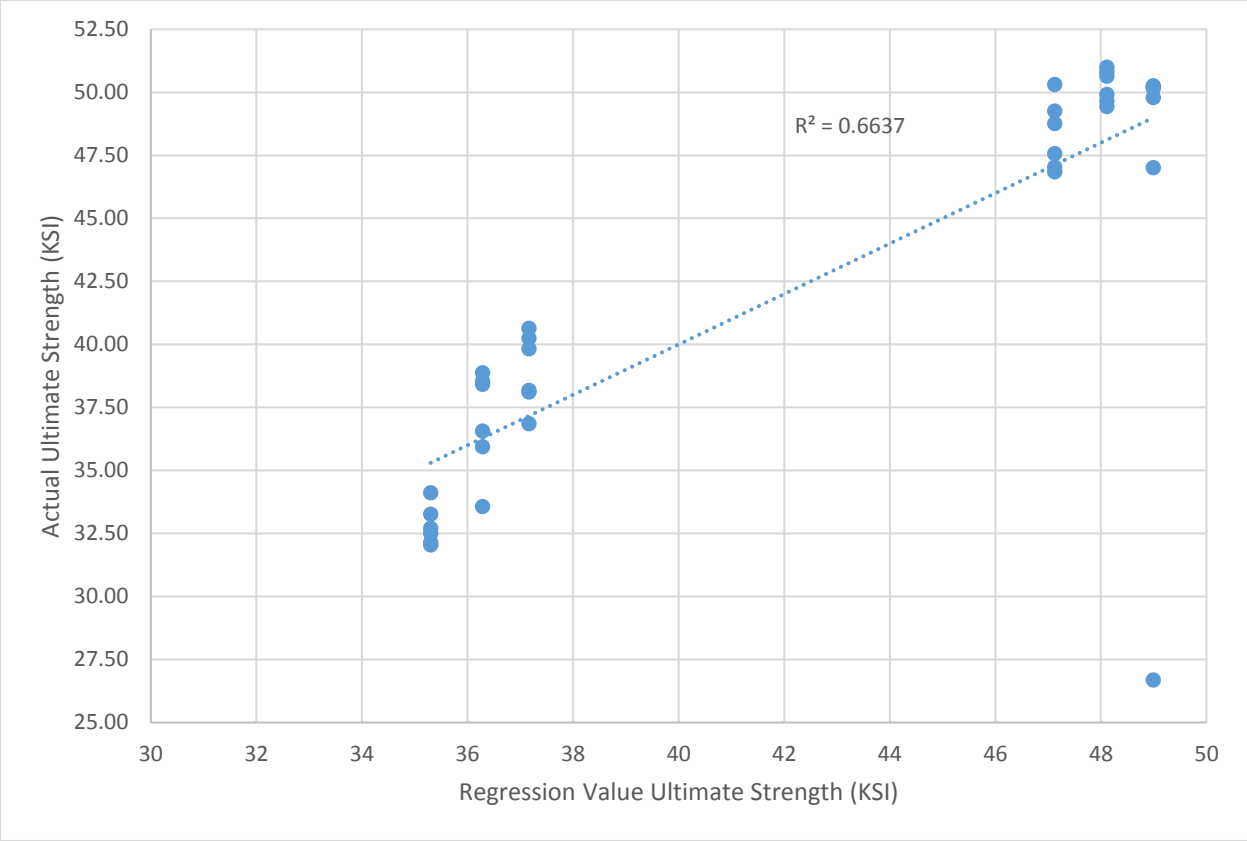

Figure 4.14: Actual Ultimate Strength vs. Regression Value Ultimate Strength

Looking at the above linear model in Figure 4.15, it can be seen from how the data points are not tightly bound around a central point that the linear regression model is not a good fit. The values are not very precise or accurate, which can be seen in the large experimental error between the actual value vs predicted value. Although looking at the data vs. the trendline, it can be seen that the regression model is not good at predicting an average value as when looking at the trendline, it is not anywhere near the center of the data points for a particular weld.

Table 4.7
Linear Regression Model Ultimate Strength

Ultimate Strength σU							
Weld	Actual	Regression Value	Percent Difference	Weld	Actual	Regression Value	Percent Difference
W1T2	49.79	48.99	1.60%	W4T2	38.18	37.17	2.66%
W1T3	50.26		2.52%	W4T3	39.83		6.68%
W1T4	50.21		2.43%	W4T4	40.64		8.54%
W1T6	50.17		2.34%	W4T6	38.11		2.47%
W1T7	26.69		83.53%	W4T7	40.24		7.64%
W1T8	47.01		4.22%	W4T8	36.85		0.85%
W2T2	50.99	48.11	5.65%	W5T2	38.87	36.29	6.65%
W2T3	49.43		2.67%	W5T3	35.94		0.96%
W2T4	49.92		3.62%	W5T4	38.42		5.55%
W2T6	49.66		3.12%	W5T6	38.53		5.82%
W2T7	50.64		4.99%	W5T7	36.57		0.77%
W2T8	50.83		5.34%	W5T8	33.57		8.09%
W3T2	49.25	47.13	4.32%	W6T2	32.14	35.30	9.83%
W3T3	50.32		6.34%	W6T3	32.05		10.14%
W3T4	47.04		0.19%	W6T4	32.5		8.62%
W3T6	48.77		3.36%	W6T6	34.11		3.49%
W3T7	47.57		0.92%	W6T7	32.71		7.92%
W3T8	46.85		0.58%	W6T8	33.26		6.13%

Examining the full set of data, trends can now be determined based off of the mechanical properties and the input welding parameters. The weld properties in the following graphs are characterized by the average mechanical properties. This is to average out any outliers due to localized defects. An example would be Weld 1 Tensile 7, which broke at 29 ksi, while the remaining five tensiles fractured at greater than 47 ksi.

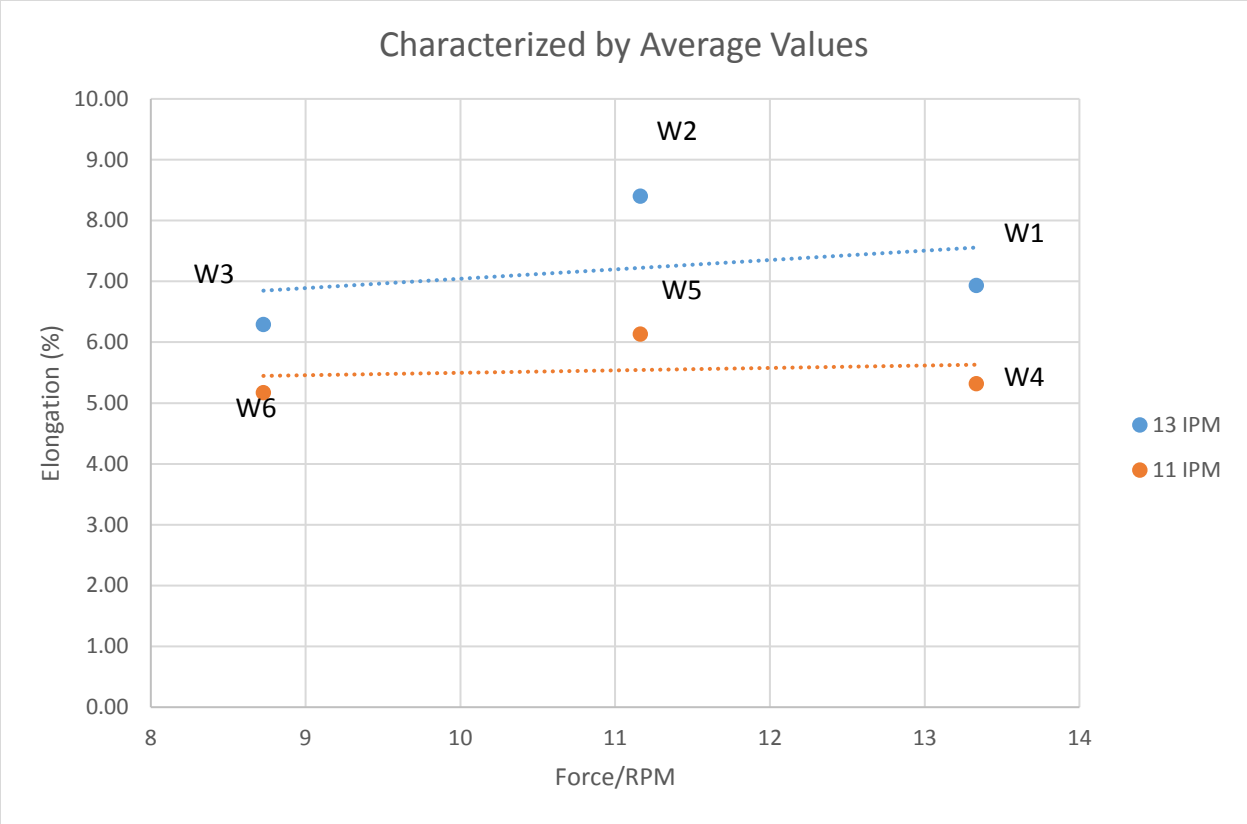

Figure 4.15: Effects of Travel Speed on Elongation, Characterized by Average Values

Looking at Figure 4.16, it appears that the Elongation of the welds do not show any insensitivity with regards to the varying travel speed. The plotted trend lines of both the 13 IPM and 11 IPM travel speed show that the values are diverging as the values of the Force/RPM increases. There appears to be no variable insensitive point possible either when extrapolating the data beyond the test data collected. This could mean that the elongation of the material is heavily affected by the travel speed of the spindle much more than the other two welding parameters.

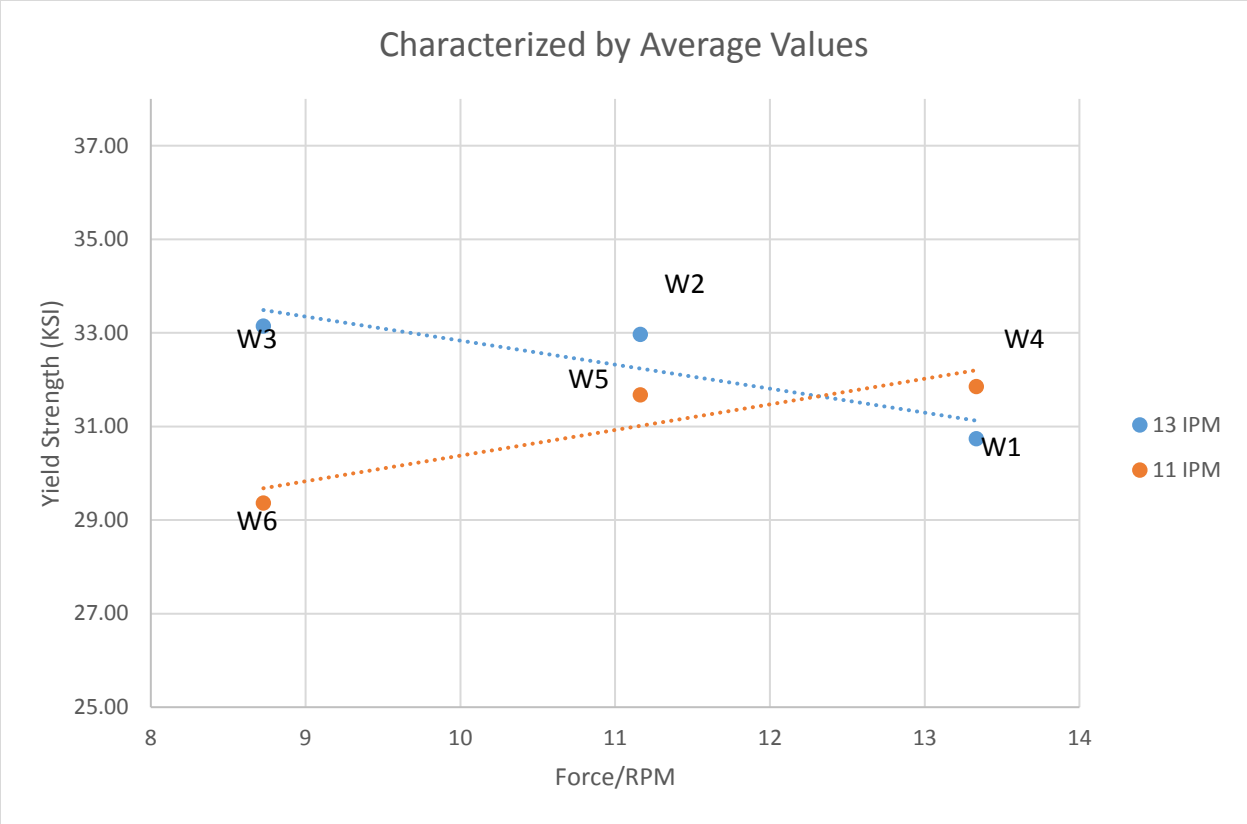

Figure 4.16: Effects of Travel Speed on Yield Strength, Characterized by Average Values

Looking at the above figure, it can be seen a clear point where the yield strength value is independent of the travel speed. This is where the two trend lines cross. When setting both trendlines equal to each other and then solving for when the yield strength is the same, it can be calculated that the exact value in which the variable insensitive point is 12.32 Force/RPM. When using this value with a forge force value of 2,400 lbfs, the appropriate value for the spindle speed should be set at 195 RPM to achieve a variable insensitive point. This is important as the values of the Forge Force or Spindle Speed can be calculated based off the given Force/RPM and the experiment can be recreated for different input parameters. It is noted that these data points are valid for 11 IPM to 13 IPM. This is still of value as certain FSW machinery may not be able to have a constant travel speed over various geometries, and scatter in travel speed may exist.

The importance of yield strength over the other mechanical properties is that it is the first point of material failure. Most structural applications can be considered non-successful if the yield strength of a material is met under any type of loading. If a material experiences plastic deformation in an aerospace structure, the aircraft will normally have to be scrapped due to safety concerns regardless of whether a high enough loading was achieved to reach the ultimate tensile strength. Being able to accurately predict the first initial point of failure is crucial in design.

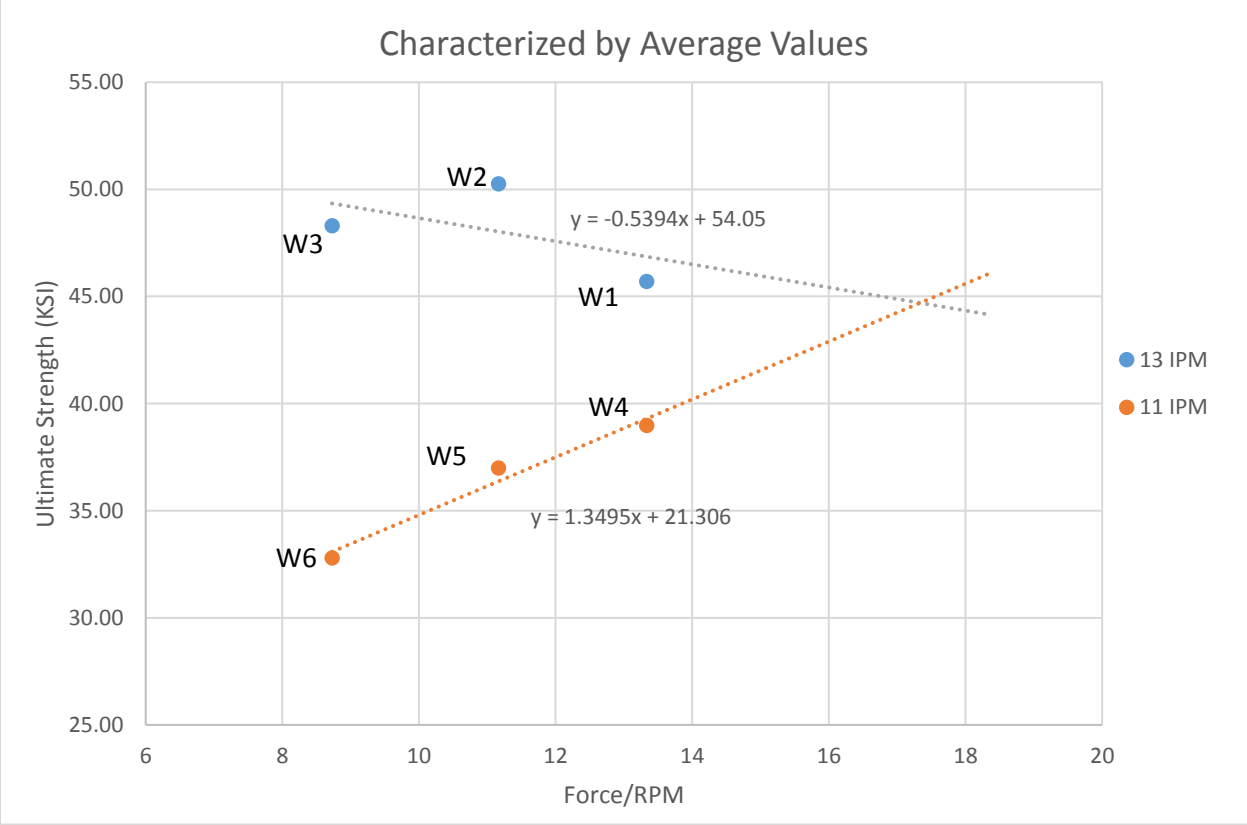

Figure 4.17: Effects of Travel Speed on Ultimate Strength, Characterized by Average Values

Looking at Figure 4.7, the data points collected do not show a variable insensitive point like the previous yield strength does, but when examining the slopes of the lines it appears that there may be a point in which a variable insensitive point is possible. When extrapolation the trend lines out past the collected data points, it can be seen that for higher values of Force/RPM, these values can

be achieved by increasing the forge force to a value of 4000 lbf, which is a typically used value in industry. The alternative would be to lower the spindle speed, but lowering the value any more could cause unnecessary stresses on the pin tool as the RPM would have to be incredibly low. Specifically, the point of interest on the graph is when the value of the Force/RPM is approximately 17.33.

It was noted that the predicted variable insensitive point for the ultimate strength was not the same value for the yield strength. This means that for any future applications of these results will have to prioritize the importance of yield strength versus ultimate strength, as based off the data from the experiment, only one can be achieved.

The effects of the travel speed can be seen on the hardness can be seen in the next figure. Looking at the overall range of hardness data points for the 2195 vs. 2219, it is predicted that low Force/RPM values will have the same hardness data ranges for both sides of the weld centerline.

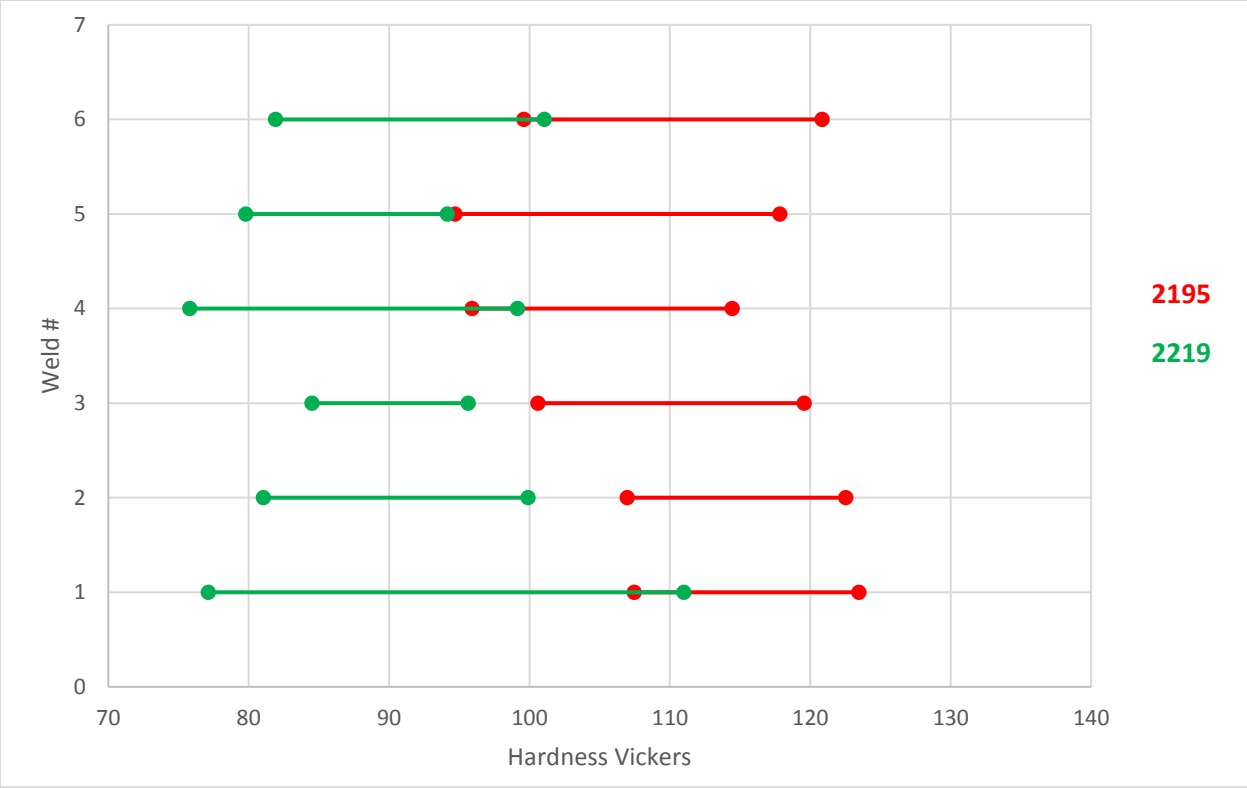

Figure 4.18: Effects of Travel Speed on Hardness

In this figure, the green lines are the overall range of hardness data for the 2219 material from the beginning of the HAZ to the point the materials meet in the weld nugget (which is always not the center of the weld), while the red lines are the 2195 material within the same range. Full hardness graphs can be found in Chapter 7.

Looking at this graph, the overall range of data points are getting closer together as the Force/RPM decreases (Welds 3 & 6). This could mean that there is a data range that is insensitive to the travel speed at low Force/RPM values, but limitations of machinery may limit how low a value of a Force/RPM value that can be achieved. Certain pin tools are required for high RPM Friction Stir Welding, so a different pin tool would have to be used to try and create those welds, which would vary the experimental process from this procedure. It is also noted that this is opposite to the trend that the Ultimate Tensile Strength is showing.

Chapter 5: Conclusions and Recommendations

5.1 Conclusions

The only mechanical property to show definite insensitivity to travel speed was the yield strength from the range of 11 IPM to 13 IPM. This is different from the previous experiments in which both the ultimate and yield strengths were insensitive to the forge force at a particular point. It can be extrapolated from the data that there does exist an insensitive point for the ultimate tensile strength, but the dataset from this particular experiment did not extend far enough to include this point. This shows that the post weld mechanical properties are more dependent on the travel speed than the forge force.

Normally when designing a weld schedule for friction stir welding, one of the mechanical properties will be optimized over the others depending on design criteria, so finding a point that is insensitive to variations in the travel speed will be beneficial as certain welding equipment may not be able to maintain a steady travel speed as it travels across a complex geometry. For example, this would allow a designer to select a travel of 12 IPM and still be able to maintain his or her manufacturing tolerances for the optimized mechanical property as it will not change as the spindle traverses across a complex geometry and experiences deviations in travel speed.

When examining the mechanical properties, having a consistent/predictable yield strength is important because this is will be the first instance of where the weld will fail. Permanent deformation in structures could result in issues with the original manufacturing tolerances.

Examining the hardness data, there was a drop off approximately 50 HV. This is because the material is flowing inward from the left-hand right-hand threaded pin tool. It appears that low values of Force/RPM will yield an insensitive data range with respect to the Travel Speed, as having a higher RPM will allow more heat into the system to have more of a mixing effect.

The length of the nose in the macrographs has an effect on the material properties, as they are trending downward as they approach a sample location with a long nose. When comparing the required forces to break each tensile, as the material had a longer nose on that particular point of the weld, a lower force was required to break the tensile specimen.

5.2 Recommendations

A wider range of process parameters could be selected, especially to investigate the predicted travel speed insensitive point involving the ultimate tensile strength. Specifically, the point of interest in where the travel speed is predicted to be insensitive is when the value of the Force/RPM is approximately 17.33. It is recommended to complete this at a Forge Force value of 4000 lbf as lowering the spindle speed anymore would cause an increase on stresses on the pin tool. A smaller gauge panel should be used instead, as the existing left-hand right-hand pin tool can be used for further experimentation involving forge force insensitivity. This is because a pin tool broke when under a load of 4000 lbf against the larger gauge panels. An alternative would be to increase the size of the pin tool to withstand the larger Forge Force at the existing panel thickness.

To greater determine the effects of the Left-Hand Right-Hand Pin Tool, it would be recommended to collect hardness samples along the short traverse of the weld to see the effects of the inward flowing material.

Chapter 6: References

[1] Murphy, Joseph; Majors, Jerry; Calmes, Jason; *Load Insensitive Welding of Self Reacting Friction Stir Welding* Lockheed Martin Corporation 2014.

[2] AlcoTec Wire Corporation *What are Unweldable Aluminum Alloys?* 2016

[3] Aerospace Specificatoin Metals, Inc., *Aluminum 2219 Material Specification Sheet* 2012

[4] Bohanon, Catherine; *Microhardness Testing of Aluminum Alloy Welds* Missouri University of Science and Technology

[5] Eller, Michael; Quiggle, Michael; Niedzinski, Michael.; *Application of Advanced AIRWARE Plate on the NASA Orion Command Module (CM) Architecture.* 2014 In Presentation at the 25thAeroMat Conference, Orlando, FL.

[6] Thomas, Wayne. *Friction Welding*. US patent #5,460,317 October 24, 1995.

[7] Mishra, Rajiv Sharan; Kumar, Nilesh, *Friction Stir Welding and Processing Science and Engineering* Springer International Publishing Switzerland 2014.

[8] Chao, Yuh J., Qi, X, and Tang W, *Heat Transfer in Friciton Stir Welding – Experimental and Numerical Studies.* ASME Vol. 125, 2003.

[9] Mishra, R. *Friction Stir Welding and Processing.* Materials Park: AMS international, 2007.

[10] Schneider, J.A., Nunes, A.C., Brendel, M.S., *The Influence of Friction Stir Weld Tool Form and Welding Parameters on Weld Structure and Properties: Nugget Bulge in Self-Reacting Friction Stir Welds*

[11] DeGarmo, E. Paul; Black, J T.; Kohser, Ronald A.; & Klamecki, Barney E., *Materials and Processing in Manufacturing.* John Wiley & Sons, 2003.

[12] Smith, Travis Lee, "*The Effect of Tool Rotation Speed and Clamping on Deformation in Friction Stir Welded 6061-T6511 Aluminum Extrusions"* (2011). University of New Orleans Theses and Dissertations. Paper 350.

[13] Callister Jr., William D.; Rethwisch, David G., *Materials Science and Engineering: An Introduction.* John Wiley & Sons 2010

[14] Gordon, J. E.; "*Structures or Why Things Don't Fall Down"* (2003). De Capo Press

[15] Budynas, Richard G., & Nisbett, J. Keith; "*Shigley's Mechanical Engineering Design*" 9th Edition 2011 The McGraw-Hill Companies

[16] Lindeburg, PE, Michael; *Mechanical Engineering Reference Manual for the PE Exam*. Thirteenth Edition, Professional Publications, Inc. 2013.

[17] Beer, Ferdinand P., Johnston, Jr. E. Russel, Dewolf, John T., & Mazurek, David F.; "*Mechanics of Materials"* 6th Edition 2012. The McGraw-Hill Companies

[18] Professional Plastics *Plastics Overview* 2016

[19] Rocha-Rangel, Enrique; *Fracture Toughness Determinations by Means of Indentation Fracture.* Universidada Politecnica de Victoria, Mexico. 2011

[20] Oberg, Erik; Jones, Franklin D.; Horton, Holbrook L.; & Ryffel, Henry H., *Machinery's Handbook 29th Edition* Industrial Press 2012

[21] Verges, Melody A.; Schilling, Paul J.; Germond, Jeffrey D.; Upadhyay, Puja; Miller, William K.; Takas, Nathan J.; Poudeu, Pierre F. P.; *(1908) Indentation Testing of Bulk* $ZR_{.05}HF_{.05}Co_{1-}$

$_xIr_xSb_{0.99}Sn_{.01}$ *Half-Heusler Alloys,* Department of Mechanical Engineering and the Advanced Materials Research Institute, University of New Orleans

[22] Khodir, Saad Ahmed; Shibayanagi, Toshiya; and Naka, Masaaki; *Control of Hardness Distribution in Friction Stir Welded AA2024-T3 Aluminum Alloy* Osaka University, Ibaraki 567-0047, Japan 2006

[23] Schultz, Jeffrey Patrick, and Creehan, Kevin *Self-reacting friction stir welding tool with the ability to add filler material*. US patent # 8,397,974 B2 March 19, 2013.

[24] Chowdhury, S.M., Chen, D. L., Bhole, S.D., and Cao, X.,*Effect of pin tool thread orientation on fatigue strength of friction stir welded AZ31B-H24 Mg butt joints.*

[25] Seidel TU, Reynolds AP. *Visualization of the material flow in AA2195 friction-stir welds using a marker strain technique.* Metal Mater Trans A 2001;32:2879–84.

[26] Eugene Wycliffe Kerr *(1908) Power and Power Transmission*, 2nd Ed., John Wiley

[27] Fisher, R.A. The Design of Experiments. Edinburough: Oliver and Boyd, 1935.

[28] Collins, Linda M; *Introduction to Factorial Experimental Designs* Penn State

[29] Collins, Linda M. et al. "*Factorial Experiments: Efficient Tools for Evaluation of Intervention Components*." American journal of preventive medicine 47.4 (2014): 498–504. PMC. Web. 26 Nov. 2016.

[30] Montgomery, Douglas C.; Peck, Elizabeth A.; Vining, G. Geoffrey; *Introduction to Linear Regression Analysis*. John Wiley & Sons, Inc. 2012

[31] Brannick, Michael T.; *Regression with Two Independent Variables* University of South Florida

[32] Frost, Jim; *Regression Analysis: How Do I Interpret R-squared and Assess the Goodness-of-Fit?* Minitab. May 30, 2013.

[33] *Introduction to Statistics* Saylor Academy 2012

[34] Simon, Laura; Young, Derek; STAT 501 *Simple Linear Regression* PennState Eberly College of Science

[35] Eller, Michael, (2015) *Friction Stir Welding Course Notes* University of New Orleans.

[36] Mishra, Rajiv Sharan; Kumar, Nilesh, *Friction Stir Welding and Processing Science and Engineering* Springer International Publishing Switzerland 2014. Pg 121.

[37] Struers Inc., Citopress Mounting Press

[38] Struers Inc., Tegramin

[39] Shimadzu Corporation Microhardness HMV-2

Chapter 7: Appendix

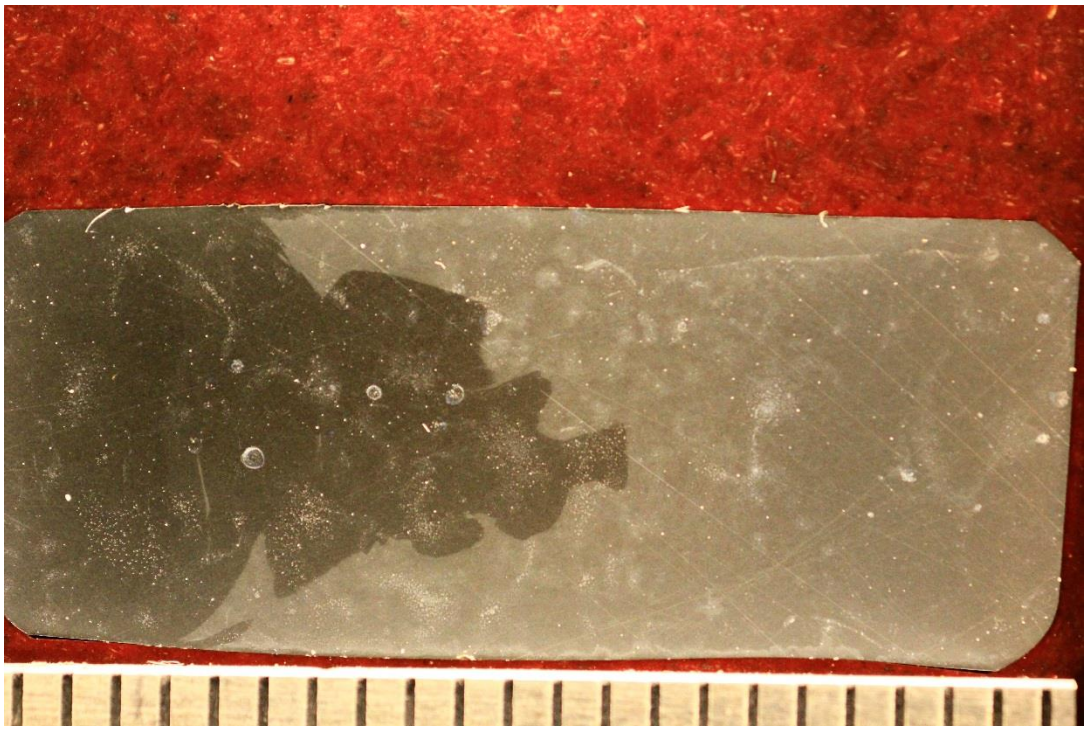

Figure 7.1: Macrograph of Weld 1 Sample 1

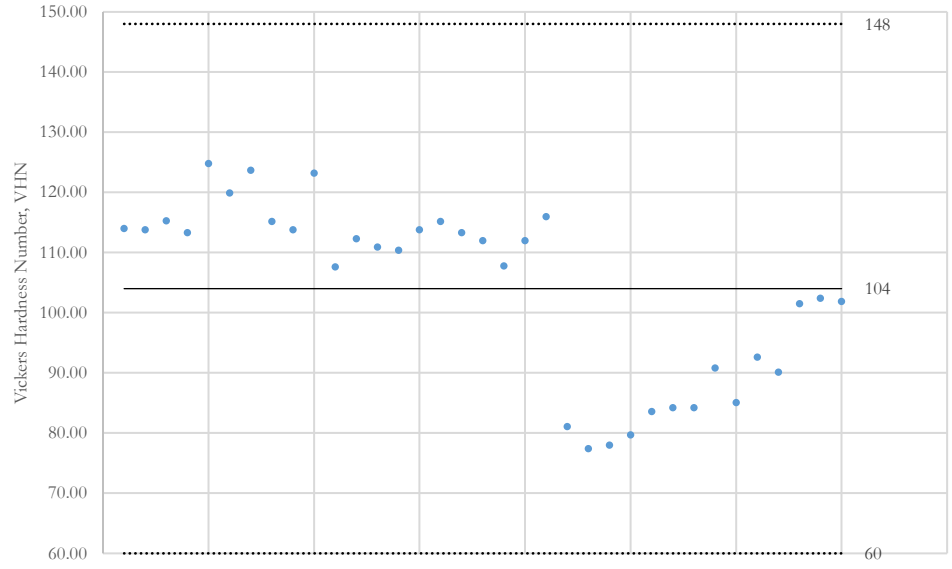

Figure 7.2: Hardness Data of Weld 1 Sample 1

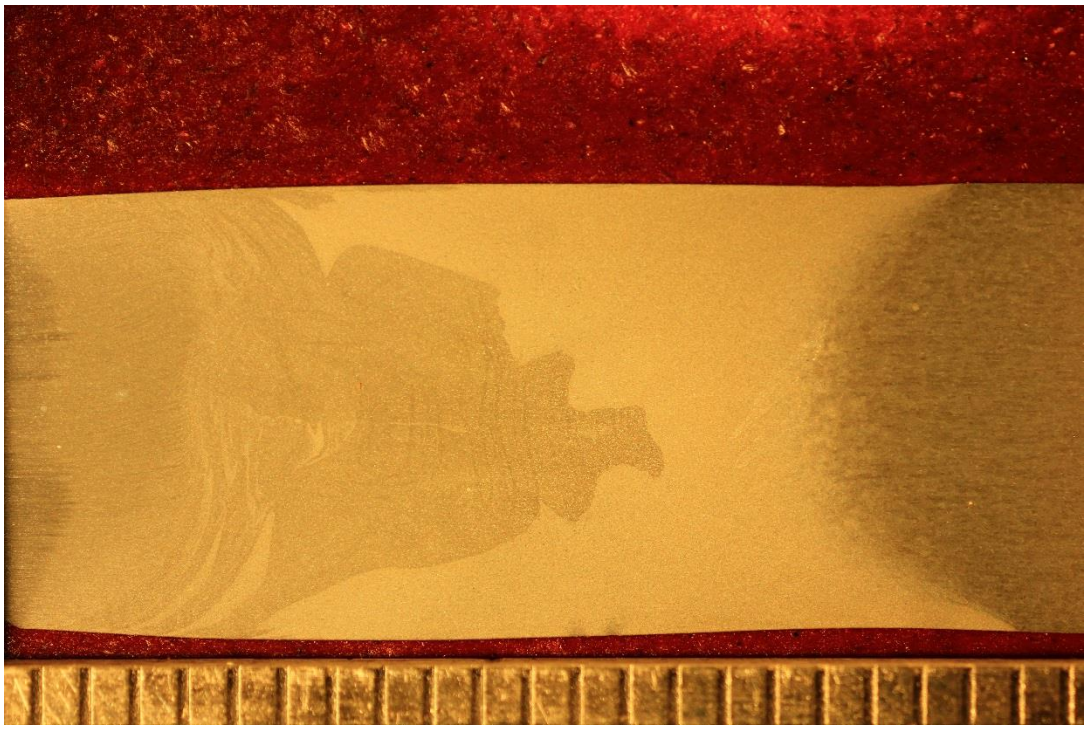

Figure 7.3: Macrograph of Weld 1 Sample 5

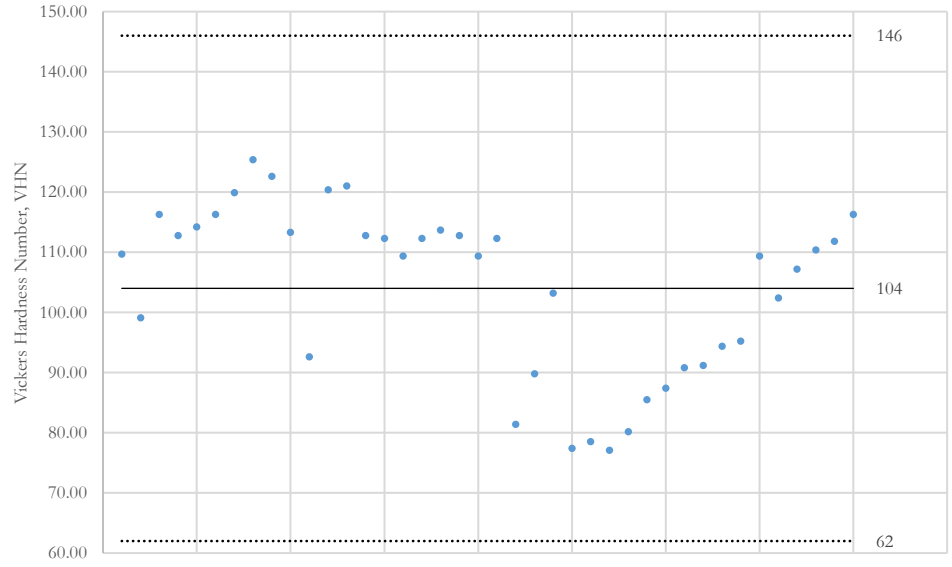

Figure 7.4: Hardness Data of Weld 1 Sample 5

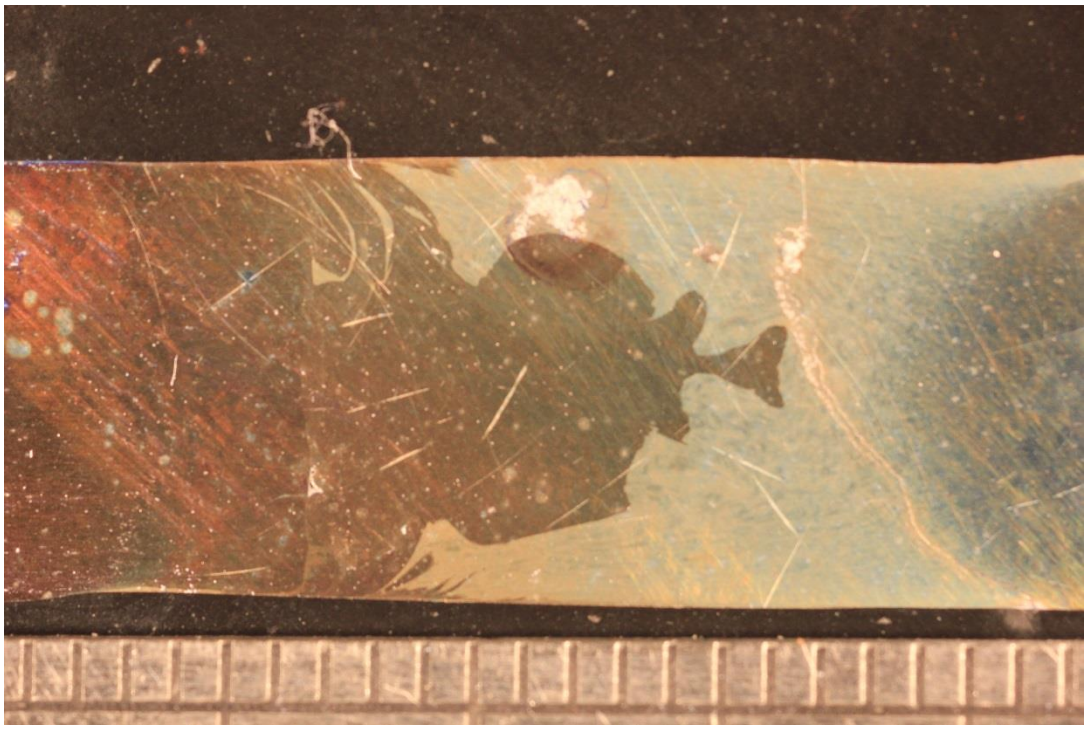

Figure 7.5: Macrograph of Weld 1 Sample 9

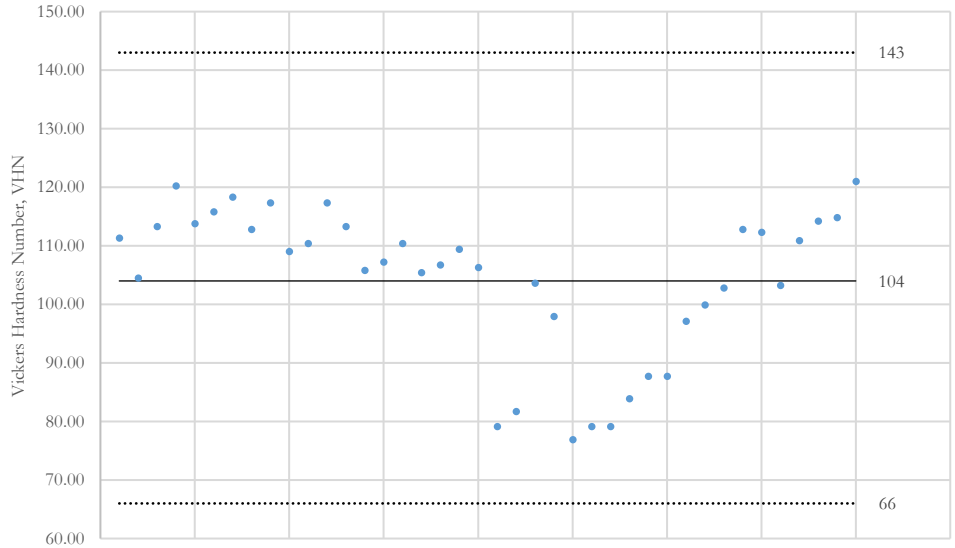

Figure 7.6: Hardness Data of Weld 1 Sample 9

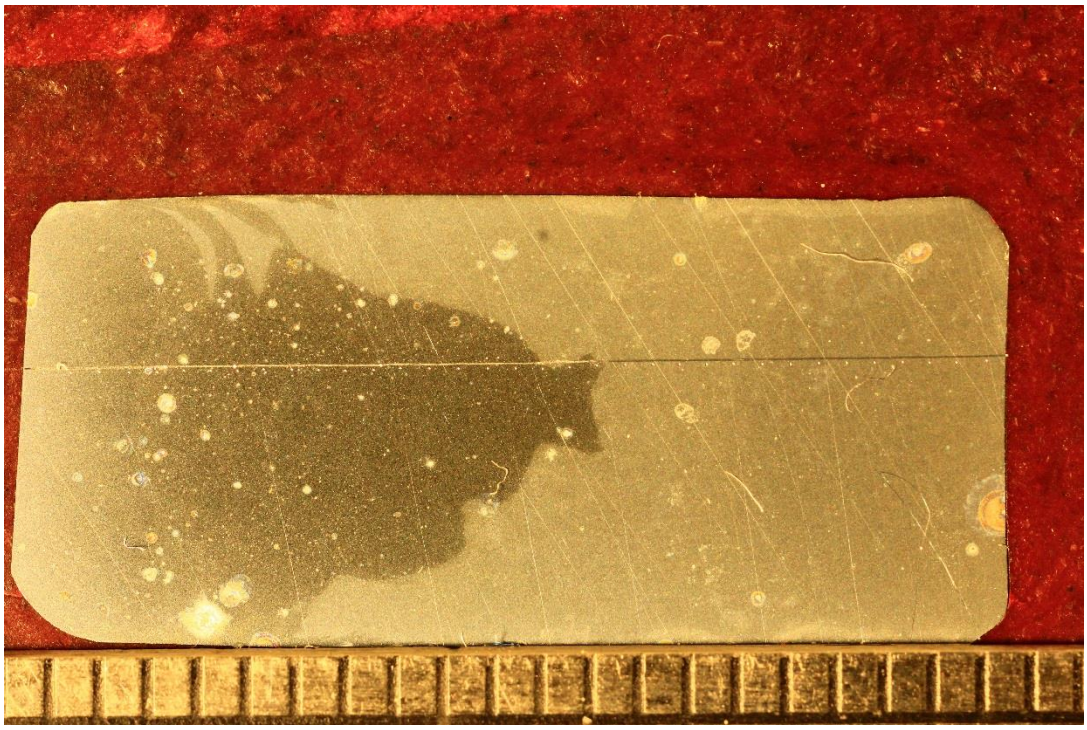

Figure 7.7: Macrograph of Weld 2 Sample 1

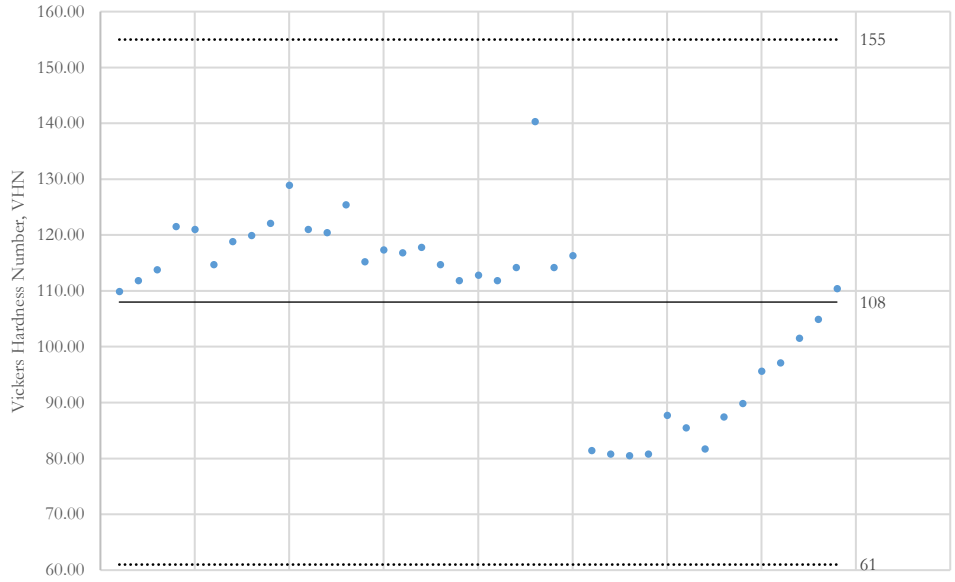

Figure 7.8: Hardness Data of Weld 2 Sample 1

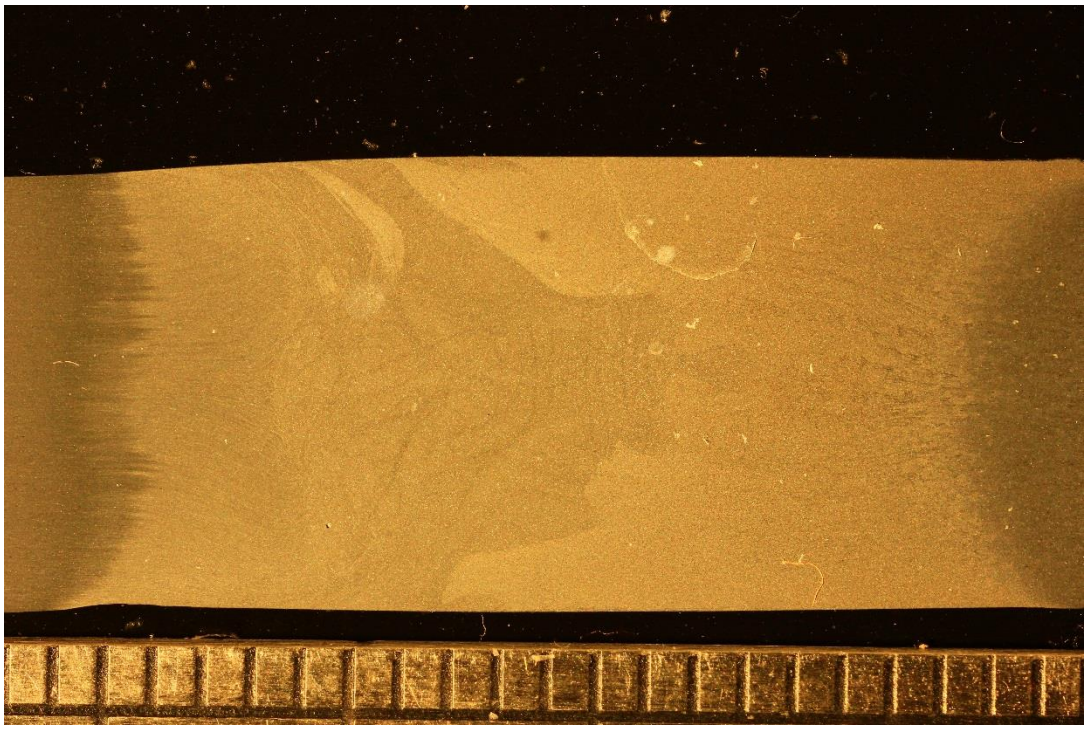

Figure 7.9: Macrograph of Weld 2 Sample 5

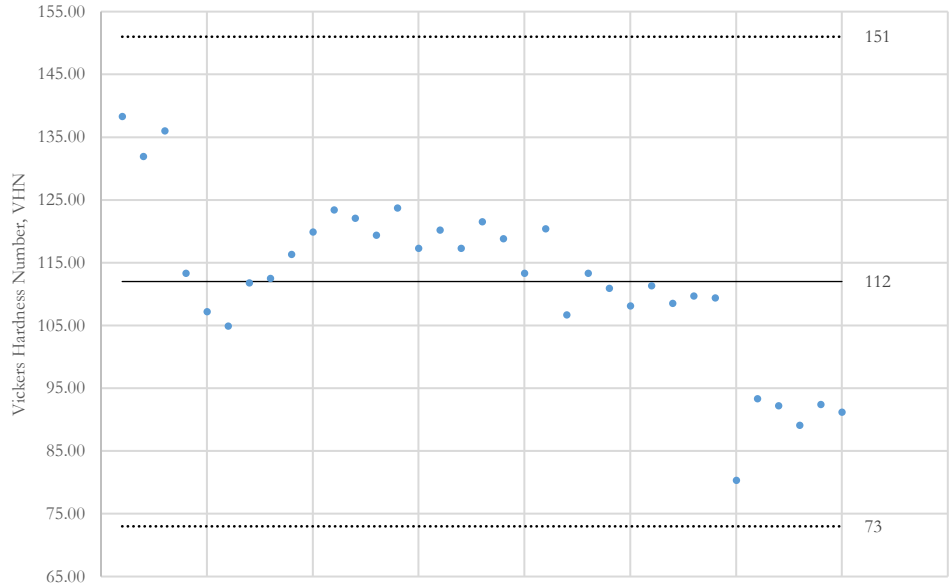

Figure 7.10: Hardness Data of Weld 2 Sample 5

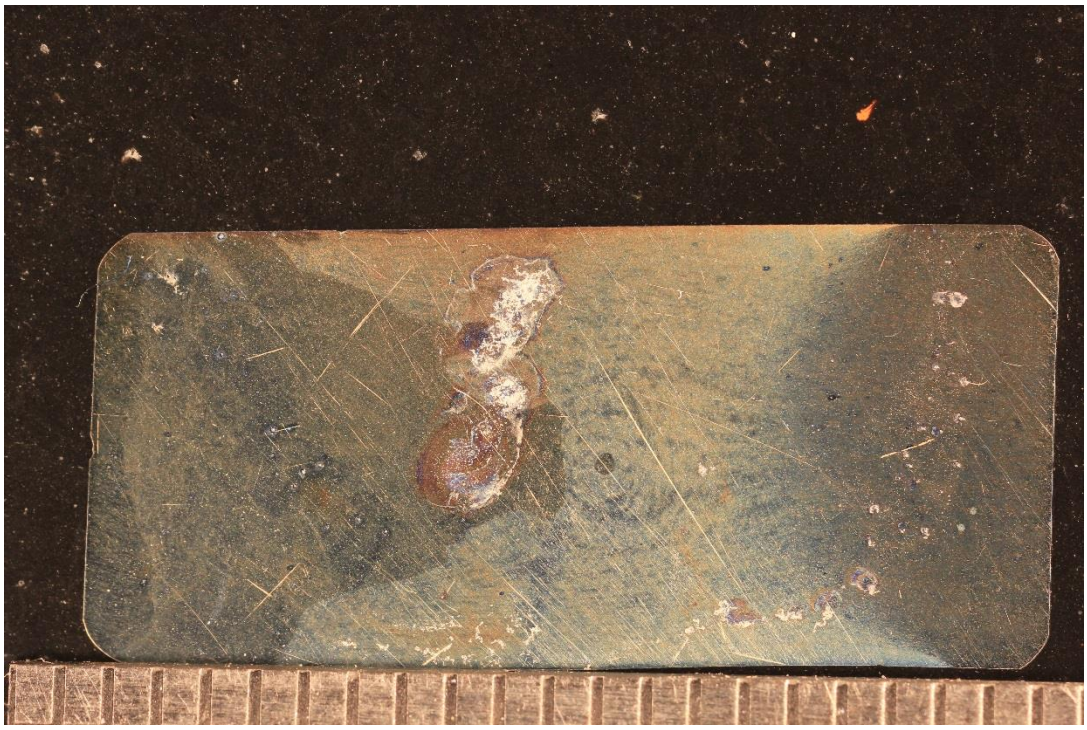

Figure 7.11: Macrograph of Weld 2 Sample 9

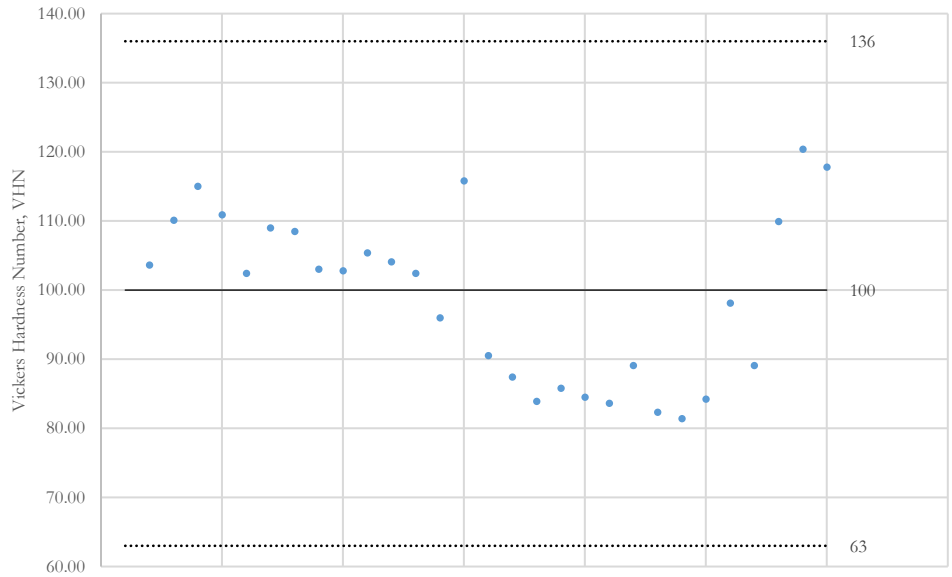

Figure 7.12: Hardness Data of Weld 2 Sample 9

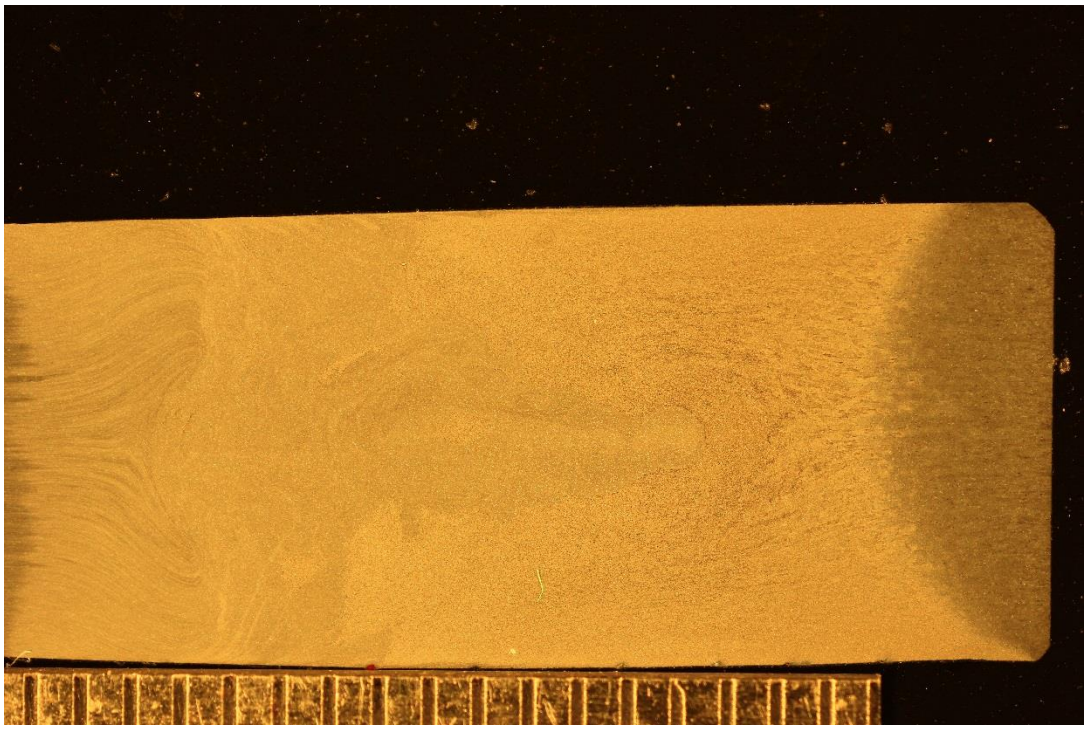

Figure 7.13: Macrograph of Weld 3 Sample 1

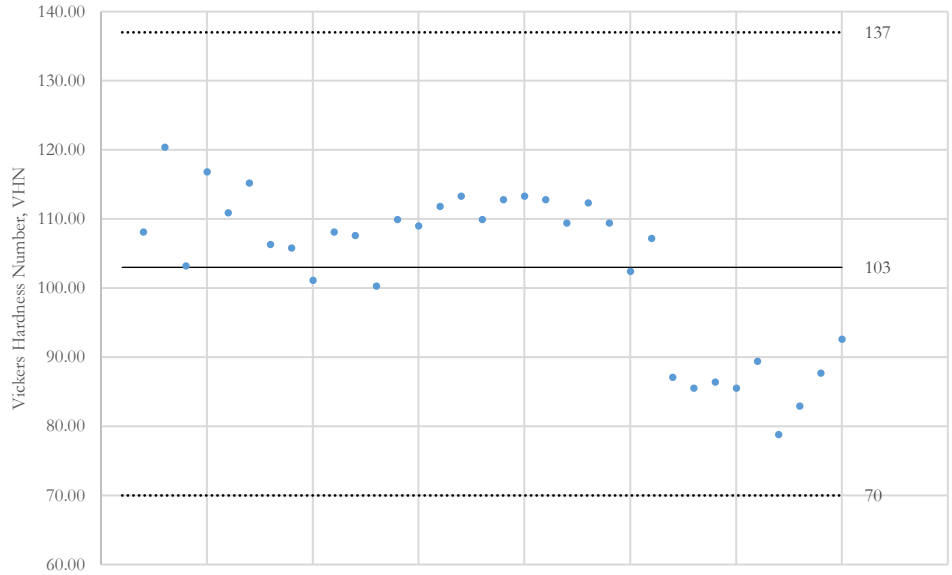

Figure 7.14: Hardness Data of Weld 3 Sample 1

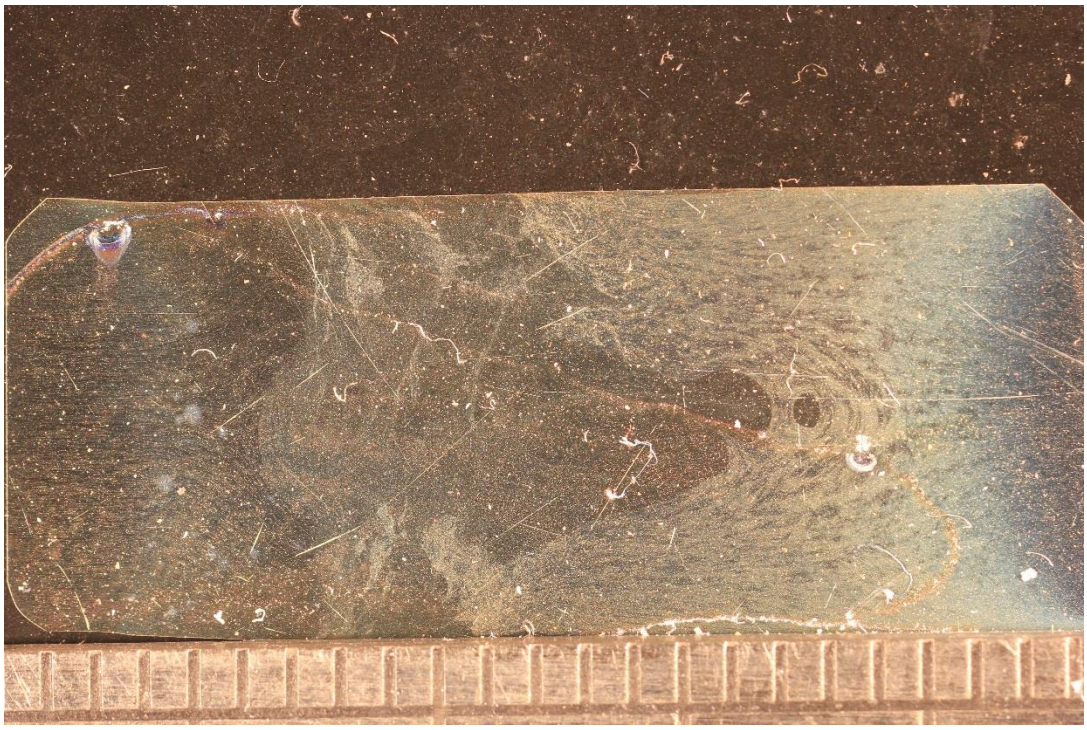

Figure 7.15: Macrograph of Weld 3 Sample 5

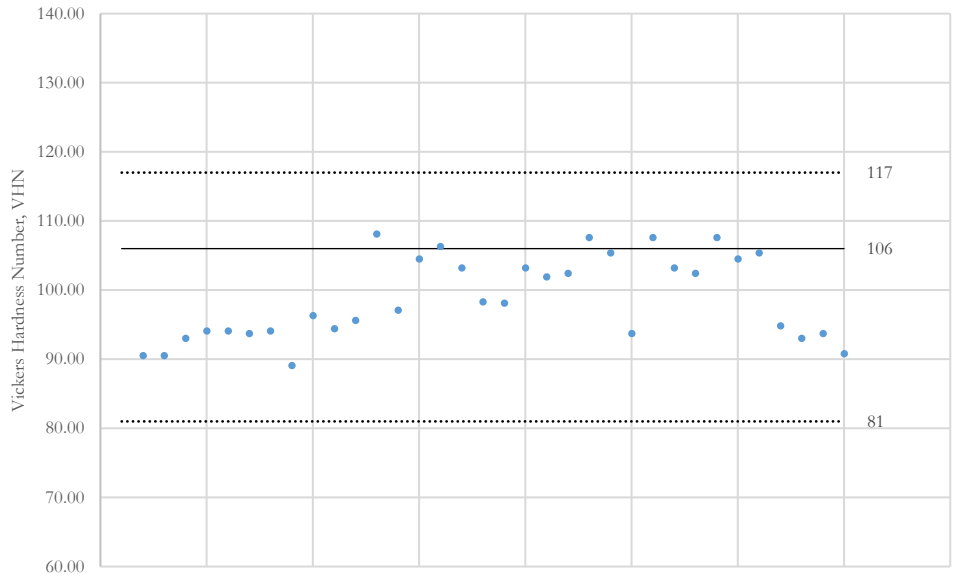

Figure 7.16: Hardness Data of Weld 3 Sample 5

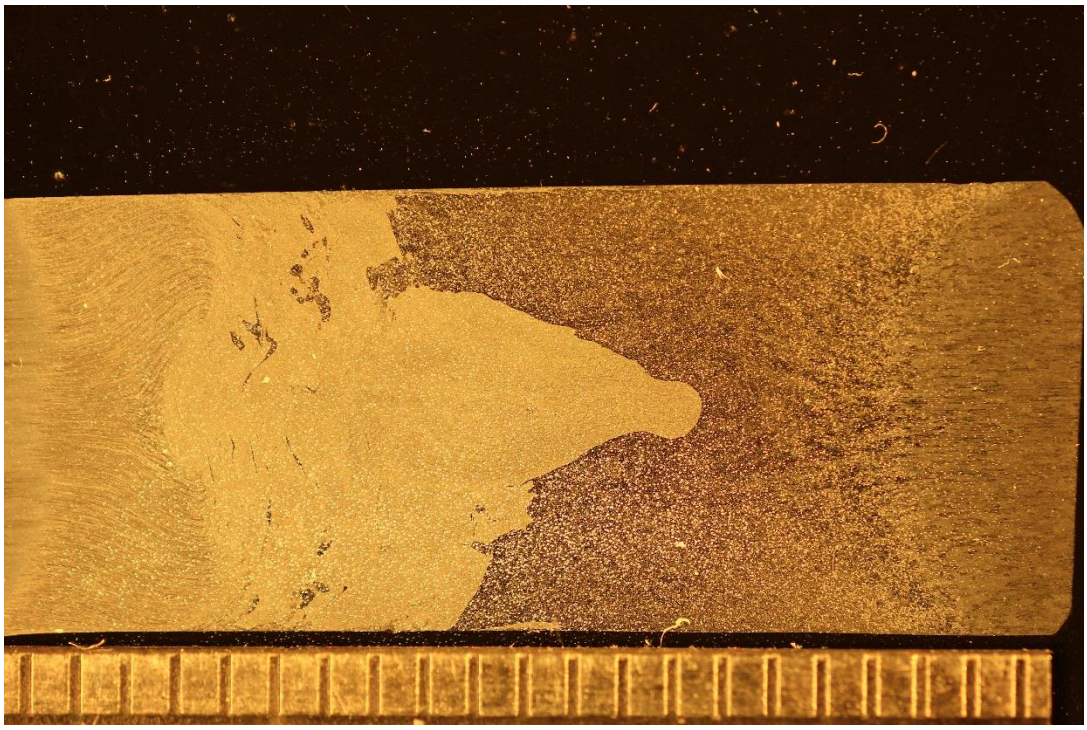

Figure 7.17: Macrograph of Weld 3 Sample 9

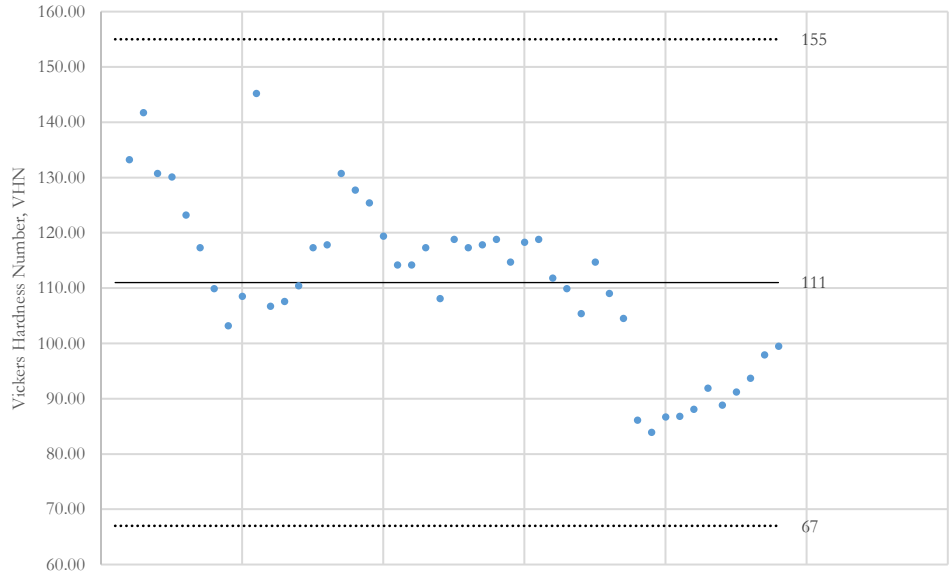

Figure 7.18: Hardness Data of Weld 3 Sample 9

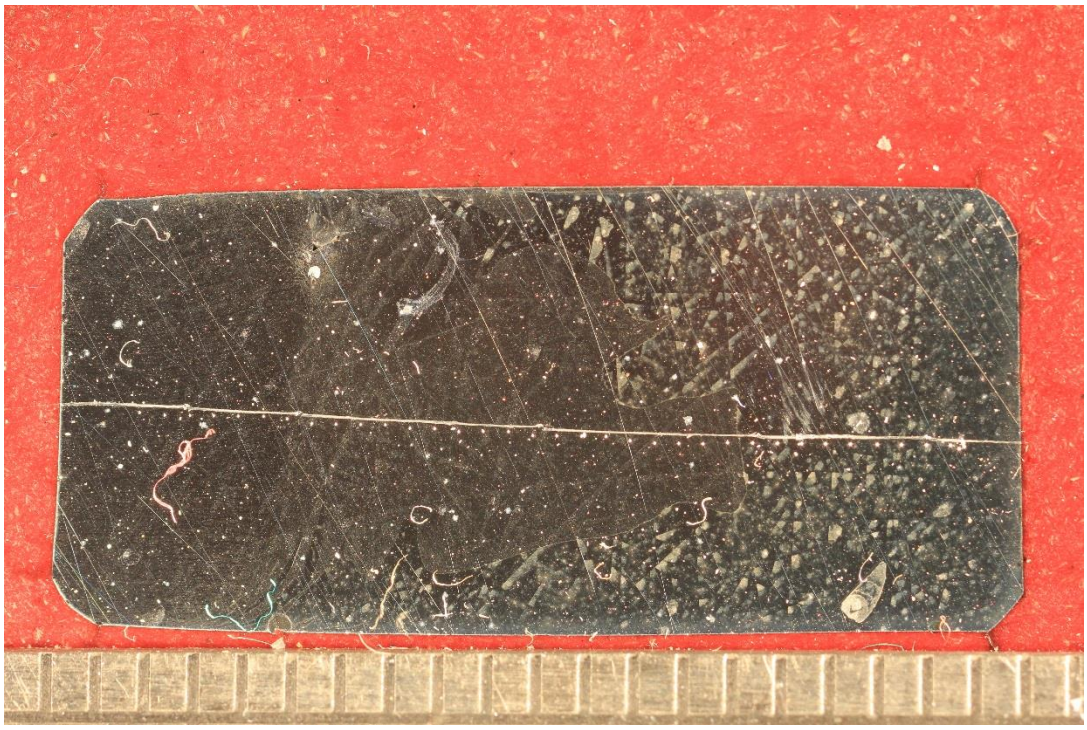

Figure 7.19: Macrograph of Weld 4 Sample 1

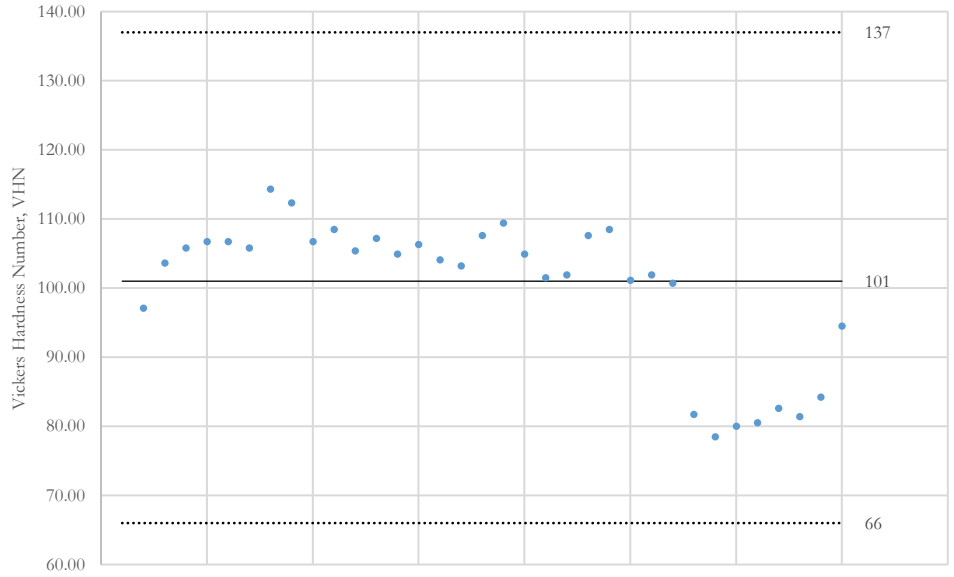

Figure 7.20: Hardness Data of Weld 4 Sample 1

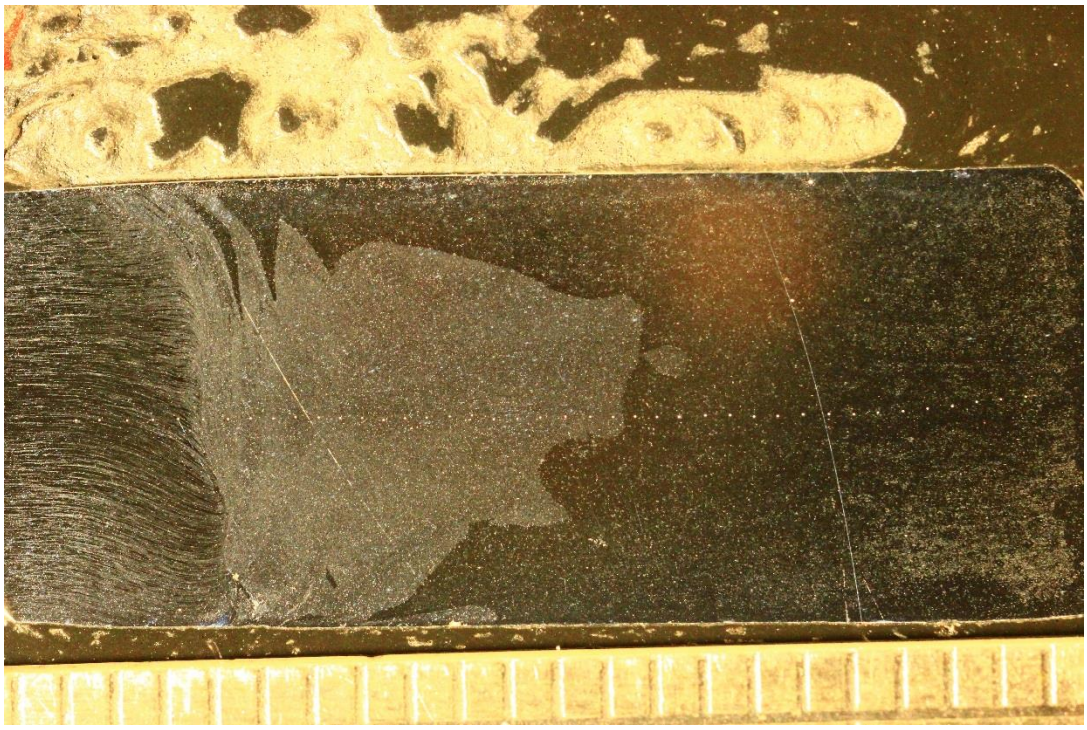

Figure 7.21: Macrograph of Weld 4 Sample 5

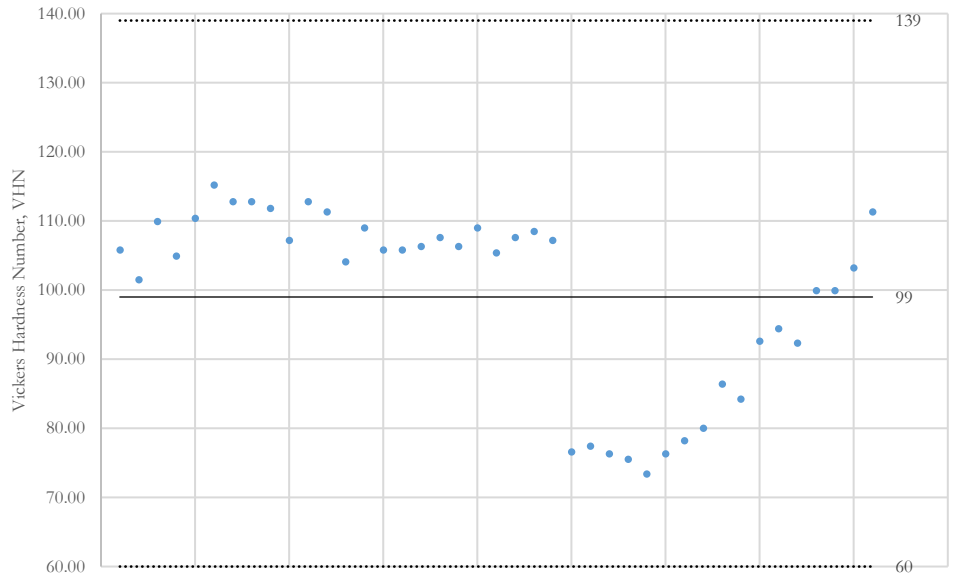

Figure 7.22: Hardness Data of Weld 4 Sample 5

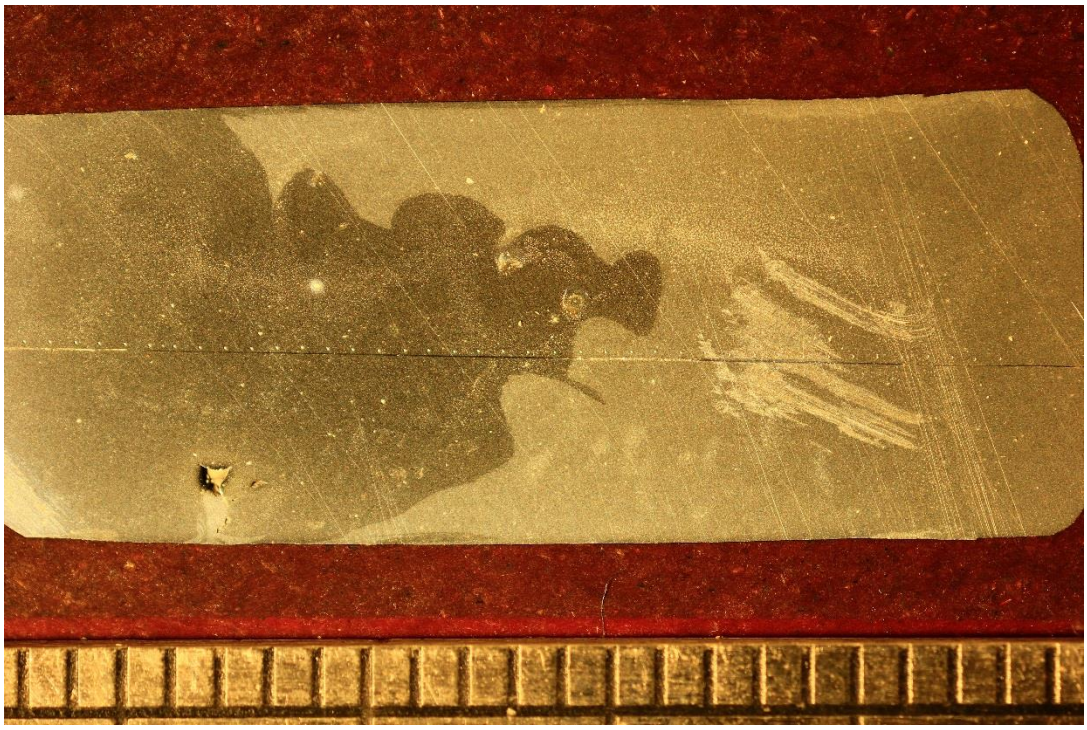

Figure 7.23: Macrograph of Weld 4 Sample 9

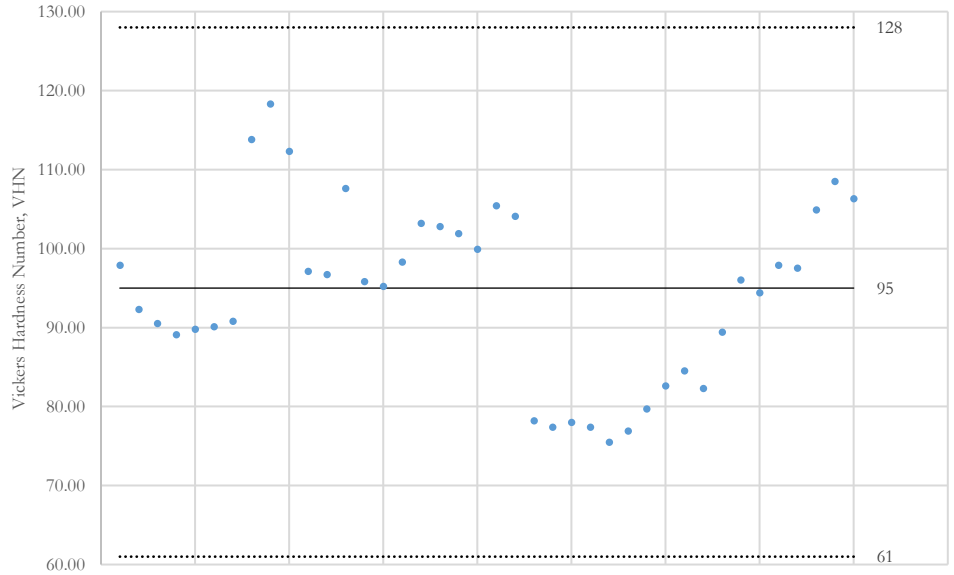

Figure 7.24: Hardness Data of Weld 4 Sample 9

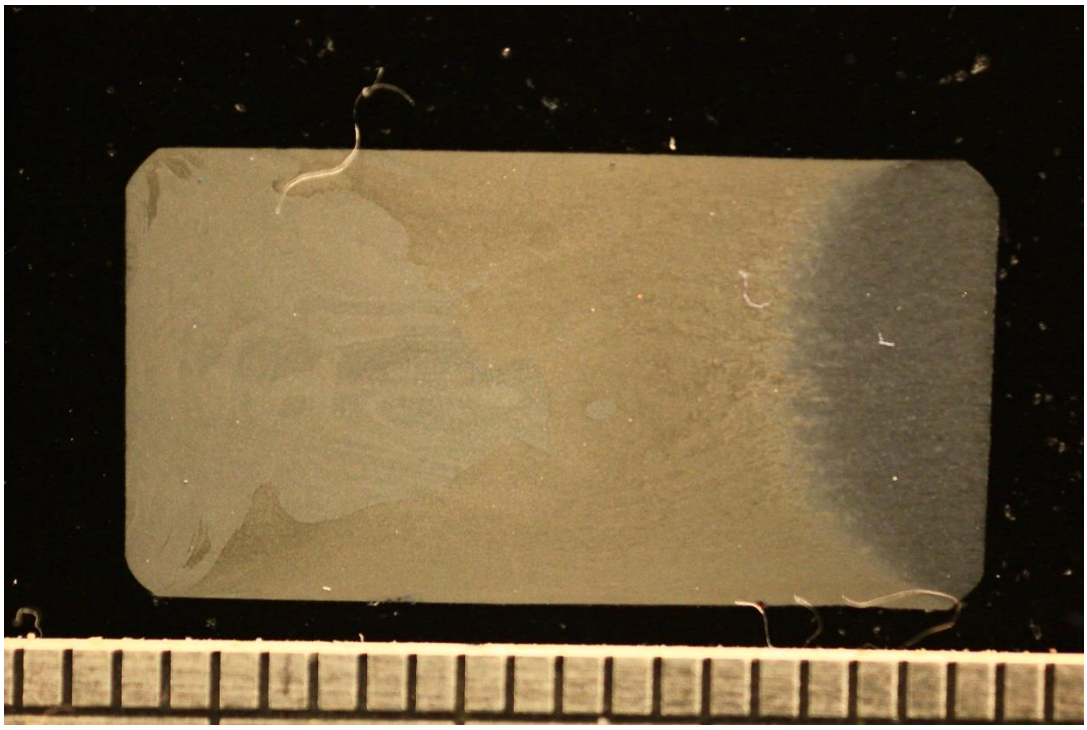

Figure 7.25: Macrograph of Weld 5 Sample 1

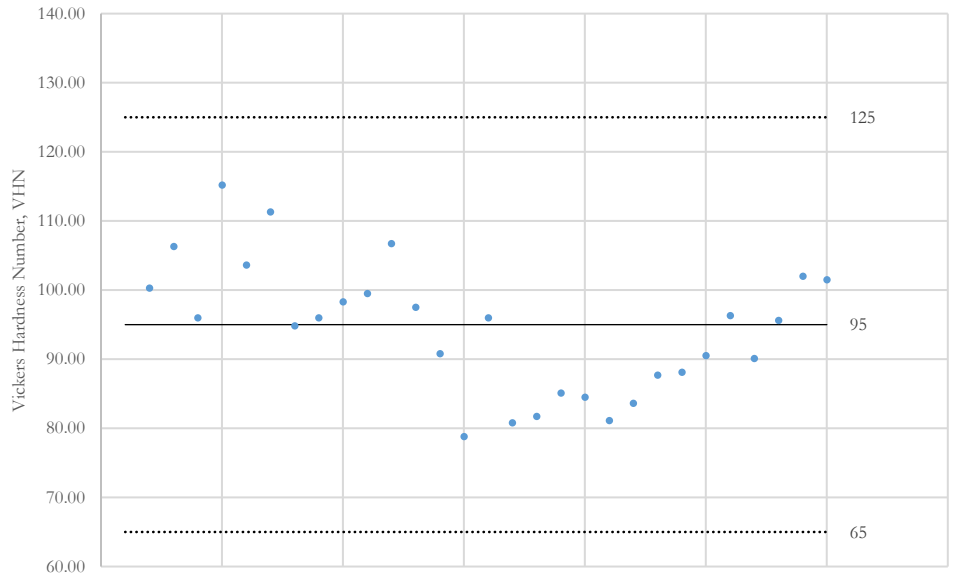

Figure 7.26: Hardness Data of Weld 5 Sample 1

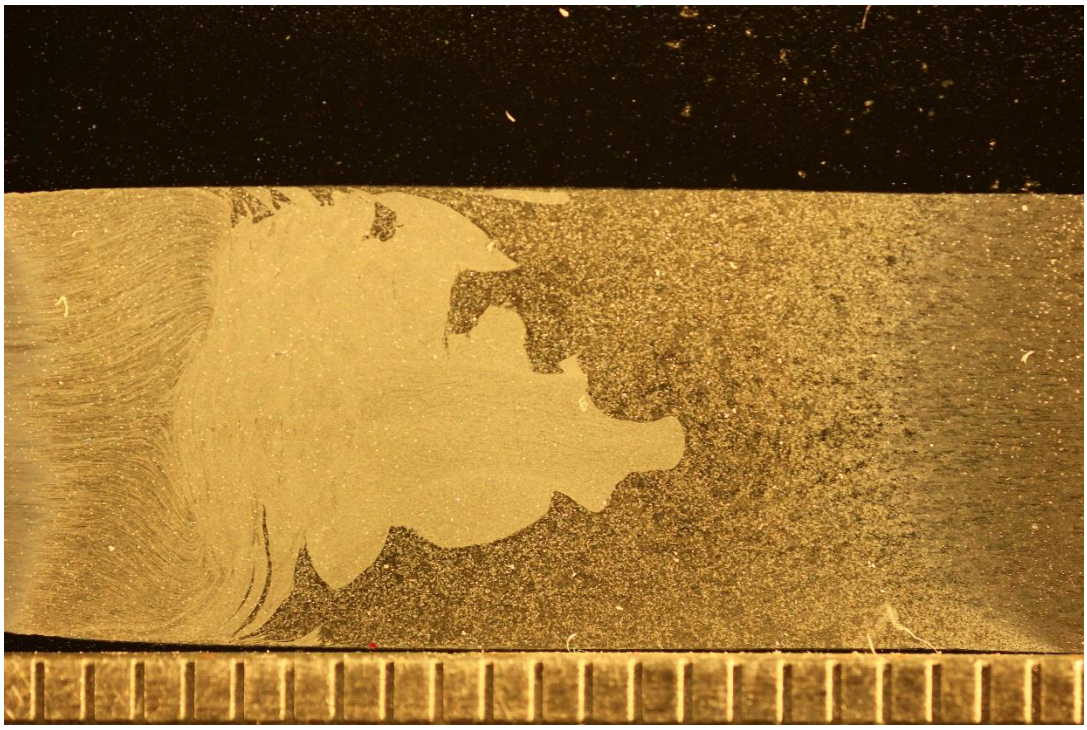

Figure 7.27: Macrograph of Weld 5 Sample 5

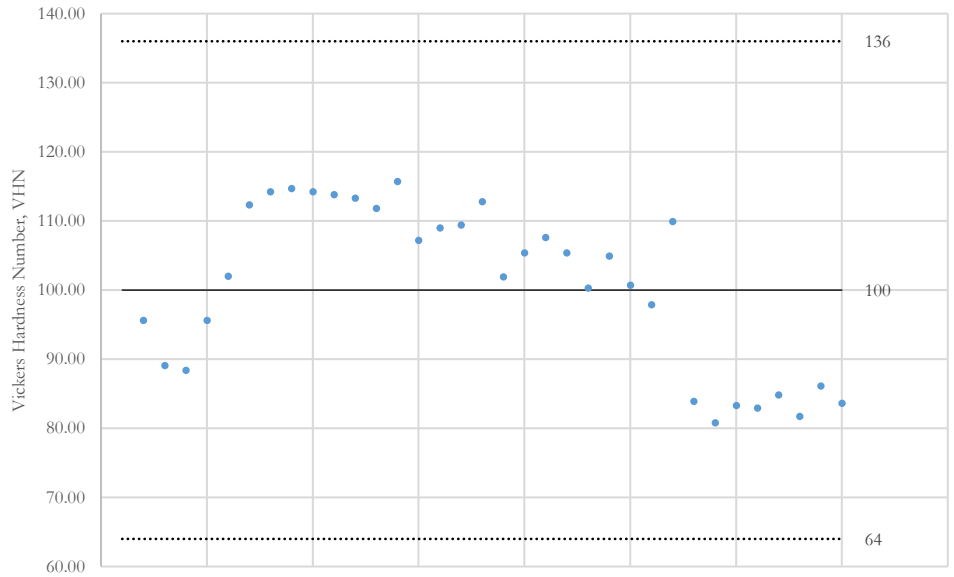

Figure 7.28: Hardness Data of Weld 5 Sample 5

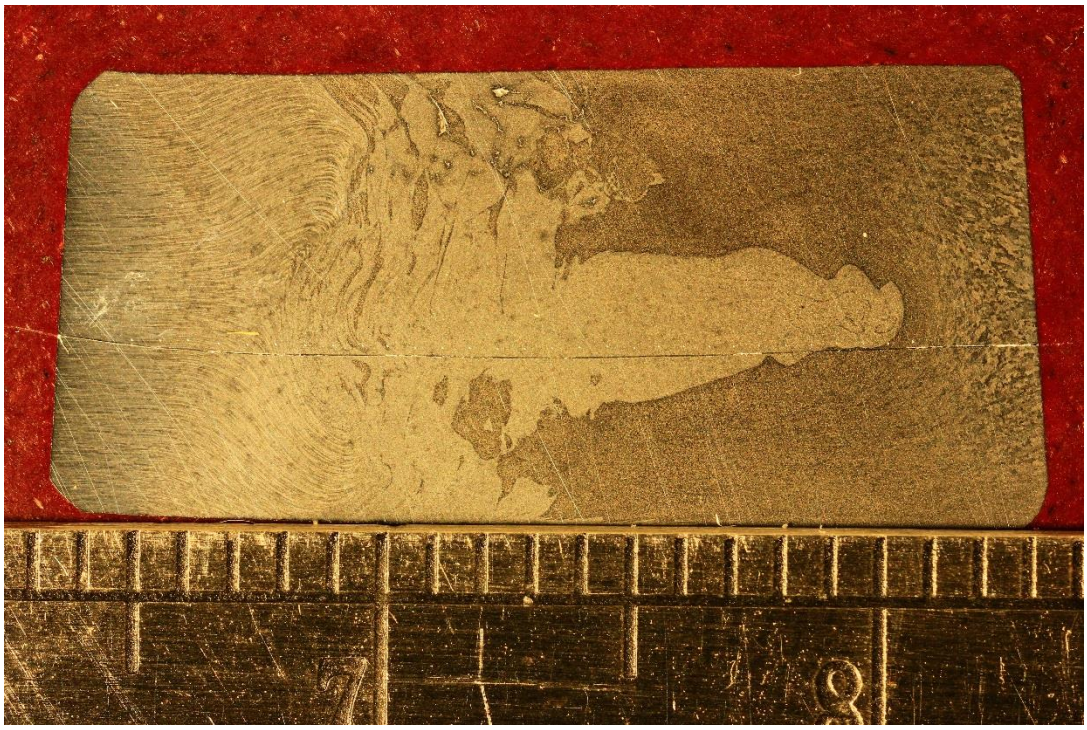

Figure 7.29: Macrograph of Weld 5 Sample 9

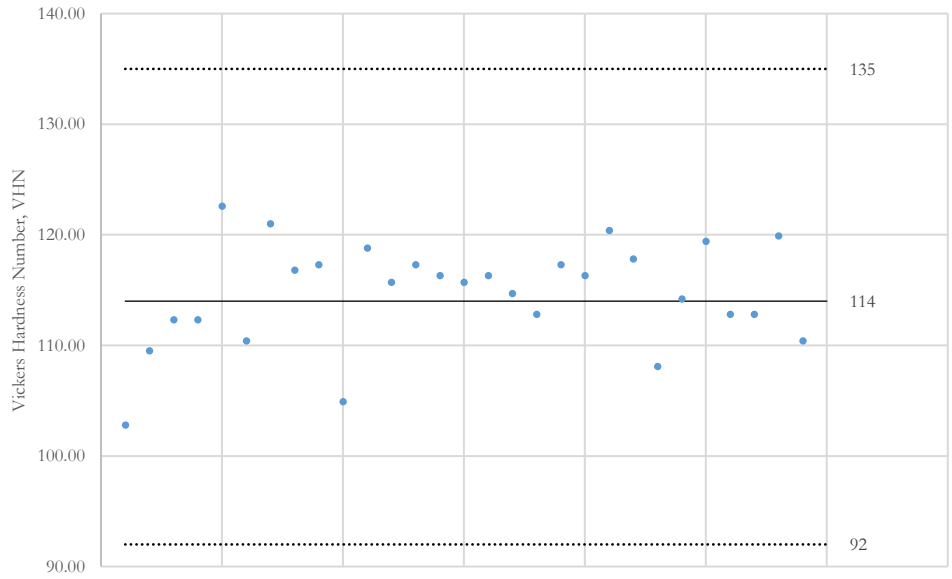

Figure 7.30: Hardness Data of Weld 5 Sample 9

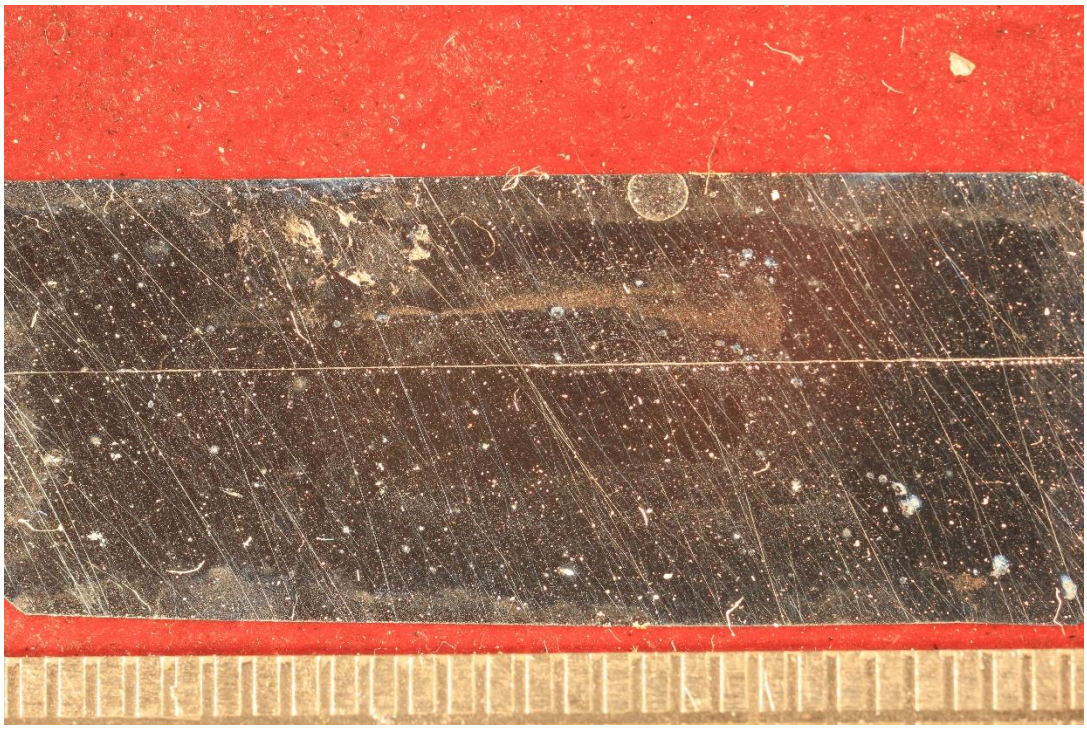

Figure 7.31: Macrograph of Weld 6 Sample 1

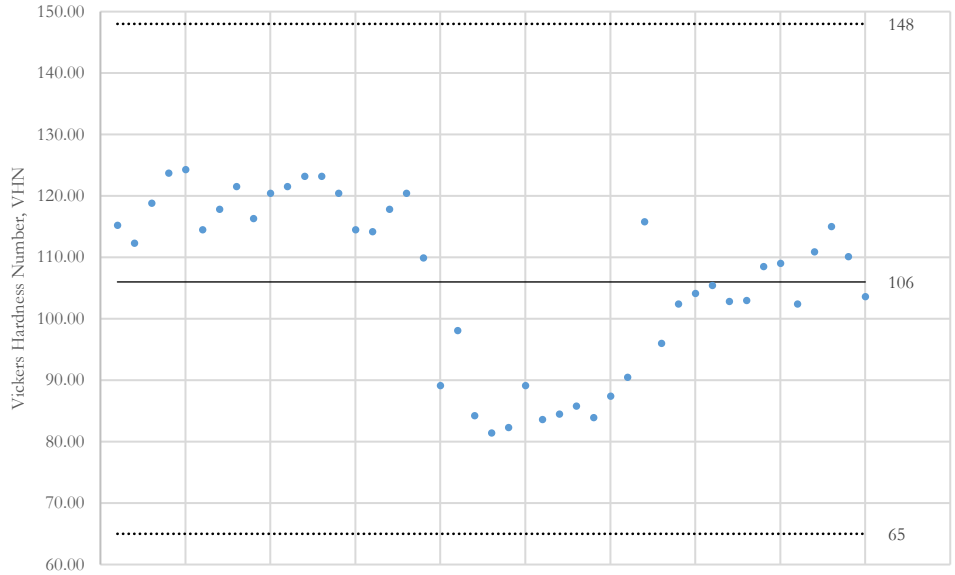

Figure 7.32: Hardness Data of Weld 6 Sample 9

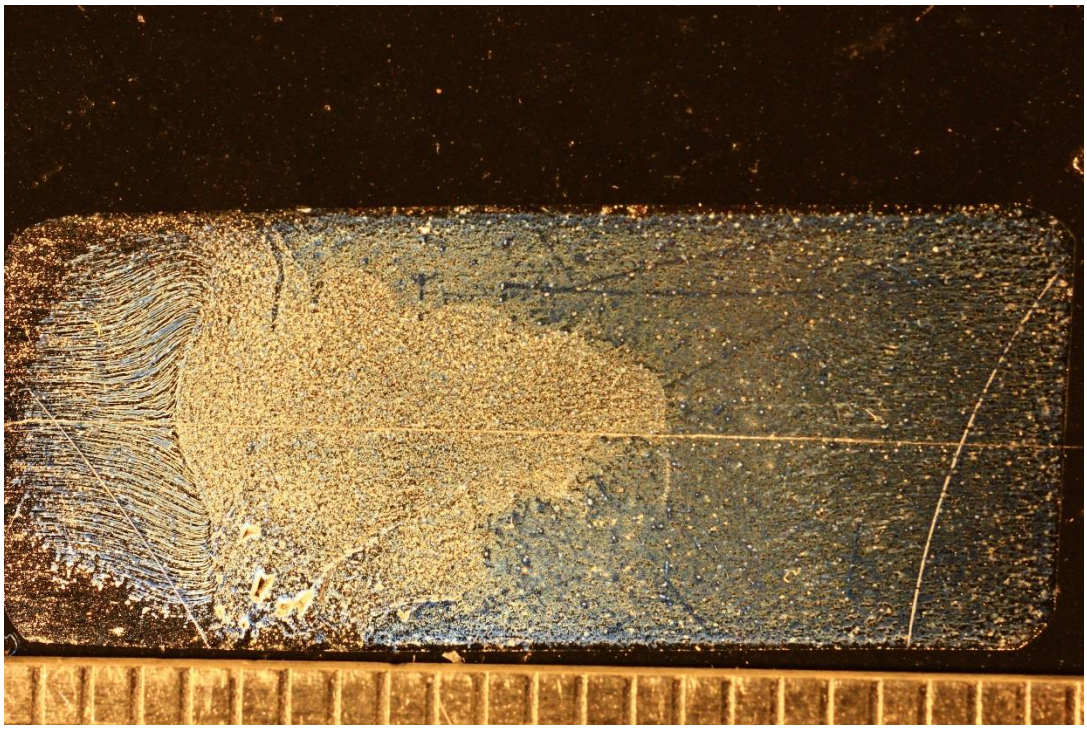

Figure 7.33: Macrograph of Weld 6 Sample 5

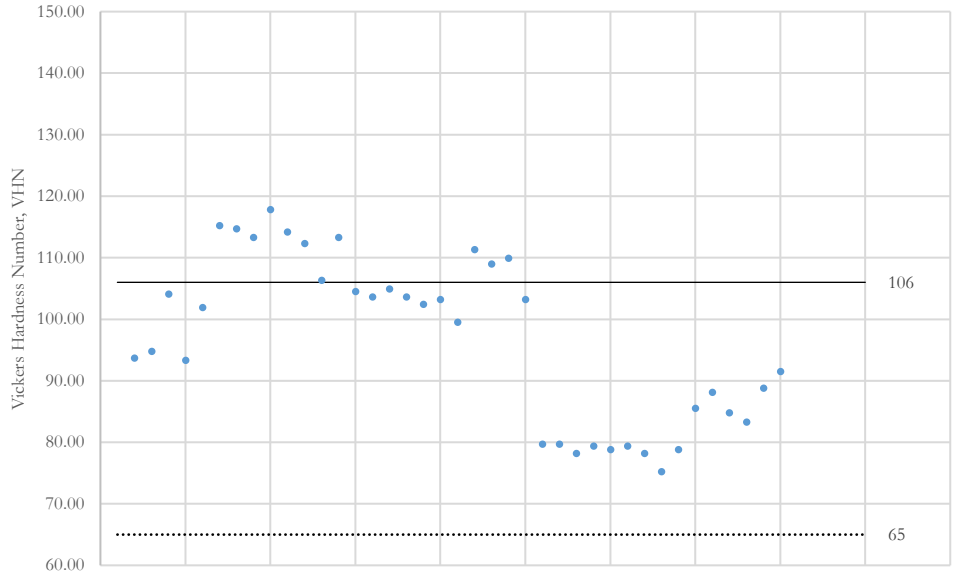

Figure 7.34: Hardness Data of Weld 6 Sample 9

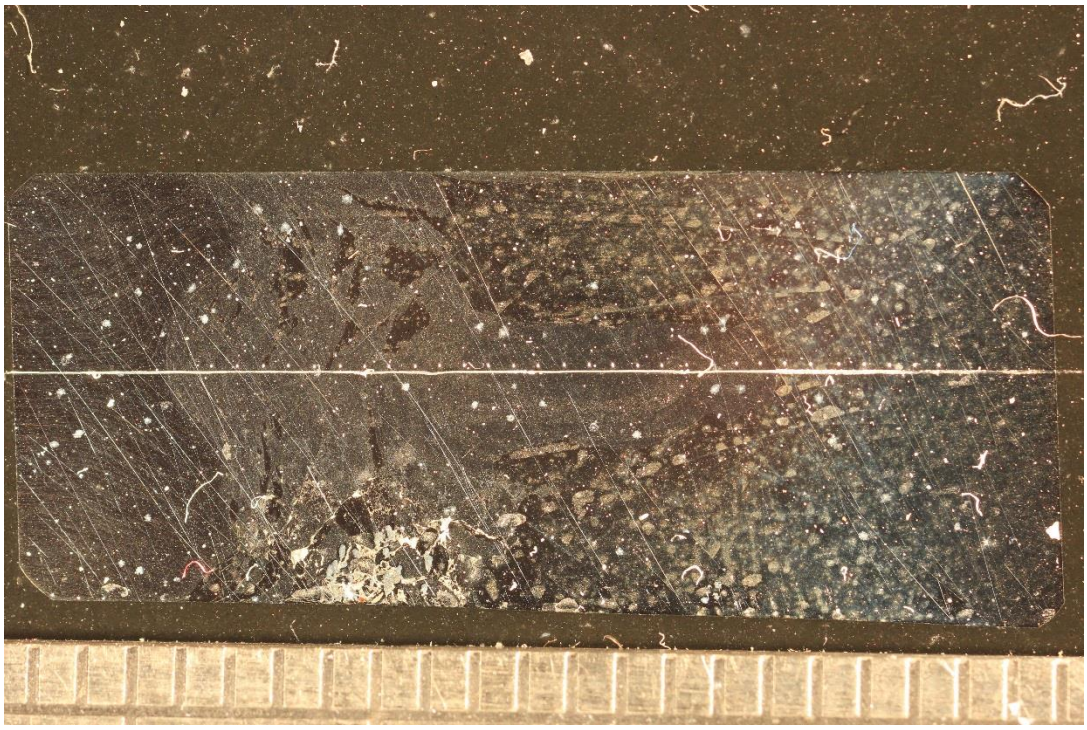

Figure 7.35: Macrograph of Weld 6 Sample 9

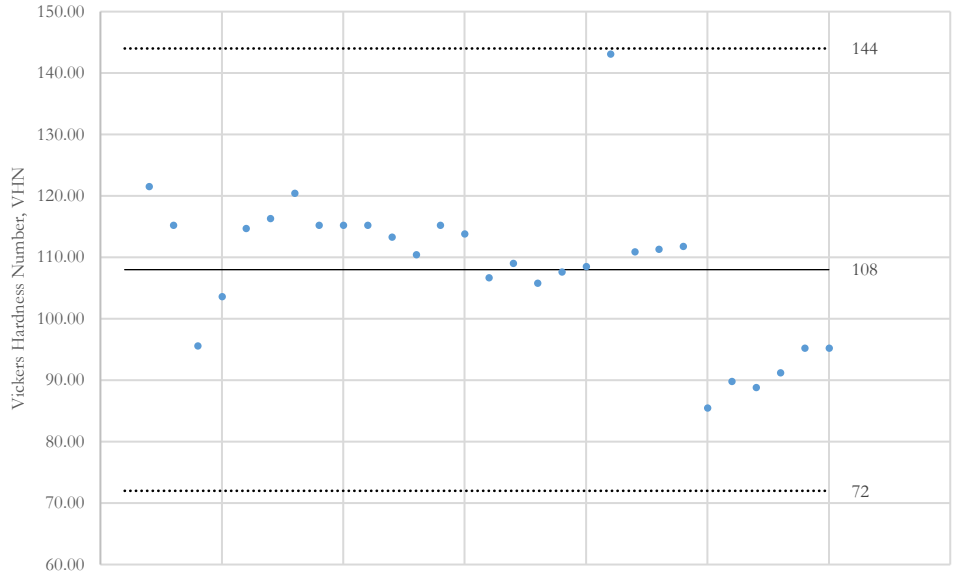

Figure 7.36: Hardness Data of Weld 6 Sample 9

Vita

Robert L. Marrero, Jr. is a graduate student in the Mechanical Engineering Department at the University of New Orleans, where he completed his Bachelors of Science in Mechanical Engineering. He has passed the Professional Engineer exam in Mechanical Engineering in the State of Louisiana and is awaiting official licensure, where he works in the Environmental Industry with a specialty in Marine Vapor Recovery Systems.